Fuel 112 (2013) 391–449

Contents lists available at SciVerse ScienceDirect

Fuel

journal homepage: www.elsevier.com/locate/fuel

Review article

An overview of the behaviour of biomass during combustion: Part I. Phase-mineral transformations of organic and inorganic matter

Stanislav V. Vassilev [a,b,*], David Baxter [a], Christina G. Vassileva [b]

[a] Institute for Energy and Transport, Joint Research Centre, European Commission, P.O. Box 2, NL-1755 ZG Petten, The Netherlands
[b] Institute of Mineralogy and Crystallography, Bulgarian Academy of Sciences, Acad. G. Bonchev Street, Block 107, Sofia 1113, Bulgaria

ARTICLE INFO

Article history:
Received 24 April 2013
Accepted 14 May 2013
Available online 31 May 2013

Keywords:
Biomass combustion
Phase-mineral transformations
Ash formation
Chemical and mineral composition
Classification

ABSTRACT

An extended overview of the phase-mineral transformations of organic and inorganic matter that occur during biomass combustion was conducted. Some general considerations and particularly problems associated with the composition of biomass and biomass ash (BA) and behaviour of biomass during burning were discussed initially. Then, reference peer-reviewed data plus own investigations were used to organise and describe systematically the above topics. It was demonstrated that the phase composition of BA is polycomponent, heterogeneous and variable and includes: (1) mostly inorganic matter (IM) composed of non-crystalline (amorphous) and crystalline to semi-crystalline (mineral) constituents; (2) subordinately organic matter (OM) consisting of char and organic minerals; and (3) some fluid matter associated with both IM and OM. Approximately 291 phases or minerals were identified in BA. These species have primary, secondary or tertiary origin in the combustion residue and they are generated from natural (authigenic and detrital) and technogenic phases or minerals originally present in biomass. Afterwards, common issues related to the composition, occurrence, transformation and origin of common constituents in biomass and BA such as: (1) OM, namely cellulose, hemicellulose, lignin, char and other organic phases plus organic minerals; and (2) IM such as silicates, oxides and hydroxides, phosphates, sulphates (plus sulphides, sulphosalts, sulphites and thiosulphates), carbonates (plus bicarbonates), chlorides (plus chlorites and chlorates), nitrates, glass, amorphous (non-glass) material and other inorganic phases; were described and compared to coal ash. As a final point, a systematization of physico-chemical transformations during biomass combustion is given. It was found that the original OM and IM in biomass during combustion transform: (1) initially to devolatilization of OM and burning of combustible gases and char with formation of intermediate and less stable oxalates, nitrates, chlorides, hydroxides, carbonates, sulphates and inorganic amorphous (non-glass) material; (2) subsequently to more stable silicates, phosphates and oxides; (3) then to melting accompanied by dissolution of the refractory minerals; with increasing combustion temperatures in the system; and (4) followed by crystallisation of melt and formation of glass accompanied by some salt condensation and hydroxylation, hydration and carbonation of newly formed phases during cooling of BA. Finally, some post-combustion transformations of the newly formed minerals and phases to stable during weathering species among silicates, hydroxides, phosphates, sulphates, carbonates, chlorides and nitrates also occur due to their hydration, hydroxylation and carbonation by moisture and CO_2 in the air through storage of BA. Certain major associations related to the occurrence, content and origin of elements and phases were identified in the BA system and they include: (1) Si–Al–Fe–Na–Ti (mostly glass, silicates and oxyhydroxides); (2) Ca–Mg–Mn (commonly carbonates, oxyhydroxides, glass, silicates and some phosphates and sulphates); and (3) K–P–S–Cl (normally phosphates, sulphates, chlorides, glass and some silicates and carbonates). These associations were applied for classification of BAs to four types and six sub-types. It was found that such systematic relationships have a key importance in both fundamental and applied aspects related to innovative and sustainable processing of biomass and BA. The ash formation mechanisms and ash fusion behaviour, as well as some indications of potential technological problems and environmental risks during combustion of biomass types and sub-types and application of their BAs will be described in Part II of the present work.

© 2013 Elsevier Ltd. All rights reserved.

---

* Corresponding author at: Institute of Mineralogy and Crystallography, Bulgarian Academy of Sciences, Acad. G. Bonchev Street, Block 107, Sofia 1113, Bulgaria. Tel.: +359 2 9797055; fax: +359 2 9797056.

E-mail address: vassilev_stan@yahoo.com (S.V. Vassilev).

0016-2361/$ - see front matter © 2013 Elsevier Ltd. All rights reserved.
http://dx.doi.org/10.1016/j.fuel.2013.05.043

Contents

1. Introduction . . . 392
2. Materials, methods and data used . . . 408
3. Results and discussion . . . 413
  3.1. General considerations about composition of biomass and biomass ash . . . 413
  3.2. General observations about behaviour of biomass during combustion . . . 416
  3.3. Behaviour of organic matter during biomass combustion . . . 421
    3.3.1. Cellulose, hemicellulose and lignin . . . 421
    3.3.2. Char and other organic phases . . . 427
    3.3.3. Organic minerals. . . . 430
  3.4. Behaviour of inorganic matter during biomass combustion. . . . 432
    3.4.1. Silicates . . . 432
    3.4.2. Oxides and hydroxides. . . . 434
    3.4.3. Phosphates . . . 434
    3.4.4. Sulphates, sulphides, sulphosalts, sulphites and thiosulphates . . . 435
    3.4.5. Carbonates and bicarbonates. . . . 436
    3.4.6. Chlorides, chlorites and chlorates . . . 436
    3.4.7. Nitrates . . . 437
    3.4.8. Glass . . . 437
    3.4.9. Inorganic amorphous (non-glass) material. . . . 441
    3.4.10. Other inorganic phases. . . . 441
  3.5. Systematization of physico-chemical transformations during biomass combustion. . . . 441
4. Conclusions. . . . 441
Acknowledgements . . . 443
References . . . 443

Nomenclature

A	ash yield	MM	marine macroalgae
AFTs	ash fusion temperatures	MP	melting point
BA	biomass ash	OM	organic matter
BC	beech wood chips	PP	plum pits
CC	corn cobs	R^2	correlation coefficient
daf	dry, ash-free basis	RH	rice husks
db	dry basis	SG	switchgrass
DTA	differential–thermal analysis	SS	sunflower shells
DWR	dry water-soluble residue	TGA	thermo-gravimetric analysis
FC	fixed carbon	VM	volatile matter
FT	fluid temperature	WS	walnut shells
HTA	high-temperature ash (⩾500 °C)	XRD	X-ray powder diffraction
IM	inorganic matter	%	weight%
LTA	low-temperature ash (100–250 °C)		

1. Introduction

It is widely accepted that biofuel combustion does not contribute to the greenhouse effect due to the CO_2 neutral conversion thanks to the renewability of biomass. The focus on bioenergy as an alternative to fossil energy has increased tremendously in recent times because of global warming problems originating mostly from fossil fuels combustion. Therefore, extensive investigations have been carried out worldwide recently to enhance biomass use instead of fossil fuels for energy conversion ([1–4] and references therein). In total about 95–97% of the world's bioenergy is currently produced by direct combustion of biomass [5–8]. As a result of that, it was estimated that approximately 480 million tonnes of biomass ash (BA) could be generated worldwide annually if the burned biomass is assumed to be 7 billion tonnes [3]. Hence, this quantity is comparable to that of coal ash, namely 780 million tonnes [9]. The perspective of increasing large-scale combustion of natural biomass and its co-combustion with semi-biomass (contaminated biomass such as municipal solid waste, refuse-derived fuel, sewage sludge, demolition wood and other industrial organic wastes) and solid fossil fuels (coal, peat, petroleum coke) seems to be one of the main drivers for biofuel promotion in many countries worldwide in the near future ([3] and references therein]).

Numerous biomass varieties with large biological diversity and distinct source and origin can be used as solid biofuel resources (Table 1). Two fundamental aspects related to the use of biomass and BA are: (1) to extend and improve the basic knowledge on composition and properties; and (2) to apply this knowledge for their most innovative and sustainable utilisation. The systematic identification, quantification and characterization of chemical and phase composition of a given solid fuel are the initial and most important steps during the investigation and application of such fuel. This composition is a unique fundamental code that depends on various factors and determines or predicts properties, quality and application perspectives, as well as technological and environmental problems related to any fuel. There is a huge amount of

Table 1
General classification of biomass varieties as solid fuel resources according to their biological diversity, source and origin.

Biomass groups	Biomass sub-groups, species and varieties
1. Wood and woody biomass	Coniferous or deciduous, angiospermous or gymnospermous and soft or hard such as stems, barks, branches (twigs), leaves (foliage), bushes (shrubs), chips, lumps, pellets, briquettes, sawdust, sawmill and others from various wood species
2. Herbaceous and agricultural biomass	Annual or perennial, arable or non-arable and field-based or processed-based biomass from various species such as: *2.1. Grasses and flowers* (alfalfa, arundo, bamboo, bana, cane, miscanthus, reed canary, ryegrass, switchgrass, timothy, others) *2.2. Straws* (barley, bean, corn, flax, mint, oat, paddy, rape, rice, rye, sesame, sunflower, triticale, wheat, others) *2.3. Stalks* (alfalfa, arhar, arundo, bean, corn, cotton, kenaf, mustard, oreganum, sesame, sunflower, thistle, tobacco, others) *2.4. Fibers* (coconut coir, flax, jute bast, kenaf bast, palm, others) *2.5. Shells and husks* (almond, cashewnut, coconut, coffee, cotton, hazelnut, millet, olive, peanut, rice, sunflower, walnut, others) *2.6. Pits* (apricot, cherry, olive, peach, plum, others) *2.7. Other residues* (fruits, pips, grains, seeds, coir, cobs, bagasse, food, fodder, marc, pulps, cakes, others) from various species
3. Aquatic biomass	Marine or freshwater, macroalgae or microalgae and multicellular or unicellular species (blue, blue-green, brown, golden, green and red algae; diatoms, duckweed, giant brown kelp, kelp, salvinia, seaweed, sweet-water weeds, water hyacinth, others)
4. Animal and human biomass wastes	Bones, chicken litter, meat-bone meal, sponges, various manures, others
5. Contaminated biomass and industrial biomass wastes (semi-biomass)	Municipal solid waste, demolition wood, refuse-derived fuel, sewage sludge, hospital waste, paper-pulp sludge, waste papers, paperboard waste, chipboard, fibreboard, plywood, wood pallets and boxes, railway sleepers, tannery waste, others
6. Biomass mixtures	Blends from the above varieties

Table 2
Phase composition of biomass.

Matter	State and type of constituents	Phases and components
1. Organic matter	*1.1. Solid, non-crystalline*	Structural ingredients (cellulose, hemicellulose, lignin), extractives, others
	1.2. Solid, crystalline	Organic minerals such as Ca–Mg–K–Na oxalates, others
2. Inorganic matter	*2.1. Solid, crystalline*	Mineral species from different mineral classes (silicates, oxyhydroxides, sulphates, phosphates, carbonates, chlorides, nitrates, others)
	2.2. Solid, semi-crystalline	Poorly crystallised mineraloids of some silicates, phosphates, hydroxides, chlorides, others
	2.3. Solid, amorphous	Amorphous phases such as various glasses, silicates, others
3. Fluid matter (mostly inorganic)	*Fluid, liquid, gas*	Moisture, gas and gas–liquid inclusions associated with both organic and inorganic matter

Table 3
Origin of phases in biomass.

Formation process	Place of formation	Time of formation	Formation mechanism
1. Natural	*1.1. Authigenic* (formed in biomass)	*1.1.1. Syngenetic* (during plant growing)	Generated by biogenic processes of growing plants (photosynthesis, diffusion, adsorption, osmosis, pinocytose, endocytose, exocytose, hydrolysis, precipitation, others)
		1.1.2. Epigenetic (after plant died)	Originated by natural processes after plants died (evaporation, precipitation)
	1.2. Detrital (formed outside biomass, but fixed in/on biomass)	*1.2.1. Pre-syngenetic* (before plant growing)	Pre-existing and finely dispersed mineral grains (commonly <1 μm) introduced into the plant by water suspensions during syngenesis (endocytose)
		1.2.2. Pre-syngenetic, syngenetic or epigenetic	Pre-existing and fine-grained particles (normally <10–100 μm) introduced by water and wind on plant surfaces and fixed in pores, voids and cracks
2. Anthropogenic	*Technogenic* (formed outside or inside biomass and fixed in/on biomass)	*Post-epigenetic* (during and after plant collecting)	Natural and/or industrial components (dust, materials, additives, contaminants, others) introduced in biomass during collecting, handling, transport and subsequent processing steps

data on the composition of biomass and BA, and the behaviour of organic matter (OM) and inorganic matter (IM) during biomass combustion on the Internet and numerous scientific reports from projects, conference proceedings and workshop presentations, as well as in databases and many publications. However, the use of such information is often unreliable because the data are not peer-reviewed. Therefore, a detailed review of the scientific literature, including more than 650 mostly peer-reviewed references and data compilations has been conducted to systematise the results obtained until now for composition and properties of biomass and BA. As initial steps, several extended and consecutive overviews related to: (1) chemical composition and classification of

Table 4
Phase composition of biomass ash.

Matter	State and type of constituent	Phase, mineral and particle morphology
Inorganic matter	*Solid, non-crystalline (amorphous)*	Spherical and spheroidal glass particles (massive, vesicular, cenospheres, plerospheres, dermaspheres, ferrospheres, ferrispheres, others)
	Solid, non-crystalline (amorphous)	Angular, irregular and other aspherical glass particles (massive, hollow, vesicular, fibres, needles, cylinders, discs, slabs, sheets, lacy, spongy, porous, elongated, rounded, agglomerates, others)
	Solid, crystalline to semi-crystalline (mineral)	Crystals, grains, aggregates, clusters, ferrospheres, ferrispheres, skeletal spheres and spheroids, agglomerates and others of various minerals or poorly crystallised mineraloids (silicates, oxides and hydroxides, sulphates, sulphides, sulphosalts, sulphites, thiosulphates, phosphates, carbonates, chlorides, chlorites, chlorates, nitrates, native elements, pure metals, metallic alloys, others)
Organic matter	*Solid, crystalline (mineral)*	Crystals, grains and aggregates of organic minerals (whewellite–weddelite and other groups)
	Solid, non-crystalline (amorphous) to semi-crystalline	Char including semi-coked, coked, soot and tar particles (angular, irregular, rounded, massive, hollow, vesicular, spongy, porous, skeleton, needles, whiskers, fibres, scaly, flaky, sheets, clusters of rosettes, cylinders, discs, slabs, spherical, spheroidal, agglomerates, others)
Fluid matter	*Fluid, liquid, gas*	Moisture and gas and gas–liquid inclusions associated with both inorganic and organic matter

Table 5
Origin of phases in biomass ash.

Origin	Formation process	Place of formation	Time of formation	Formation mechanism
Primary	*Natural*	Biomass	Before and during plant growing, and after plant died	Original phases or minerals that have undergone no phase transformations during combustion
Secondary	*Anthropogenic (technogenic)*	Combustion installation	During combustion	New phases generated by solid, liquid and gas reactions among pre-existing and newly formed compounds (absorption, adsorption, aggregation, agglomeration, amorphization, carbonation, carbonization, chloridation, coagulation, coalescence, condensation, crystallisation, decarbonation, decomposition, dehydration, dehydroxylation, disintegration, destruction, desulphation, diffusion, dissociation, dissolution, evaporation, fragmentation, hydration, hydroxylation, melting, nitration, nucleation, oxidation, phosphation, polymorphic transformation, precipitation, recrystallization, reduction, segregation, sintering, softening, solidification, solid-state reactions, sulphation, swelling, thermophoresis, vaporisation, vitrification, volatilization, combined conversions, others)
Tertiary	*Natural*	Transportation facility and disposal site	During transport and storage of combustion residues	New minerals or phases originated by wheathering (absorption, adsorption, amorphization, carbonation, crystallisation, decarbonation, decomposition, dehydration, dehydroxylation, destruction, desulphation, diffusion, dissociation, dissolution, evaporation, hydration, hydroxylation, oxidation, polymorphic transformation, precipitation, recrystallization, solid-state reactions, sulphation, vitrification, others)

biomass [1]; (2) organic and inorganic phase composition and classification of biomass [2]; (3) phase-mineral and chemical composition and classification of BA [3]; and (4) potential utilisation, technological and ecological advantages and challenges of BA [4], respectively, have been performed and published recently. The extensive reference peer-reviewed data plus own investigations for both biomass and BA systems were used to describe the above topics.

The occurrence and origin of phases in biomass and BA have been described in detail recently [2,3] and summarized herein (Tables 2–5). However, some of the major and still open questions are related to the limited knowledge of phase and mineral transformations and chemical interactions that occur during thermo-chemical conversion (combustion, pyrolysis, gasification, liquefaction) of biomass. A detailed knowledge for the composition of biomass and BA and behaviour of OM and IM during biomass combustion has primary importance in both basic and applied aspects and can assist directly or indirectly in:

(1) Establishment of a uniform nomenclature and standards.
(2) Identification of combined chemical and phase-mineral associations and their application for creation of advanced and precise classifications.
(3) Explanation or prognosis of composition and properties, as well as phase-mineral transformations and chemical interactions during combustion.
(4) Characterization of formation mechanisms of solid combustion products.
(5) Prediction and assessment of technological, ecological and health problems or benefits such as:
    - Performance during processing.
    - Economically valuable or environmentally hazardous components.
    - Specification of appropriate or potential innovative (effective, muticomponent, wasteless) modes of sustainable utilisation.
    - Novel, effective and environmentally sound biomass combustion technologies.
    - Reduction or elimination of various technological problems (agglomeration, corrosion, abrasion–erosion, slagging, fouling) and environmental risks and health concerns such as global and local contaminations of the air, water, soil and plants by toxic and potentially toxic compounds originated from gas, liquid and solid emissions; associated with biomass fuels and their combustion products.

Numerous studies of the behaviour of solid biofuels and their products during thermo-chemical conversion such as combustion, to a lesser extent pyrolysis (including torrefaction as low-temperature pyrolysis) and gasification, and more rarely liquefaction, as well as co-combustion, co-pyrolysis and co-gasification of coal with biomass have been performed worldwide and published [1–8,10–371]. As a result, extensive data for formation of bottom ashes, slags, fly ashes, chars and other residues during thermal treatment of different biomass varieties have been generated in the above investigations. Some advanced approaches and studies of phase and mineral transformations at different temperature intervals during combustion and occasionally gasification of biomass varieties such as: apple pulp; brassica; cassava; eucalyptus bark and stem; meat–bone meal; olive kernel, cake and tree pruning; parasol tree leaves; pine sawdust; poplar; pulp-paper mill residue; stalks (corn, cotton, pepper); straws (rice, wheat, mixed); sunflower husk; thistle; vine shoots; wastes (animal, food, sewage sludge); and wood (citrus tree, fire-pine, olive tree); have also been performed [12,20,75,79,99,116,129,156,164,186,201,202,205,310,329,333,343,348,367]. Thus, significant information for the phases and minerals identified in biomass and BA plus combustion behaviour of OM and IM is available and such data have been collected and arranged systematically, chronologically and alphabetically where possible herein. These results provide a sound foundation for an initial database that can be used for characterization of biomass during combustion. However, it was also found that serious problems related to composition and behaviour of OM and IM during biomass combustion occur and most of them are similar to those determined for chemical and phase studies of biomass and BA [1–4]. Therefore, an attempt to summarize these problems was undertaken and is described below:

(1) A serious omission is the limited description of the specific type, place and manner of collection, as well as storage and processing conditions of biomass varieties and their BAs used as samples or feedstock. For instance, the use of biomass specification such as: wood, fuelwood or firewood; soft or hard wood; stem or bark; forest or agricultural residue; straw; grass; manure; coppicing or dedicated energy crop; and short rotation coppice or crop; do not provide sufficient information for the reliable identification and characterization of a particular type of biomass and its behaviour during combustion. The exact fuel and ash status of the samples studied, namely as-collected or as-received, air-dried and oven-dried basis, is also very often not reported, which presents a serious challenge for some interpretations.

(2) The long term experience and knowledge achieved for the composition and phase transformations of the most studied fuels and their ashes, namely for coal, peat, petroleum coke and municipal solid waste or refuse-derived fuel ([3,372–379] and references therein) have not been implemented very successfully in the field of biomass and BA. Therefore, the use of unsuitable scientific approaches, models and procedures, incomplete data or inappropriate terms and interpretations is common in many investigations of biomass and BA ([1–4] and see also below and Part II).

(3) The lack of generally accepted terminology, classification systems and standards worldwide for the chemical and phase composition of biomass and BA leads to very serious misunderstanding during the investigations. The biggest problem seems to be the absence of appropriate phase classifications for biomass and BA in contrast to some other fuels and their ashes. For example, there are systematic and relatively strict phase specifications for coal and coal ash (which can also be applied to biomass and BA) including: (1) IM (crystalline and non-crystalline) such as mineral classes, groups and species, and amorphous phases; and (2) OM, namely different lithotypes, microlithotype groups and macerals, and chars produced from them; which are well recognised worldwide and relatively well characterised ([1–3,372,373,380,381] and references therein).

(4) The organic and inorganic phases in biomass and BA are a result of natural and anthropogenic formation processes (Tables 1–5) and a significant fraction in these solid fuels and their combustion products can contain other non-biomass phases [1–3]. Therefore, the contaminated biomass (semi-biomass) should always be considered separately from biomass generated from natural resources due to the different origin, composition and potential use.

(5) The detailed and complete data sets from simultaneous chemical and phase-mineral analyses for numerous biomass varieties and their solid combustion products are scarce. Thus, limited systematic interpretations can be made from such investigations.

(6) The methods for phase and mineral investigations of biomass and BA have not been developed and implemented very well. Extraction procedures are dominantly used for the identification and quantification of the inorganic and organic phase composition of biomass and BA. Unfortunately, the direct methods for determination of phases in biomass and BA are not commonly applied and some analytical concerns associated with biomass and BA have been discussed ([1–3] and references therein).

(7) Sequential chemical fractionation is mostly used to distinguish the speciation (modes of occurrence or chemical forms of combination) of elements in biomass fuels and their ashes. However, this indirect procedure cannot be applied to identify the actual modes of occurrence of elements in a multicomponent system. Leaching alone has many limitations and can be used only to provide preliminary information for some possible associations of elements in phases [2,3]. Other direct methods commonly applied for coal and coal products ([382,383] and references therein) provide better information and they should always be used simultaneously with leaching procedures.

(8) Most studies used the data from ash yield of biomass or the bulk chemical composition of ash to explain mineral matter, mineral composition, inorganic matter or inorganics in biomass and BA, which is not fully correct and can lead to confusion in many cases [1–3].

(9) There are still insignificant or quite limited data about the combined exploration of the thermal behaviour of OM (cellulose, hemicellulose, lignin, organic minerals) and IM (diverse species of silicates, oxyhydroxides, sulphates, phosphates, carbonates, chlorides, nitrates and other inorganic phases) constituents for biomass varieties from different types and sub-types during combustion of biomass or its co-combustion with other solid fuels (see below and Part II).

(10) The common scientific approach used is to study the concentration and behaviour of individual elements (Al, C, Ca, Cl, Fe, Mg, K, N, Na, P, S, Si and trace elements) for explaining and evaluating different technological and environmental problems related to biomass combustion. However, the experience from the studies of other solid fuels shows that the actual reasons for such problems in multicomponent systems like those for biomass and BA are mostly connected with the abundance and behaviour of modes of element occurrence (specific phases or minerals containing this element) in such fuels and their products ([1–4,378,381,384] and references therein).

(11) Many findings about the behaviour of OM and IM during biomass heating are based only on theoretical equilibrium and stoichiometric calculations of chemical data. These indirect investigations may be quite unrealistic for actual predictions of phases in a multicomponent system under non-equilibrium conditions. Such calculations can be used only to provide a preliminary prediction prior to direct (input, output) phase studies of the systems (see Section 3.2).

(12) The variable ash-melting points of biomass fuels have been discussed in numerous studies. However, it should be stated that melting points occur only for pure (monocomponent) or simple systems, while BA (similar to coal ash) as a multi-component system of powder material cannot have a specific melting point [385]. Therefore, BA has three or four characteristic and measurable ash fusion temperatures because ash melting occurs over a wide temperature range ([3] and see below and Part II).

(13) The systematic studies on trace elements in biomass and BA, as well as challenges and advantages related to modes of BA utilisation are only at an initial stage and they need further clarification by more extensive investigations [4].

The above listed problems show that additional, systematic and detailed chemical and phase-mineral studies of biomass and BA

Table 6
Chemical ash composition of biomass groups and sub-groups (86 varieties of biomass) plus algae and four solid fossil fuel types based on high-temperature ash analyses (normalised to 100%), wt.%. The Mn contents are additionally given.

Biomass group and sub-group	SiO_2	CaO	K_2O	P_2O_5	Al_2O_3	MgO	Fe_2O_3	SO_3	Na_2O	TiO_2	Sum	Mn	Samples
1. Wood and woody biomass (WWB)													
Mean	22.22	43.03	10.75	3.48	5.09	6.07	3.44	2.78	2.85	0.29	100.00	1.32	28
Minimum	1.86	5.79	2.19	0.66	0.12	1.10	0.37	0.36	0.22	0.06		0.08	28
Maximum	68.18	83.46	31.99	13.01	15.12	14.57	9.54	11.66	29.82	1.20		3.57	28
2. Herbaceous and agricultural biomass (HAB)													
Mean	33.39	14.86	26.65	6.48	3.66	5.62	3.26	3.61	2.29	0.18	100.00	0.13	44
Minimum	2.01	0.97	2.29	0.54	0.10	0.19	0.22	0.01	0.09	0.01		0.02	44
Maximum	94.48	44.32	63.90	31.06	14.60	16.21	36.27	14.74	26.20	2.02		0.46	44
2.1. Grasses (HAG)													
Mean	46.18	11.23	24.59	6.62	1.39	4.02	0.98	3.66	1.25	0.08	100.00	0.31	10
Minimum	8.73	2.98	2.93	3.14	0.67	1.42	0.58	0.83	0.09	0.01			10
Maximum	84.92	44.32	53.38	20.33	2.59	8.64	1.73	9.89	6.20	0.28			10
2.2. Straws (HAS)													
Mean	43.94	14.13	24.49	4.13	2.71	4.66	1.42	3.01	1.35	0.16	100.00	0.09	9
Minimum	7.87	2.46	12.59	0.98	0.10	1.67	0.41	1.18	0.16	0.02		0.02	9
Maximum	77.20	30.68	38.14	10.38	5.57	14.10	2.82	4.93	3.52	0.33		0.28	9
2.3. Other residues (HAR)													
Mean	24.47	16.58	28.25	7.27	4.90	6.62	4.84	3.80	3.05	0.22	100.00	0.16	25
Minimum	2.01	0.97	2.29	0.54	0.11	0.19	0.22	0.01	0.12	0.01		0.02	25
Maximum	94.48	44.13	63.90	31.06	14.60	16.21	36.27	14.74	26.20	2.02		0.46	25
3. Animal biomass (AB)													
Mean	2.90	49.04	7.67	28.17	1.69	2.75	0.35	3.91	3.50	0.02	100.00	0.05	2
Minimum	0.02	41.22	3.16	15.40	1.01	1.38	0.25	3.59	0.60	0.01		0.01	2
Maximum	5.77	56.85	12.19	40.94	2.37	4.11	0.45	4.24	6.41	0.03		0.09	2
4. Mixture of biomass (MB)													
Mean	44.19	17.48	6.00	5.72	10.82	3.52	6.34	2.66	2.53	0.74	100.00	0.16	4
Minimum	34.75	11.51	3.11	1.08	9.77	2.31	4.19	1.88	1.25	0.52			4
Maximum	57.83	25.70	7.76	18.07	11.35	4.77	10.44	4.62	3.18	0.95			4
5. Contaminated biomass (CB)													
Mean	35.73	18.30	3.45	3.64	15.41	3.60	9.78	3.45	1.90	4.74	100.00	0.15	8
Minimum	3.39	7.63	0.16	0.20	3.08	1.57	0.82	0.99	0.54	0.32		0.02	8
Maximum	60.10	26.81	9.70	15.88	53.53	6.45	22.18	10.55	4.06	27.58		0.23	8
All varieties of biomass (AVB)													
Mean	29.76	25.27	17.91	5.71	5.51	5.42	4.00	3.28	2.48	0.66	100.00	0.75	86
Minimum	0.02	0.97	0.16	0.20	0.10	0.19	0.22	0.01	0.09	0.01		0.01	86
Maximum	94.48	83.46	63.90	40.94	53.53	16.21	36.27	14.74	29.82	27.58		3.57	86
Natural biomass													
Mean	29.14	25.99	19.40	5.92	4.49	5.60	3.41	3.27	2.54	0.24	100.00	0.81	78
Minimum	0.02	0.97	2.19	0.54	0.10	0.19	0.22	0.01	0.09	0.01		0.01	78
Maximum	94.48	83.46	63.90	40.94	15.12	16.21	36.27	14.74	29.82	2.02		3.57	78
Aquatic biomass (A)													
Marine macroalgae	1.65	12.39	15.35	9.76	0.85	12.50	1.87	25.74	19.88	0.01	100.00	0.03	11
Solid fossil fuels													
Peat	37.53	9.97	1.12	2.75	20.14	2.14	13.83	12.11	0.10	0.31	100.00	0.08	1
Lignite (mean)	44.87	13.11	1.48	0.20	17.11	2.50	10.80	8.64	0.48	0.81	100.00	0.07	5
Sub-bituminous coal (mean)	54.74	7.05	1.67	0.08	22.86	2.14	5.30	4.07	1.09	1.00	100.00	0.05	10
Bituminous coal (mean)	56.14	4.90	1.61	0.22	24.82	1.55	6.68	2.16	0.77	1.15	100.00	0.05	22
Coal (mean)	54.06	6.57	1.60	0.50	23.18	1.83	6.85	3.54	0.82	1.05	100.00	0.05	37
Coal (minimum)	32.04	0.43	0.29	0.10	11.32	0.31	0.79	0.27	0.09	0.62		0.02	37
Coal (maximum)	68.35	27.78	4.15	1.70	35.23	3.98	16.44	14.42	2.90	1.61		0.18	37

Table 7
Occurrence, common abundance and possible origin of minerals and phases identified in biomass ash.

Phase, mineral	Chemical formula	Quantity[a]	Origin[b]		
			Primary	Secondary	Tertiary
1. Inorganic matter					
1.1. Silicates					
Afwillite	$Ca_3(SiO_3,OH)_2 \cdot 2H_2O$ or $Ca_3(Si_2O_4)(OH)_6$	A		•	*
Akermanite	$Ca_2MgSi_2O_7$	A		•	
Albite	$NaAlSi_3O_8$	A-M	*	•	
Amorphous silica	SiO_2	A-F	•	*	
Amphibole	$NaCa_2(Mg,Fe,Al)_5(Si,Al)_8O_{22}(OH)_2$	A	*	•	*
Anorthite	$CaAl_2Si_2O_8$	A-F	*	•	
Augite	$(Ca,Na)(Mg,Fe,Al,Ti)(Si,Al)_2O_6$	A	*	•	
Biotite[c]	$K(Mg,Fe)_3AlSi_3O_{10}$ $(OH,F)_2$	A	•	*	*
Bredigite	$Ca_7Mg(SiO_4)_4$	A	*	•	
Ca aluminosilicates		A-F		•	
Ca chlorosilicate	$Ca_2SiO_3Cl_2$	A-M		•	
Ca–Fe–Mg silicate	$Ca(Fe,Mg)Si_2O_6$	A-M		•	
Ca–Mg silicates		A-M		•	
Ca–Na aluminosilicate	$Ca_{0.9}Na_{0.1}Al_{1.8}Si_{2.2}O_8$	A		•	
Ca silicate hydrate	$CaO.SiO_2 \cdot H_2O$	A-M		*	•
Ca silicates	$CaSiO_4$, $CaSi_2O_5$, $Ca_4Si_2O_8$, $Ca_8Si_5O_{18}$, others	A-M		•	
Cd silicate	$CdSiO_3$	A		•	
Chlorite	$(Mg,Fe)_5Al_2Si_3O_{10}(OH)_8$	A	•	*	*
Clay minerals		A-M	•	*	*
Clinochlore	$(Mg,Fe)_5Al(Si_3Al)O_{10}(OH)_8$	A	•	*	*
Cordierite	$(Mg,Fe)_2Al_3(Si_5AlO_{18})$	A		•	
Cristobalite	SiO_2	A-F	*	•	
Cs silicate[c]		A	•	*	
Diopside	$CaMgSi_2O_6$ or $CaMg(SiO_3)_2$	A-M	*	•	
Enstatite	$MgSiO_3$	A	*	•	
Faujasite	$Na_2Al_2Si_{3.3}O_{10.6} \cdot 7H_2O$	A		*	•
Fayalite	Fe_2SiO_4	A-Mi	*	•	
Fe gehlenite	$Ca_2FeAlSiO_7$	A		•	
Feldspars	$NaAlSi_3O_8$–$CaAl_2Si_2O_8$, $KAlSi_3O_8$	A-F	*	•	
Ferrosillite	$FeSi_2O_6$	A		•	
Forsterite	Mg_2SiO_4	A-Mi	*	•	
Garnet (andradite, pyrope, grossular)	$Ca_3Fe_2Si_3O_{12}$, $Mg_3Al_2Si_3O_{12}$, $Ca_3Al_2Si_3O_{12}$	A		•	
Gehlenite	$Ca_2Al_2SiO_7$	A-M		•	
Gismondite	$Ca_2Al_4Si_4O_{16} \cdot 9H_2O$	A		*	•
Hatrurite	Ca_3SiO_5	A		•	
Hedenbergite	$CaFeSi_2O_6$ or $Ca(Fe,Mg)(SiO_3)_2$	A	*	•	
Illite	$(K,H_2O)Al_2(Al,Si)Si_3O_{10}(OH)_2$	A-M	•	*	*
Jadeite	$NaAlSi_2O_6$	A		•	
Kalsilite–kaliophilite	$KAlSiO_4$	A-Mi		•	
K aluminosilicates		A-M		•	
Kaolinite	$Al_2Si_2O_5(OH)_4$	A-M	•	*	*
K–Ca aluminosilicate		A-M		•	
K–Ca silicates	K_2CaSiO_4, $K_4CaSi_3O_9$, others	A-F		•	
K feldspars	$KAlSi_3O_8$	A-F	*	•	
K–Mg silicate	$K_2MgSi_3O_8$	A		•	
K silicates	$K_2Si_4O_9$, $K_6Si_2O_7$, others	A-Mi		•	
Larnite	Ca_2SiO_4	A-M		•	
Leucite	$KAlSi_2O_6$	A-F		•	
Makatite	$Na_2Si_4O_8(OH)_2 \cdot 4(H_2O)$	A		*	•
Melilite (akermanite–gehlenite)	$Ca_2MgSi_2O_7$–$Ca_2Al_2SiO_7$	A-M		•	
Merwinite	$Ca_3Mg(SiO_4)_2$	A-M		•	
Metakaolinite	$Al_2Si_2O_5$	A-Mi		•	
Mg aluminosilicates[c]		A	*	•	
Mg silicate		A-Mi		•	
Microcline	$KAlSi_3O_8$	A-Mi	*	•	
Monticellite	$CaMgSiO_4$	A-Mi		•	
Montmorillonite[c]	$(Na,Ca)_{0.3}(Al,Mg,Fe)_2Si_4O_{10}(OH)_2 \cdot xH_2O$	A	•	*	*
Mullite	$Al_6Si_2O_{13}$	A-Mi		•	
Muscovite	$KAl_2AlSi_3O_{10}(OH,F)_2$	A-Mi	•	*	*
Na–Ca silicate	Na_2CaSiO_4	A-Mi		•	
Na melilite	$NaCaAlSi_2O_7$	A-Mi		•	
Na–Mg silicate	$Na(Mg_{0.5}Si_{0.5})O(Si_2O_6)$	A		•	
Na silicate (water glass)	$Na_2Si_3O_7$ or Na_2SiO_3	A-M		•	
Na tremolite	$(Ca,Na)_23Mg_5Si_8O_{22}$ $(OH)_2$	A	•	*	*
Opal[c] (amorphous or crystalline, silicic acid polymerized, biogenic silica, silica phytolith)	$SiO_2 \cdot nH_2O$	A	•	*	
Orthoclase	$KAlSi_3O_8$	A-M	*	•	
Paranatrolite	$Na_2Al_2Si_3O_{10} \cdot 3H_2O$	A		*	•
Plagioclases	$NaAlSi_3O_8$-$CaAl_2Si_2O_8$	A-F	*	•	
Quartz	SiO_2	A-F	*	•	
Rankinite	$Ca_3Si_2O_7$	A-Mi		•	
Riebeckite	$Na_2Fe_3Fe_2Si_8O_{22}(OH)_2$	A	*	•	*

(*continued on next page*)

Table 7 (*continued*)

Phase, mineral	Chemical formula	Quantity[a]	Origin[b]		
			Primary	Secondary	Tertiary
Sanidine	$KAlSi_3O_8$ or $(K,Na)(Si,Al)_4O_8$	A-M	*	•	
Sepiolite	$Mg_4Si_6O_{15}(OH)_2 \cdot 6H_2O$	A	*	*	•
Serandite	$Na(Mn,Ca)_2Si_3O_8(OH)$	A		•	*
Serendibite	$CaMg_3O(Si_3O_9)$ or $Ca_2(Mg,Al)_6(Si,Al,B)_6O_{20}$	A-F		•	
Silica minerals	SiO_2	Mi-F	*	•	*
Sillimanite	Al_2SiO_5	A		•	
Suolunite	$Ca_2Si_2O_5(OH)_2 \cdot (H_2O)$	A		•	*
Talc	$Mg_3Si_4O_{10}(OH)_2$	A	*	•	*
Tridymite	SiO_2	A-M	*	•	
Vermiculite	$(Mg,Fe,Al)_3(Si,Al)_4O_{10}(OH)_2 \cdot 4H_2O$	A	*	•	*
Willemite	Zn_2SiO_4	A		•	
Wollastonite	α-$CaSiO_3$ or α-$Ca_3Si_3O_9$	A-M	*	•	
Zeolites	$(Ca,Sr,Ba,Na_2,K_2)Al_2Si_{2-10}O_{8-24} \cdot 2{-}8H_2O$	A-Mi	*	*	•
Zn-bearing silicates		A		•	
1.2. Oxides and hydroxides					
Al hydroxide[c]	$Al(OH)_3$	A	*	•	*
Al oxides[c]		A	*	•	
Alumina	γ-Al_2O_3	A-Mi		•	
Brucite[c]	$Mg(OH)_2$	A	*	*	•
Ca–Al oxides	$Ca_3Al_2O_3$, $Ca_3Al_2O_6$	A-Mi		•	
Ca–Fe oxide	$Ca_XFe_YO_Z$	A-Mi		•	
Ca–Mn oxides	Ca_2MnO_4, $Ca_4Mn_3O_{10}$	A-Mi		•	
Cd-bearing oxides		A		•	
Corundum	Al_2O_3	A-Mi	*	•	
Cr-bearing oxides		A		•	
Cr–Fe oxide	$(Cr,Fe)_2O_3$	A		•	
Cu–Al oxides[c]		A	*	•	
Cu–Fe oxide[c]		A	*	•	
Cuprite	Cu_2O	A		•	
Fe oxide		A-M	*	•	*
Gahnite	$ZnAl_2O_4$	A		•	
Gibbsite	α-$Al(OH)_3$	A-Mi	*	•	*
Goethite	α-$FeOOH$	A-Mi	*	•	*
Hematite	α-Fe_2O_3	A-M	*	•	*
Hydrocalumite	$Ca_2Al(OH)_6[Cl_{1-x}(OH)_x] \cdot 3(H_2O)$ or $Ca_4Al_2Cl_2O_6 \cdot 10H_2O$	A		*	•
K–Al oxides	$K_2Al_2O_4$ or $K_2Al_{19}O_{29.5}$	A-Mi		•	
K–Fe oxide	K_3FeO_2	A-Mi		•	
K hydroxide	KOH	A-Mi		•	*
K oxide	K_2O	A		•	
Lime	CaO	A-F		•	
Macedonite	$PbTiO_3$	A		•	
Maghemite	γ-Fe_2O_3	A-Mi	*	•	*
Magnetite	$FeFe_2O_4$	A-Mi	*	•	
Mg–Cr–Fe oxide	$Mg(Cr,Fe)_2O_4$	A-Mi		•	
Mg–Fe–Al oxide	$MgFeAlO_4$	A		•	
Mg–Mn oxide	Mg_6MnO_8	A		•	
Monteponite	CdO	A		•	
Na hydroxide	$NaOH$	A-Mi		•	*
Na oxide	Na_2O	A		•	
Ni oxide[c]		A	*	•	
Pd oxide	PdO	A		•	
Periclase	MgO	A-M		•	
Plattnerite	PbO_2	A		•	
Portlandite	$Ca(OH)_2$	A-F	*	*	•
Rutile	TiO_2	A	*	•	
Sn oxide[c]		A	*	•	
Spertiniite	$Cu(OH)_2$	A		•	*
Spinels[c]	$MgAl_2O_4$–$Mg(AlFe)_2O_4$	A	*	•	
Srebrodolskite	$Ca_2Fe_2O_5$	A-Mi		•	
Tenorite	CuO	A		•	
Wulfingite	$Zn(OH)_2$	A		•	*
Wustite	FeO	A		•	
Zincite	ZnO	A		•	
Zn–Al oxide		A		•	
Zn ferrite	$(Zn,Fe)Fe_2O_4$	A		•	
Zn oxide[c]		A	*	•	
Zn–Mn oxide[c]		A	*	•	
Zn–Ti oxide	$Zn_XTi_YO_4$	A		•	
1.3. Phosphates					
Al phosphates		A-Mi		•	
Apatite	$Ca(PO_4)_3(Cl,F,OH,CO_3)$ or $Ca_5(PO_4)_3(Cl,F,OH,CO_3)$	A-M	*	•	*
Apatite (Ca deficient)	$Ca_{10-x}(HPO_4)_x(PO_4)_{6-x}(OH)_{2-x}$	A	*	•	*
Berlinite	$AlPO_4$	A		•	
Ca–Fe phosphate (similar to whitlockite)	$Ca_9FeH(PO_4)_7$	A		•	
Ca–K phosphate	$CaKPO_4$	A-Mi		•	

Table 7 (*continued*)

Phase, mineral	Chemical formula	Quantity[a]	Origin[b]		
			Primary	Secondary	Tertiary
Ca–K phosphate	$CaK_2P_2O_7$	A		•	
Ca–Mg–K phosphate	$Ca_9MgK(PO_4)_7$	A-Mi		•	
Ca phosphates	$Ca_3(PO_4)_2$, $Ca_3P_2O_8$, others	A-M		•	
Chloroapatite	$Ca(PO_4)_3(Cl)$ or $Ca_5(PO_4)_3(Cl)$	A-Mi	*	•	
Durapatite	$Ca_5HO_{13}P_3$	A		•	
Fe phosphates	$FePO_4$, $Fe_7(PO_4)_6$	A-Mi	*	•	
Hydroxylapatite	$Ca(PO_4)_3(OH)$, $Ca_5(PO_4)_3(OH)$ or $Ca_{10}(PO_4)_6(OH)_2$	A-M	*	•	*
K–Ca phosphate	$KCa(PO_4)$	A-Mi		•	
K hydrogen phosphate[c]	K_2HPO_4	A	*	•	
K dihydrogen phosphate	KH_2PO_4	A	*	•	
K phosphates	KPO_3, K_3PO_4, $K_5P_3O_{10}$, others	A-Mi		•	
K pyrophosphate hydrate	$K_4P_2O_7 \cdot 3H_2O$	A		*	•
Mg–Ca phosphate[c]	$MgCaPO_4$	A-Mi	*	•	
Mg phosphates		A-Mi		•	
Mg pyrophosphate	$Mg_2P_2O_7$	A		•	
Mn phosphate[c]		A	*	•	
Na–K phosphate		A-Mi		•	
Na phosphates	$Na_6P_2O_8$, others	A-Mi		•	
Whitlockite	$Ca_9Fe(PO_4)_7$ or $Ca_3(PO_4)_2$	A-Mi		•	
Zn phosphate		A		•	
1.4. Sulphates, sulphides, sulphosalts, sulphites and thiosulphates					
Amorphous K, Na, Ca and Mg sulphates		A-M	*	•	*
Anhydrite	$CaSO_4$	A-M	*	•	
Aphthitalite	$(K,Na)_3Na(SO_4)_2$	A		•	
Arcanite	K_2SO_4	A-M	*	•	
Barite[c]	$BaSO_4$	A	*	•	
Bassanite	$CaSO_4 \cdot 0.5H_2O$	A-Mi		•	*
Ca–K sulphates		A-M		•	
Ca langbeinite	$K_2Ca_2(SO_4)_3$ or $K_2CaMg(SO_4)_3$	A-Mi		•	
Ca–Mg sulphate	$CaMg_3(SO_4)_4$	A-Mi		•	
Ca sulphate		A-M		•	
Cd sulphate		A		•	
Celestine[c]	$SrSO_4$	A	*	•	
Chalcanthite	$CuSO_4 \cdot 5H_2O$	A		*	•
Ettringite	$Ca_6Al_2(SO_4)_3(OH)_{12} \cdot 26H_2O$	A-Mi		*	•
Fe sulphate[c]	$Fe_2(SO_4)_3$	A	*	•	
Fe–Zn sulphide[c]		A	*	•	
Glaserite	$K_3Na(SO_4)_2$	A-M		•	
Gypsum	$CaSO_4 \cdot 2H_2O$	A-M		*	•
Jarosite[c]	$KFe_3(SO_4)_2(OH)_6$	A	*	•	*
K sulphide	K_2S	A		•	
Langbeinite	$K_2Mg_2(SO_4)_3$	A-Mi		•	
Mg sulphate (dehydrated kieserite)	$MgSO_4$	A-Mi		•	
Mg thiosulphate	MgS_2O_3	A		•	
Millosevichite	$Al_2(SO_4)_3$	A	*	•	
Na thiosulphate	$Na_2S_2O_3$	A		•	
Oldhamite	CaS	A		•	
Picromerite	$K_2Mg(SO_4)_2 \cdot 6H_2O$	A		*	•
Pyrite[c]	FeS_2	A	*	•	
Sulphides	Compounds with sulphide anion (S^{2-})	A	*	•	
Sulphites	Compounds with sulphite anion (SO_3^{2-})	A	*	•	
Syngenite	$K_2Ca(SO_4)_2 \cdot H_2O$	A-Mi		*	•
Syngenite (dehydrated)	$K_2Ca(SO_4)_3$	A-Mi		•	
Thenardite	Na_2SO_4	A-Mi	*	•	
Zn sulphide[c]		A	*	•	
Xanthoconite	Ag_3AsS_3	A		•	
1.5. Carbonates and bicarbonates					
Ankerite	$Ca(Mg,Fe)(CO_3)_2$	A-M	*	•	*
Arterite	$Mg_2CO_3(OH)_2 \cdot 3H_2O$	A-Mi		*	•
Baylissite	$K_2Mg(CO_3)_2 \cdot 4H_2O$	A-Mi		*	•
Butschliite (dimorphous with fairchildite)	$K_2Ca(CO_3)_2$	A-Mi		•	*
Ca-K carbonate	$Ca_2K_2(CO_3)_3$	A-Mi		•	*
Calcite	$CaCO_3$	Mi-F	*	•	*
Cr-bearing carbonates		A		•	*
Dolomite	$CaMg(CO_3)_2$	A-Mi	*	•	*
Eitelite	$Na_2Mg(CO_3)_2$	A		•	*
Fairchildite	$K_2Ca(CO_3)_2$	A-M		•	*
Hydrocalcite	$CaCO_3 \cdot H_2O$	A-Mi		*	•
Hydrotalcite	$Mg_6Al_2CO_3(OH)_{16} \cdot 4H_2O$	A-Mi		*	•
Hydrozincite	$Zn_5(CO_3)_2(OH)_6$	A		•	*
Kalicinite	$KHCO_3$	A-Mi		•	*
K carbonate (potash)	K_2CO_3	A-M		•	*
K–Na–Ca–Mg carbonates[c]		A	*	•	*
Magnesite	$MgCO_3$	A-Mi	*	•	*

(*continued on next page*)

Table 7 (*continued*)

Phase, mineral	Chemical formula	Quantity[a]	Origin[b]		
			Primary	Secondary	Tertiary
Magnesite (Fe-rich)[c]	$(Mg,Fe)CO_3$	A	*	•	*
Natrite	Na_2CO_3	A-Mi		•	*
Natrofairchildite	$Na_2Ca(CO_3)_2$	A-Mi		•	*
Nesquehonite	$MgCO_3 \cdot 3H_2O$	A		*	•
Nyerereite	$(Na_{0.82}K_{0.18})_2Ca(CO_3)_2$	A		•	*
Paraalumohydrokalcit	$CaAl_2(CO_3)_2(OH)_4 \cdot 6H_2O$	A		*	•
Pirssonite	$Na_2Ca(CO_3)_2 \cdot 2H_2O$	A		*	•
Siderite	$FeCO_3$	A-M		•	*
1.6. Chlorides, chlorites and chlorates					
Bi chloride[c]		A	*	•	
Ca chloride	$CaCl_2$	A		•	
Ca chlorite hydrate	$Ca(ClO)_2 \cdot 3H_2O$	A		*	•
Ca hydroxylchloride (chloride hydroxide)	CaOHCl or CaClOH	A-Mi		•	*
Ca–K chlorides	Chlorocalcite type ($KCaCl_3$)	A-Mi		•	
Cd chloride	$CdCl_2$	A		•	
Chlorocalcite	$KCaCl_3$	A-Mi	*	•	
Cotunnite	$PbCl_2$	A		•	
Cu hydroxylchloride (chloride hydroxide)	CuClOH	A		•	*
Fe chloride		A		•	
Halite	NaCl	A-F	*	•	*
K halite	$K_{0.2}Na_{0.8}Cl$ or $K_{0.4}Na_{0.6}Cl$	A-M		•	
K perchlorate[c]	$KClO_4$	A		•	
Nantokite	CuCl	A		•	
Sylvite	KCl	A-F	*	•	*
Tolbachite	$CuCl_2$	A		•	
Zn chloride	$ZnCl_2$	A		•	
Zn chloride hydrate	$ZnCl_2 \cdot 1.3H_2O$	A		*	•
1.7. Nitrates					
Ca nitrate hydrate[c]	$Ca(NO_3)_2 \cdot 2H_2O$	A		*	•
Nitrates[c]		A	*	•	*
Nitre (niter)[c]	KNO_3	A	*	•	
Nitrocalcite[c]	$Ca(NO_3)_2 \cdot 4H_2O$	A		*	•
1.8. Glass	Various elements	A-F	*	•	*
1.9. Other inorganic phases					
Inorganic amorphous (non-glass) material		A-F	*	•	*
Au-Ni phase[c]		A	•		
Bi-bearing phase[c]		A	•		
Elemental Al	Al	A	•		
Elemental Cu	Cu	A	*	•	
Elemental Pb	Pb	A	*	•	
K–Mo selenide	$K_2Mo_3Se_{18}$	A		•	
Margaritasite	$(Cs,K,H_3O)_2(UO_2)_2V_2O_8 \cdot H_2O$	A		*	•
Metallic alloys and pure metals	Various elements	A	•	*	
Native Au, Fe, Mn and Zn[c]		A	•		
Ni–Fe–As phases[c]		A	•		
2. Organic matter					
2.1. Organic phases					
Char (unburned organic matter, semi-coke, coke, soot, tar, others)		A-F		•	
Chlorobenzene	C_6H_5Cl	A		•	
Chlorophenol	C_6H_5ClO	A		•	
Cyanides	Salts of CN^-	A		•	
Na cyanate	NaOCN	A		•	
Polychlorinated dioxins	Chlorinated hydrocarbons	A		•	
Polychlorinated furans	Halogenated organic compounds	A		•	
Polycyclic aromatic hydrocarbons	Polyaromatic or polynuclear hydrocarbons	A		•	
2.2. Organic minerals					
Ca–Mn oxalate[c]	$(Ca,Mn)C_2O_4 \cdot 2H_2O$	A	*	*	•
Ca oxalate[c]	$CaC_2O_4 \cdot nH_2O$	A	*	*	•
K–Na–Ca–Mg oxalates[c]		A	*	*	•
K oxalate[c]	$K_2C_2O_4$	A	*	•	
Oxalates[c]	Phases with C_2O_4	A	*	*	•
Weddelite (Ca oxalate dihydrate)[c]	$Ca(CO_2)_{2.}(H_2O)_2$ or $CaC_2O_4 \cdot 2H_2O$	A	*	*	•
Whewellite (Ca oxalate dehydrate)[c]	CaC_2O_4	A		•	
Whewellite (Ca oxalate monohydrate)[c]	$CaC_2O_4 \cdot H_2O$	A	*	*	•
3. Fluid matter		*A-M*	•	*	

[a] F, forming (>10%); M, major (1–10%); Mi, minor (0.1–1%); A, accessory (<0.1%);

[b] Primary constuents in biomass ash are pre-existing or original minerals and phases in biomass that have undergone no phase transformations during combustion; secondary constituents in biomass ash are new phases formed during combustion process; and tertiary constituents are new minerals or phases formed during transport and storage of biomass ash. Their origin can be: •, dominant; and *, subordinate.

[c] Identified only in biomass or low-temperature ash produced in oxygen plasma (100–250 °C).

Table 8
Possible physico-chemical formations, transformations and reactions during biomass combustion and transport and storage of biomass ash.

Phase, mineral	Formation, transformation or reaction and reference used
Akermanite ($Ca_2MgSi_2O_7$)	Formation: crystallisation at 700–1300 °C [376,377], 1161–1299 °C [202], 1500–1600 °C [329] Formation: solid-state reaction at 700–1300 °C [376,377] Formation: melt crystallisation at 1161–1299 °C [202], 1500–1600 °C [329] Transformation: dissolution in melt at 1100–1600 °C [376,377]
Al (organically bound)	Transformation: oxidation to Al_2O_3 at 500–700 °C [376,377]
Albite ($NaAlSi_3O_8$)	Formation: crystallisation at $\geqslant$575 °C [336], $\geqslant$900 °C [331], 930–980 °C [333] Formation reaction: $Al_2O_3{\cdot}2SiO_2(s) + 2NaCl(g) + H_2O(g) \rightarrow Na_2O{\cdot}Al_2O_3{\cdot}2SiO_2(s) + 2HCl(g)$ [132,159,176] Formation reaction: $5SiO_2 + Al_2O_3{\cdot}SiO_2 + 2NaCl + H_2O \rightarrow 2NaAlSi_3O_8 + 2HCl$ ($\geqslant$575 °C) [336] Formation reaction: $5SiO_2 + Al_2O_3{\cdot}SiO_2 + NaSO_4 \rightarrow 2NaAlSi_3O_8 + SO_3$ ($\geqslant$575 °C) [336]
Al–Si spinel ($2Al_2O_3{\cdot}3SiO_2$)	Formation reaction: $2(Al_2O_3{\cdot}2SiO_2) \rightarrow 2Al_2O_3{\cdot}3SiO_2 + SiO_2$ (970 °C) [75]
Alumina (Al_2O_3)	Formation: crystallisation of amorphous alumina at 700–1300 °C [376,377]
Alunite ($KAl_3(SO_4)_2(OH)_6$)	Transformation: dehydroxylation (530–550 °C) → separation of Al_2O_3 (730–740 °C) → loss of SO_3 (820–830 °C) (references in [376,377])
Amphibole ($NaCa_2(Mg,Fe,Al)_5(Si,Al)_8O_{22}(OH)_2$)	Transformation: amphibole → loss of combined water (440–470 °C) → oxidation of Fe^{2+} (400–800 °C) → dehydroxylation, decomposition and formation of meta-phases (750–850 °C) → recrystallization to pyroxene, hematite, cristobalite (1000–1150 °C) (references in [376,377])
Anhydrite ($CaSO_4$)	Formation: crystallisation at 100–1000 °C [376,377,389], 500–815 °C [343], $\geqslant$575 °C [336], 630–1000 °C [333] Formation: gypsum dehydration at 100–300 °C [376,377,389] Formation: bassanite dehydration at 200–400 °C [376,377] Formation: sulphation of CaO released from organic matter at 200–1000 °C [376,377,389] Formation: sulphation of CaO released from calcite, ankerite and dolomite at 500–1000 °C [389] Formation reaction: $CaO + H_2SO_4$ (or $H_2O + SO_2 + 0.5O_2$) $\rightarrow CaSO_4 + H_2O$ [387] Formation reaction: $CaO(s) + SO_3(g) \rightarrow CaSO_4(s,l)$ [346] Formation reaction: $CaO + SO_2 + 0.5O_2 \rightarrow CaSO_4$ [79,336,387] Formation reaction: $2CaO(s) + 2SO_2(g) + O_2 \rightarrow 2CaSO_4(s)$ [355] Transformation: desulphation at 800–1300 °C [376,377,389]
Ankerite ($Ca(Mg,Fe)(CO_3)_2$)	Formation: carbonation of Ca, Mg and Fe oxyhydroxides at 200–400 °C [376,377] Transformation: decarbonation at 500–800 °C [376,377,389] Transformation: decarbonation to lime, periclase and wustite as two stages process: (1) at 610–770 °C (mostly 727 °C); and (2) at 900 °C (references in [376,377])
Anorthite ($CaAl_2Si_2O_8$)	Formation: solid-state reaction at 800–1100 °C and melt crystallisation at > 1100 °C [376,377] Transformation: dissolution in melt at 1100–1600 °C [376,377]
Apatite ($Ca(PO_4)_3(Cl,F,OH,CO_3)$)	Transformation: decomposition at 1400 °C (references in [376,377])
Aragonite ($CaCO_3$)	Transformation: polymorphic to calcite at 390–420 °C (references in [376,377])
Arcanite (K_2SO_4)	Formation: crystallisation at 200–900 °C [389], 400–1000 °C [20], $\geqslant$400 °C [310], 500–815 °C [343], 600 °C [261], 650–900 °C [66] Formation: sulphation of K_2O released from organic matter at 200–800 °C [389] and jarosite at 300–900 °C [389] Formation reaction: $6KCl(s,l) + Fe_2O_3(s)$ 8 $3SO_2(g) + 1.5O_2(g) \rightarrow 3K_2SO_4(s) + 2FeCl_3(s,l,g)$ [65] Formation reaction: $2KCl(s) + SO_2(g) + O_2(g) \rightarrow K_2SO_4(s) + Cl_2(g)$ [65,260] Formation reaction: $2KCl(s,g,l) + SO_2(g) + 0.5O_2(g) + H_2O(g) \rightarrow K_2SO_4(s,g,l) + 2HCl(g)$ [56,65,132,176,199,235,260,281,387] Formation reaction: $4KCl(s,g) + 2SO_2(g) + O_2(g) + 2H_2O(g) \rightarrow 2K_2SO_4(s,g) + 4HCl(g)$ [208,311] Formation reaction: $2KOH(g) + SO_3(g) \rightarrow K_2SO_4(l,g) + H_2O(g)$ [346] Formation reaction: $2KOH(g) + SO_2(g) + 0.5O_2(g) \rightarrow K_2SO_4(g,l,s) + H_2O(g)$ [235,387] Formation reaction: $KSO_3Cl + H_2O \rightarrow KHSO_4 + HCl$; and $KHSO_4 + KCl \rightarrow K_2SO_4 + HCl$ [208] Transformation: α-arcanite → β-arcanite (578 °C) → K_2SO_4 evaporation (1200 °C) [165,210] Transformation: desulphation at 800–1100 °C [389] Transformation: desulphation and kaliophilite formation at 900 °C [42]
Ba (organically bound)	Transformation: oxidation to BaO at 200–700 °C [389]
Barite ($BaSO_4$)	Formation: sulphation of Ba oxide released from organic matter at 200–900 °C [376,377,389] Transformation: desulphation at 900–1300 °C [376,377,389], 1582 °C (references in [376,377])
Bassanite ($CaSO_4{\cdot}0.5H_2O$)	Formation: gypsum semi-dehydration at 100–300 °C [376,377,389] Transformation: dehydration at 200–400 °C [376,377]
Biomass ($C_{42}H_{60}O_{28}$)	Transformation: combustion reaction such as $C_{42}H_{60}O_{28} + 43O_2 \rightarrow 42CO_2 + 30H_2O$ + ash [350,353] Transformation: combustion reaction such as biomass + O_2 → charcoal + MO + MCO_3 + CO_2 + H_2O (M is mostly Ca, Mg, K, Na) [12] Transformation: release of elements (Al, Ba, C, Ca, Cl, Fe, H, K, Mg, N, Na, O, P, S, Si, Ti, trace elements) associated with organic matter during combustion mostly at 200–700 °C [376,377,389] Transformation: gasification such as biomass + some air → fuel gas ($CO + H_2 + CH_4 + CO_2 + N_2 + H_2O$) + char, tar and ash [391] Transformation: pyrolysis in inert atmosphere such as $C_3(H_2O)_2$ → CHO intermediates (C, $HOCH_2$, H_2O, char, tars, oils, water) → char with inorganic matter + exothermal (CO_2, CH_4) and endothermal (CO, H_2) gas production [85]
Biotite ($K(MgFe)_3AlSi_3O_{10}(OH,F)_2$)	Transformation: crystallisation of magnetic spinel, maghemite, leucite and mullite at >1100 °C (references in [376,377])

(*continued on next page*)

Table 8 (*continued*)

Phase, mineral	Formation, transformation or reaction and reference used
Boehmite (γ-AlOOH)	Transformation: dehydroxylation to α-Al_2O_3 at 450–580 °C (references in [376,377])
Brucite ($Mg(OH)_2$)	Formation: hydroxylation of Mg oxide at $\leqslant$400 °C [376,377] Transformation: dehydroxylation to periclase at 320 °C [219], 350–450 °C (references in [376,377]); 400–500 °C [376,377]
Ca aluminosilicates	Formation: $CaO + Al_2O_3 + SiO_2 \rightarrow$ Ca aluminosilicates (>950 °C) [79] Transformation: dissolution in melt at 1100–1600 °C [376,377]
Ca arsenate ($Ca_3(AsO_4)_2$)	Formation reaction: $3CaO + As_2O_3 + O_2 \rightarrow Ca_3(AsO_4)_2$ (>500 °C) [79]
Ca bicarbonate ($Ca(HCO_3)_2$)	Formation reaction: $CaCO_3 + H_2O + CO_2 \rightarrow Ca(HCO_3)_2$ (as Ca bicarbonate solution at ambiente temperature) [12]
Ca chloride ($CaCl_2$)	Formation reaction: $CaO(s) + 2HCl(g) \rightarrow CaCl_2(s,l,g) + H_2O(g)$ (550–700 °C) [132,159,235,311,346,387] Formation reaction: $CaCO_3 + 2HCl \rightarrow CaCl_2 + H_2O + CO_2$ [387] Formation reaction: $Ca(OH)_2 + 2HCl \rightarrow CaCl_2 + 2H_2O$ [387]
Calcite ($CaCO_3$) (see also Ca oxalates)	Formation: crystallisation at 300–600 °C [79], 400–650 °C [20], $\geqslant$400 °C [310], 420 °C [116,185], $\leqslant$500 °C [376,377], 500 °C [146,253] Formation: carbonation of Ca oxyhydroxides at $\leqslant$500 °C [376,377] Formation reaction: $2CaC_2O_4 + O_2 \rightarrow 2CaCO_3 + 2CO_2$ (420 °C) [116,185] Formation reaction: $CaC_2O_4 \rightarrow CaCO_3 + CO$ (500 °C) [146,253] Formation reaction: $CaO(s) + CO_2(g) \rightarrow CaCO_3(s)$ [346,355] Formation reaction: $Ca(OH)_2 + CO_2 \rightarrow CaCO_3 + H_2O$ [12,36,48,49] Transformation: decarbonation to lime at 400–850 °C [133], 500–900 °C [376,377,389], 600–780 °C [156], 615–775 °C [20], 645 °C [332], 650–900 °C [14], 700–950 °C and mostly 877–927 °C (references in [376,377]), 750 °C [390]
Ca–K carbonates	Transformation: decarbonation at 600–900 °C [14]
Ca–Mg silicates ($Ca_2MgSi_2O_7$, $CaMg(SiO_3)_2$)	Formation: crystallisation at 1000–1150 °C [20], 1100–1300 °C [376,377] Formation: melt crystallisation at 1100–1300 °C [376,377] Formation: reaction of dolomite ($CaMg(CO_3)_2$) with $SiO_2 \rightarrow CaMg(SiO_3)_2$, $Ca_2MgSi_2O_7$ and $MgSiO_3$ [42] Transformation: dissolution in melt at 1100–1600 °C [376,377]
Ca–Na aluminosilicate ($Ca_{0.9}Na_{0.1}Al_{1.8}Si_{2.2}O_8$)	Formation: crystallisation at 530 °C [261]
Ca (organically bound)	Transformation: oxidation to lime at 200–700 °C [389], 300–600 °C [376,377]
Ca oxalates (weddelite, $CaC_2O_4{\cdot}2H_2O$ and whewellite, $CaC_2O_4{\cdot}H_2O$)	Transformation of whewellite: $CaC_2O_4{\cdot}H_2O \rightarrow CaC_2O_4 + H_2O$ (170–200 °C) $\rightarrow CaCO_3 + CO$ (300–600 °C) $\rightarrow CaO + CO_2$ (700–1000 °C) [79] Transformation of dehydrated weddelite and whewellite: $2CaC_2O_4 + O_2 \rightarrow 2CaCO_3 + 2CO_2$ at 420 °C [116,185], 500 °C [253], 500–700 °C [146,185]
Ca phosphates ($Ca_3(PO_4)_2$, $Ca_3P_2O_8$)	Formation: crystallisation of $Ca_3(PO_4)_2$ at 1200–1600 °C [329] Formation reaction: $3CaO(s) + P_2O_5(g) \rightarrow Ca_3P_2O_8(s)$ [346]
Carbohydrates	Transformation: decomposition at 180–270 °C [254]
Carbonates	Formation: crystallisation at 400–650 °C [20] Transformation: decarbonation at 500–800 °C [254], 500–900 °C [376,377,389], 600–800 °C [185,210], 700–800 °C [201], 700–1050 °C [79] Transformation: decarbonation of Ca–Mg–K–Na carbonates to $CaO + MgO + K_2O + Na_2O + CO_2$ at 700–1050 °C [79]
Ca selenate	Formation reaction: $CaO + SeO_2 + 0.5O_2 \rightarrow CaSeO_4$ [79]
Ca silicate hydrate ($CaO{\cdot}SiO_2{\cdot}H_2O$)	Formation (puzzolanic) reaction: $SiO_2 + Ca(OH)_2 + H_2O \rightarrow$ Ca silicate hydrate (ambient temperature) [36] Transformation: dehydration at 135–185 °C [283]
Ca silicates	Formation: crystallisation at 400–1300 °C [376,377], 900 °C [20] Formation: interaction between quartz and calcite at 400–800 °C [376,377] Formation: interaction between quartz and anhydrite at 400–1300 °C [376,377] Formation: melt crystallisation at 1100–1300 °C [376,377] Transformation: dissolution in melt at 1100–1600 °C [376,377]
Celestine ($SrSO_4$)	Transformation: desulphation to Sr oxide at 1005 °C (references in [376,377])
Cellulose ($(C_6H_{10}O_5)_n$, $CH_{1.67}O_{0.83}$, $(C_5H_{10}O_5)_x$, $C_6H_{10}O_5$ or $C_6(H_2O)_5$)	Transformation: decomposition/oxidation at 240–360 °C [189], 250–360 °C [16], 250–400 °C [347], 270–370 °C [254], 280–400 °C [350], 305–375 °C [285,296], 315–400 °C [233], 350–500 °C [308] Transformation: peak decomposition/oxidation at 325 °C [209], 330 °C [319], 340–370 °C [24], 351–375 [146], 354 [308], 357 °C [347]
Cellulose–hemicellulose	Transformation: decomposition/oxidation at 177–377 °C [144], 180–270 °C [254], 200–370 °C [332], 250–350 °C [24]
Chalcedony (SiO_2)	Formation and transformation: crystallisation and recrystallization at $\leqslant$300 °C) [376,377]
Chalcocite (Cu_2S)	Transformation to $CuSO_4$ and CuO at 520 °C (references in [376,377])
Chalcopyrite ($CuFeS_2$)	Transformation to Cu_5FeS_4, $CuSO_4$, CuO, Cu_2O and hematite at 530–600 °C (references in [376,377])
Char	Char decomposition/oxidation at 370–490 °C [332], 380–600 °C [338], 450–720 °C [16], 500–900 °C [367], 550–900 °C [350], 600–700 °C [75], 820–950 °C [72]
Chlorite ($(MgFe)_5Al_2Si_3O_{10}(OH)_8$)	Transformation: chlorite $\rightarrow$ decomposition of brucite layer (550–750 °C) $\rightarrow$ dehydration of talc layer (750–820 °C) $\rightarrow$ additional dehydration (820–860 °C) $\rightarrow$ crystallisation of olivine (>860–900 °C) (references in [376,377])

Table 8 (*continued*)

Phase, mineral	Formation, transformation or reaction and reference used
	Transformation: dehydroxylation at 600–900 °C [376,377] Transformation: crystal lattice destruction at 800–1100 °C [376,377]
Clay minerals (see specific clay minerals)	Transformation: crystallisation of amorphous and cryptomere clay minerals at 200–300 °C [376,377] Transformation: loss of crystallisation water and consequent structural collapse and amorphization at 400–700 °C [116] Transformation: dissolution in melt at 1100–1600 °C [376,377]
Corundum (Al_2O_3)	Transformation: dissolution in melt at 1100–1600 °C [376,377]
Covelline (CuS)	Transformation: covelline → chalcocite (370 °C) → $CuSO_4$ and CuO (520 °C) (references in [376,377])
Cristobalite (SiO_2) (see silica minerals)	Formation: crystallisation at 718–767 °C [201] and melt crystallisation at 1100–1400 °C [376,377] Transformation: dissolution in melt at 1100–1600 °C [376,377]
Diaspore (α-AlOOH)	Transformation to α-Al_2O_3 at 540–585 °C (references in [376,377])
Diopside ($CaMgSi_2O_6$)	Formation: crystallisation at 1000–1150 °C [20], 1100–1300 °C [376,377], 1163–1263 °C [202] Formation: melt crystallisation at 1100–1300 °C [376,377], 1163–1263 °C [202] Formation: reaction of dolomite with $SiO_2 \rightarrow CaMgSi_2O_6$ [42] Transformation: dissolution in melt at 1100–1600 °C [376,377]
Dolomite ($CaMg(CO_3)_2$)	Formation: carbonation of Ca and Mg oxyhydroxides at 300–500 °C [376,377] Formation: crystallisation at $\geqslant$400 °C [310] Transformation: decarbonation as two stages process: (1) $MgCO_3$ part forms MgO at 650–750 °C; and (2) $CaCO_3$ part is decomposed to CaO at 800–900 °C [42] Transformation: decarbonation as two stages process: (1) formation of calcite and periclase at 740–800 °C (mostly 745 °C); and (2) formation of lime at 815–930 °C (mostly 870 °C) (references in [376,377]) Transformation: decarbonation at 500–900 °C [376,377,389]
Ettringite ($Ca_6Al_2(SO_4)_3(OH)_{12}{\cdot}26H_2O$)	Formation reaction: $Ca_3Al_2O_6 + 3CaSO_4{\cdot}2H_2O + 26H_2O \rightarrow Ca_6Al_2(SO_4)_3(OH)_{12}{\cdot}26H_2O$ [36], or $Ca_3Al_2O_6 + 3CaSO_4 + 32H_2O \rightarrow Ca_6Al_2(SO_4)_3(OH)_{12}{\cdot}26H_2O$ [48,49] Transformation: dehydration at 135–185 °C [283]
Extractives	Transformation: peak decomposition at 180 °C [146]
Fairchildite ($K_2Ca(CO_3)_2$)	Formation: crystallisation at $\geqslant$400 °C [310]
Fe chlorides ($FeCl_2$, $FeCl_3$)	Formation reaction: $FeCl_2 + HCl + 0.25O_2 \rightarrow FeCl_3 + 0.5H_2O$ [65] Formation reaction: $Fe_2O_3 + 6HCl \rightarrow 2FeCl_3 + 3H_2O$ [387] Formation reaction: $Fe_3O_4 + 8HCl \rightarrow FeCl_2 + 2FeCl_3 + 4H_2O$ [387]
Fe chloride and arcanite	Formation reaction: $Fe_2O_3(s) + 6KCl(s,l) + 3SO_2(g) + 1.5O_2(g) \rightarrow 2FeCl_3(s,l,g) + 3K_2SO_4(s)$ [65]
Fe chloride and Na oxide	Formation reaction: $Fe_2O_3(s) + 6NaCl(s,l) \rightarrow 2FeCl_3(g) + 3Na_2O(s,l)$ [65]
Fe (organically bound)	Transformation: oxidation to hematite at 200–700 °C [376,377,389]
Fe phosphate ($FePO_4$)	Formation: crystallisation at 630 °C [333]
Fe sulphates ($FeSO_4$, $Fe_2(SO_4)_3$)	Formation: sulphatation of sulphides (ambient temperature) and sulphatation of Fe oxide originated from pyrite and marcasite (100–500 °C), organic matter (200–700 °C), jarosite (300–900 °C), siderite (400–800 °C) and ankerite (500–800 °C) [389] Formation reaction: $2FeCl_3(s,l,g) + 3SO_2(g) + 3O_2(g) \rightarrow Fe_2(SO_4)_3(s) + 3Cl_2(g)$ [65] Transformation: desulphation of $Fe_2(SO_4)_3$ to hematite at 480–810 °C (references in [376,377]) Transformation: desulphation of $FeSO_4$ to hematite at 500–900 °C [389], 603–810 °C (references in [376,377])
Galena (PbS)	Transformation to $PbSO_4$ and PbO at 840 °C (references in [376,377])
Gehlenite ($Ca_2Al_2SiO_7$)	Formation: crystallisation at $\geqslant$575 °C [336], 700–1300 °C [376,377], $\geqslant$900 °C [331] Formation: solid-state reaction at 700–1300 °C [376,377] Formation reaction: $SiO_2 + Al_2O_3 + 2CaO \rightarrow Ca_2Al_2SiO_7$ ($\geqslant$575 °C) [336] Transformation: dissolution in melt at 1100–1600 °C [376,377]
Gibbsite (α-$Al(OH)_3$)	Transformation: gibbsite → boehmite (325–330 °C) → α-Al_2O_3 (500–550 °C) (references in [376,377])
Glass (or melt)	Formation: initial melt/glass at 400–600 °C [131], 515 °C [311], 572 °C [201], 584–815 [261], 600 °C [188,220], 600–815 °C [261,338], 620–825 °C [97], 950 °C [168] Formation: initial silicate melt/glass at 550–900 °C [42], 816 °C [201], 982 °C [202], 1050 °C [79] Formation: silicate melt/glass at 816–1325 °C [201], 1100–1200 °C [48] Formation: melt cooling and vitrification at 1100–1600 °C [376,377]
Goethite (α-FeOOH)	Formation: hydroxylation of Fe oxide at $\leqslant$200 °C [376,377] Transformation: dehydroxylation to hematite at 190–380 °C (references in [376,377]), 400–600 °C [376,377]
Gypsum ($CaSO_4{\cdot}2H_2O$)	Formation: precipitation of solution at $\leqslant$200 °C [376,377] Formation: hydration of bassanite and anhydrite (ambient temperature) [376,377] Formation reaction: $CaSO_4 + 2H_2O \rightarrow CaSO_4{\cdot}2H_2O$ [48] Transformation: gypsum → bassanite (100–150 °C, mostly 145 °C) → γ-anhydrite (150–200 °C, mostly 174 °C) → β-anhydrite (350–370 °C, mostly 364 °C) → lime (900–1300 °C, mostly 1050–1220 °C) (references in [376,377]) Transformation: dehydration at 100–300 °C [376,377,389] Transformation reaction: $CaSO_4{\cdot}2H_2O \rightarrow CaSO_4 + 2H_2O$ ($\geqslant$575 °C) [336]
Halite (NaCl)	Formation: crystallisation at 600 °C [261] Formation reaction: $Na + HCl(g) + O \rightarrow NaCl + OH$ [174]

(*continued on next page*)

Table 8 (*continued*)

Phase, mineral	Formation, transformation or reaction and reference used
	Formation reaction: $NaOH(g) + HCl(g) \rightarrow NaCl(g,l) + H_2O(g)$ [346]
Hatrurite (Ca_3SiO_5)	Formation: crystallisation at > 525 °C [129]
HBr	Formation reaction: $Br_2 + H_2O \rightarrow 2HBr + 0.5O_2$ [387]
HCl	Formation at 200–400 °C [59] Formation reaction: $Cl_2 + H_2O \rightarrow 2HCl + 0.5O_2$ [387]
HCl and SO_3	Formation reaction: $Cl_2 + SO_2 + H_2O \rightarrow SO_3 + 2HCl$ (Cl capture by S) [211]
Hematite (Fe_2O_3)	Formation: crystallisation at 100–1400 °C [376,377,389], $\geqslant$575 °C) [336], 630–1000 °C [333] Formation: from oxidation of pyrite and marcasite (100–500 °C), organic matter (200–700 °C), jarosite (300–900 °C), siderite (400–800 °C) and ankerite (500–800 °C) [389] Formation: melt crystallisation at 1100–1400 °C [376,377] Formation reaction: $2FeCl_2 + 1.5O_2 \rightarrow Fe_2O_3 + 2Cl_2$ [260] Formation reaction: $2FeCO_3 + 0.5O_2 \rightarrow Fe_2O_3 + 2CO_2$ ($\geqslant$575 °C) [336] Formation reaction: $Fe_3O_4 + FeCl_2 + O_2 \rightarrow 2Fe_2O_3 + Cl_2$ [260] Formation reaction: $4FeS_2 + 11O_2 \rightarrow 2Fe_2O_3 + 8SO_2$ (references in [336,376,377]) Formation reaction: $4FeS_2 + 15O_2 + 8H_2O \rightarrow 2Fe_2O_3 + 8H_2SO_4$ ($\geqslant$575 °C) [336] Transformation: reduction at 900–1400 °C [376,377] Transformation: dissolution in melt at 1100–1600 °C [376,377]
Hemicellulose ($(C_5H_8O_4)_n$, $CH_{1.64}O_{0.78}$ or $C_5(H_2O)_4$)	Transformation: decomposition/oxidation at 150–350 °C [347], 190–320 °C [350], 200–260 °C [189], 200–270 °C [254], 220–315 °C [233], 220–320 °C [16], 225–325 °C [285,296], 250–350 °C [308] Transformation: peak decomposition/oxidation at 230 °C [209], 287 °C [347], 290 °C [319], 299 °C [308], 300 °C [146]
Hexahydrite ($MgSO_4.6(H_2O)$)	Transformation: dehydration at 100–200 °C [376,377]
Illite ($(KH_2O)Al_2(AlSi)Si_3O_{10}(OH)_2$)	Transformation: illite → release of adsorbed and interlayer water (50–200 °C) → dehydroxylation without lattice destruction (370–700 °C) → lattice destruction (850–950 °C) → formation of spinel and amorphous phase (900–1000 °C) → formation of amorphous SiO_2 and leucite (1000–1100 °C) → crystallisation of quartz or cristobalite, cordierite, enstatite, mullite, corundum and spinel (1100–1300 °C) (references in [376,377]) Transformation: illite → dehydration (50–200 °C) → dehydroxylation (600–900 °C) → crystal lattice destruction (700–1100 °C) [376,377]
Inorganic amorphous matter	Formation: amorphization of inorganic matter at 550 °C [116]
Jadeite ($NaAlSi_2O_6$)	Formation: crystallisation at 600 °C [261]
Jarosite ($KFe_3(SO_4)_2(OH)_6$)	Transformation: jarosite → dehydroxylation (470–480 °C) → loss of SO_3 (800 °C) (references in [376,377]) Transformation: dehydroxylation and desulphation at 300–900 °C [376,377,389]
Kalicinite ($KHCO_3$)	Transformation reaction: $2KHCO_3 \rightarrow K_2CO_3 + CO_2 + H_2O$ (100–200 °C) [344]
Kaliophilite ($KAlSiO_4$)	Formation reaction: $Al_2Si_2O_5(OH)_4 + 2KCl \rightarrow 2KAlSiO_4 + H_2O + 2HCl$ (700–800 °C) [42]
Kalsilite–kaliophilite ($KAlSiO_4$)	Formation: crystallisation at 700–900 °C [42], $\geqslant$815 °C [310] Formation reaction: $Al_2O_3{\cdot}2SiO_2(s) + 2KCl(g,l,s) + H_2O(g) \rightarrow 2KAlSiO_4(s) + 2HCl(g)$ [235,310,333] Formation reaction: $Al_2O_3{\cdot}2SiO_2(s) + 2KOH(g) \rightarrow K_2O{\cdot}Al_2O_3{\cdot}2SiO_2(s) + H_2O(g)$ [235] Formation reaction: $Al_2Si_2O_5(OH)_4 + 2KCl \rightarrow 2KAlSiO_4 + H_2O + 2HCl$ (700–900 °C) [42] Formation reaction: $Al_2Si_2O_5(OH)_4 + K_2CO_3 \rightarrow 2KAlSiO_4 + 2H_2O + CO_2$ (700–900 °C) [42] Formation reaction: $Al_2Si_2O_5(OH)_4 + K_2SO_4 \rightarrow 2KAlSiO_4 + 2H_2O + SO_3$ (700–900 °C) [42]
K–Al sulphate ($K_3Al(SO_4)_3$)	Formation: reaction between kaolinite and arcanite → $K_3Al(SO_4)_3$ + muscovite (700 °C) [42] Transformation: desulphation at 690–800 °C [42]
K aluminosilicate	Formation reaction: $Al_2O_3{\cdot}SiO_2(s) + K_2SO_4(g,l,s) \rightarrow K_2O{\cdot}Al_2O_3{\cdot}SiO_2(s) + SO_2(g) + 0.5O_2(g)$ (700–800 °C) [59,235]
Kaolinite ($Al_2Si_2O_5(OH)_4$)	Transformation: kaolinite → release of adsorbed and interlayer water (100–150 °C) → dehydroxylation and lattice destruction (450–650 °C) → formation of mullite, sillimanite, spinel, γ-Al_2O_3, amorphous SiO_2 (920–1030 °C) → crystallisation of amorphous SiO_2 to cristobalite, γ-Al_2O_3 to corundum and sillimanite to mullite (1200–1300 °C) (references in [376,377]) Transformation: kaolinite → dehydration (50–200 °C) → dehydroxylation (600–900 °C) → crystal lattice destruction (300–1100 °C) [376,377]
K-bearing oxides (K_2MO_4, $K_2M_2O_4$, K_2MO_2)	Formation reaction: $M(s) + 2KCl(g) + 2O_2(g) \rightarrow K_2MO_4(s,l) + Cl_2(g)$ (M is mostly Fe, Cr and Ni) [65] Formation reaction: $M_2O_3(s) + 2KCl(s,l) + 0.5O_2(g) \rightarrow K_2M_2O_4(s,l) + Cl_2(g)$ (M is mostly Fe, Cr and Ni) [65] Formation reaction: $0.5M_2O_3(s) + 2KCl(s,l) + 1.25O_2(g) \rightarrow K_2MO_4(s,l) + Cl_2(g)$ (M is mostly Fe, Cr and Ni) [65] Formation reaction: $M_2O_3(s) + 4KCl(g) + 2.5O_2(g) \rightarrow 2K_2MO_4(s,l) + 2Cl_2(g)$ (M is mostly Fe, Cr and Ni) [65] Formation reaction: $MO(s) + K_2O(s,l) \rightarrow K_2O{\cdot}MO(s,l)$ (M is mostly Fe, Cr and Ni) [65]
K carbonate (K_2CO_3)	Formation: crystallisation at 200–400 °C [59], 500–900 °C [367] Formation reaction: $2KOH(g) + CO_2(g) \rightarrow K_2CO_3(l,g) + H_2O(g)$ [346] Transformation: decarbonation at 830–1000 °C [59], 840 °C [97],$\geqslant$900 °C [14]
K–Ca silicate (K_2CaSiO_4)	Formation: crystallisation of K_2CaSiO_4 at >525 °C) [129], 700–1000 °C [20] Formation: reaction of $CaO(s) + K_2SiO_3(l) \rightarrow$ K–Ca silicate (l) [346]
K (elemental)	Formation reaction: $KCl(l) + 0.5H_2 \rightarrow K(g) + HCl$ [387]
K feldspars (see orthoclase and sanidine)	Formation: crystallisation at 400–1000 °C [20], $\geqslant$575 °C [336], 1100–1300 °C [376,377] Formation: melt crystallisation at 1100–1300 °C [376,377]

Table 8 (*continued*)

Phase, mineral	Formation, transformation or reaction and reference used
	Formation reaction: $Al_2O_3 \cdot 2SiO_2(s) + 2KCl(g) + H_2O(g) \rightarrow K_2O.Al_2O_3 \cdot 2SiO_2(s) + 2HCl(g)$ [132,159,176] Formation reaction: $5SiO_2 + Al_2O_3 \cdot SiO_2 + K_2SO_4 \rightarrow 2KAlSi_3O_8 + SO_3$ (⩾575 °C) [336]
K–Fe oxides (K_3FeO_2, $K_2Fe_2O_4$)	Formation: crystallisation of K_3FeO_2 at ⩾400 °C [310] Formation reaction: $K_2CO_3 + Fe_2O_3 \rightarrow K_2Fe_2O_4 + CO_2$ [72,102] Formation reaction: $K_2O + Fe_2O_3 \rightarrow K_2Fe_2O_4$ [102]
K–Fe sulphate ($K_3Fe(SO_4)_3$)	Formation reaction: $12KCl(s,l) + 2Fe_2O_3(s) + 12SO_2(g) + 9O_2(g) \rightarrow 4K_3Fe(SO_4)_3(s,l) + 6Cl_2(g)$ [65] Formation reaction: $3K_2SO_4(s) + Fe_2O_3(s) + 3SO_2(g) \rightarrow 2K_3Fe(SO_4)_3(s,l)$ [65]
K hydroxide (KOH)	Formation at 830–1000 °C [59] Formation reaction: $K(g) + OH(g) \rightarrow KOH(g)$ [174] Formation reaction: $KCl(g) + H_2O \rightarrow KOH(g) + HCl(g)$ [174,387]
K (organically bound)	Transformation: oxidation to K_2O at 200–700 °C [389]
K oxide (K_2O)	Formation reaction: $2\ K(g) + 0.5O_2 \rightarrow K_2O(l)$ [68]
K perchlorate ($KClO_4$)	Formation: crystallisation at <250 °C [22] Transformation: decomposition at 200–700 °C [22]
K phosphate (KPO_3, K_5P3O_{10})	Formation: crystallisation of $K_5P_3O_{10}$ at 1200–1600 °C [329] Formation reaction: $2KOH(g) + P_2O_5(g) \rightarrow 2KPO_3(l,g) + H_2O(g)$ [346]
K silicates (K_2SiO_3, $K_6Si_2O_7$, $K_2O.nSiO_2$)	Formation: crystallisation of K silicates at 530 °C [261], 700–830 °C [59], 850–1150 °C [133] Formation: crystallisation of $K_6Si_2O_7$ at 530 °C [261] Formation reaction: $SiO_2(s) + KCl(g) + H_2O(g) \rightarrow K_2SiO_3(l,s) + 2HCl(g)$ [355] Formation reaction: $SiO_2 + 2KCl(l) + H_2O \rightarrow K_2SiO_3 + 2HCl$ [387] Formation reaction: $3SiO_2(s) + 2KCl(g,l,s) + H_2O(g) \rightarrow K_2O.3SiO_2(s) + 2HCl(g)$ [235] Formation reaction: $4SiO_2 + K_2CO_3 \rightarrow K_2O.4SiO_2 + CO_2$ [72,102] Formation reaction: $nSiO_2 + K_2CO_3 \rightarrow K_2O \cdot nSiO_2 + CO_2$ (850–1150 °C) ($n = 1, 2, 4$) [133] Formation reaction: $SiO_2(s) + 2KOH(g) \rightarrow K_2SiO_3(l,s) + H_2O(g)$ [235,346,355] Formation reaction: $SiO_2(s) + K_2SO_4(g,l,s) \rightarrow K_2O \cdot SiO_2(s) + SO_2(g) + 0.5O_2(g)$ [235]
Larnite (Ca_2SiO_4)	Formation: crystallisation at 500–1200 °C [376,377], ⩾525 °C [129], ⩾600 °C) [310], 718–1425 °C [201], 1249–1541 °C [202] Formation: reaction between calcite and wollastonite at 500–900 °C [376,377] Formation: solid-state reactions at 500–1200 °C [376,377] Formation: melt crystallisation (1249–1541 °C) [202] Transformation: dissolution in melt at 1100–1600 °C [376,377]
Lepidocrocite (γ-FeOOH)	Transformation: lepidocrocite → maghemite (304 °C) → hematite (508 °C) (references in [376,377])
Leucite ($KAlSi_2O_6$)	Formation: melt crystallisation at 1134–1217 °C [202] Formation: a reaction product between the alkali rich melt and mullite (ceramic lining) [369] Formation reaction: $2SiO_2 + Al_2Si_2O_5(OH)_4 + K_2SO_4 \rightarrow 2KAlSi_2O_6 + 2H_2O + SO_3$ [42] Formation reaction: $2SiO_2 + Al_2Si_2O_5(OH)_4 + 2KCl \rightarrow 2KAlSi_2O_6 + H_2O + 2HCl$ [42,333]
Lignin ($[C_9H_{10}O_3(OCH_3)_{0.9\text{-}1.7}]_n$, $C_9H_{10}O_2$, $C_{10}H_{11}O_{3.5}$, $C_{10}H_{12}O_3$, $C_{11}H_{14}O_4$, $C_{40}H_{44}O_6$ or $C_{40}H_{44}O_{14}$)	Transformation: decomposition/oxidation at 160–900 °C [233], 180–500 °C [16], 200–600 °C [146], 250–500 °C [285,296], 277–>600 °C [319], 280–500 °C [189], 320–450 °C [350], 350–500 °C [24], 350–700 °C [347], 370–490 °C [332], >500 °C [308] Transformation: peak decomposition/oxidation: (350–450 °C) [189], (482 °C) [308], (510–520 °C) [24], (527 °C) [144]
Lime (CaO)	Formation: crystallisation at 200–1300 °C [376,377,389], 400–850 °C [133], 500–900 °C [367], 600–780 °C [156], 615–775 °C [20], 645 °C [332], 650–900 °C [14], 700–950 °C and mostly 877–927 °C (references in [376,377]), 700–1000 °C [79], 700–1150 °C [20], 750 °C [390], 900–1100 °C [327] Formation: oxidation of organically bound Ca at 200–700 °C [389] Formation from: ankerite decarbonation at 500–800 °C, calcite and dolomite decarbonation at 500–900 °C, anhydrite desulphation at 800–1300 °C [376,377,389] Formation reaction: $CaCO_3 \rightarrow CaO + CO_2$ [253] Formation reaction: $CaSO_4 \rightarrow CaO + SO_3$ (800–1300 °C) [376,377,389] Formation reaction: $CaSO_4 + CO \rightarrow CaO + SO_2 + CO_2$ [79] Transformation: dissolution in melt at 1100–1600 °C [376,377]
Maghemite (γ-Fe_2O_3)	Formation: crystallisation at 1000 °C [333]
Magnesite ($MgCO_3$)	Transformation: to periclase at 560–650 °C (references in [376,377])
Magnetite ($FeFe_2O_4$)	Formation: melt crystallisation at 1100–1400 °C [376,377] Formation reaction: $3FeCl_2 + 2O_2 \rightarrow Fe_3O_4 + 3Cl_2$ [260] Transformation: magnetite → maghemite (275–375 °C) → hematite (590–650 °C) (references in [376,377]) Transformation: dissolution in melt at 1100–1600 °C [376,377]
Marcasite (FeS_2)	Transformation: polymorphic to pyrite at 100–400 °C [376,377], 400–460 °C (references in [376,377]) Transformation: oxidation to Fe sulphates at < 500 °C [376,377,389]
Melanterite ($FeSO_4 \cdot 7H_2O$)	Transformation to hematite at 482 °C (references in [376,377])
Melilite (see akermanite and gehlenite)	Formation: solid-state reaction at 700–1300 °C [376,377] Transformation: dissolution in melt at 1100–1600 °C [376,377]
Metakaolinite ($Al_2Si_2O_5$)	Formation: $Al_2Si_2O_5(OH)_4 \rightarrow Al_2O_3 \cdot 2SiO_2 + 2H_2O$ [159,333]
Metal (elemental form)	Formation reaction: $M + CO/C \rightarrow M + CO_2$ [75]

(*continued on next page*)

Table 8 (*continued*)

Phase, mineral	Formation, transformation or reaction and reference used
Metal chlorides (MCl, MCl_2)	Formation reaction: $M(s) + Cl_2(g) \rightarrow MCl_2(s)$ [54,65,75] Formation reaction: $M(s) + 2HCl(g) \rightarrow MCl_2(g) + H_2(g)$ (M is mostly Fe, Cr and Ni) [54,65] Formation: $MCl_2(s) \rightarrow MCl_2(g)$ (M is mostly Fe, Cr and Ni) [65] Formation reaction: $MO(s) + 0.5Cl_2(g) \rightarrow MCl(s,l,g) + 0.5O_2(g)$ (M is mostly Fe, Cr and Ni) [65] Formation reaction: $MO + 2HCl \rightarrow MCl_2 + H_2O$ [54]
Metal oxides (MO_X, M_2O_3, M_3O_4)	Formation reaction: $M + CO_2 \rightarrow MO_X + CO$ [75] Formation reaction: $M + O_2 \rightarrow MO_X$ [75] Formation reaction: $4\,M(s) + 3O_2(g) \rightarrow 2M_2O_3(s)$ (M is mostly Fe, Cr and Ni) [65] Formation reaction: $2MCl_2(g) + 1.5O_2(g) \rightarrow M_2O_3(s) + 2Cl_2(g)$ (M is mostly Fe, Cr and Ni) [65] Formation reaction: $3MCl_2(g) + 2O_2(g) \rightarrow M_3O_4(s) + 3Cl_2(g)$ (M is mostly Fe, Cr and Ni) [65] Formation reaction: $4\,MCl_2(g) + 3O_2(g) \rightarrow 2M_2O_3(s) + 4Cl_2(g)$ (M is mostly Fe, Cr and Ni) [65] Formation reaction: $4MCl_2(g) + O_2(g) + 4H_2O(g) \rightarrow 2M_2O_3(s) + 8HCl(g)$ (M is mostly Fe, Cr and Ni) [65]
Metal oxide and chloride (M_2O_3, MCl)	Formation reaction: $4M(s) + 3O_2(g) + MCl(s,l) \rightarrow 2M_2O_3(s) + MCl(s,l)$ (M is mostly Fe, Cr and Ni) [65]
Metal sulphates (MSO_4, M_2SO_4)	Formation reaction: $M + SO_2 + O_2 \rightarrow MSO_4$ [54] Formation reaction: $MO + SO_2 + 0.5O_2 \rightarrow MSO_4$ [54] Formation reaction: $2MCl + SO_2 + 1/2O_2 + H_2O \rightarrow M_2SO_4 + 2HCl$ (M is mostly K and Na) [176]
Mg chloride ($MgCl_2$)	Formation reaction: $MgCO_3 + 2HCl \rightarrow MgCl_2 + H_2O + CO_2$ [387] Formation reaction: $MgO(s) + 2HCl(g) \rightarrow MgCl_2(g,l) + H_2O(g)$ [346,387] Formation reaction: $Mg(OH)_2 + 2HCl \rightarrow MgCl_2 + 2H_2O$ [387]
Mg (organically bound)	Transformation: oxidation to MgO at 200–700 °C [376,377,389]
Mg sulphate ($MgSO_4$)	Formation: crystallisation at 200–1100 °C [389], ⩾575 °C [336] Formation: sulphation of MgO released from organic matter at 200–1100 °C [389] and from ankerite and dolomite at 500–1100 °C [389] Formation reaction: $MgO + H_2SO_4$(or $H_2O + SO_2 + 0.5O_2$) $\rightarrow MgSO_4 + H_2O$ [387] Formation reaction: $MgO + SO_2 + 0.5O_2 \rightarrow MgSO_4$ [79,336,387] Transformation: desulphation of $MgSO_4$ to periclase at 1100–1200 °C [389] and 1122–1124 °C (references in [376,377])
Monticellite (CaMgSiO4)	Formation: crystallisation at ⩾575 °C [336], 600–1300 °C [376,377] Formation: solid-state reaction at 600–1300 °C [376,377] Formation reaction: $CaO + MgO + SiO_2 \rightarrow CaMgSiO_4$ (⩾575 °C) [336] Transformation: dissolution in melt at 1100–1600 °C [376,377]
Montmorillonite ($(NaCa)_{0.3}(AlMgFe)_2Si_4O_{10}(OH)_2\cdot xH_2O$))	Transformation: montmorillonite → release of adsorbed and interlayer water (100–180 °C) → dehydroxylation without lattice destruction (500–730 °C) → lattice destruction (850–900 °C) → formation of spinel and amorphous phase (900–950 °C) → formation of quartz or cristobalite, cordierite, enstatite, mullite (1000–1300 °C) (references in [376,377]) Transformation: montmorillonite → dehydration (50–200 °C) → dehydroxylation (600–900 °C) → crystal lattice destruction (800–1100 °C) [376,377]
Mullite ($Al_6Si_2O_{13}$)	Formation: crystallisation at 800–1600 °C [376,377], 1150 °C [75] Formation: solid-state reaction at 800–1400 °C [376,377] Formation: melt crystallisation at 1100–1600 °C [376,377] Formation: $2(2Al_2O_3\cdot 3SiO_2) \rightarrow 2(3Al_2O_3\cdot 2SiO_2) + 5SiO_2$ (1150 °C) [75] Transformation: dissolution in melt at 1100–1600 °C [376,377]
Muscovite ($KAl_2AlSi_3O_{10}(OH,F)_2$)	Formation: reaction between kaolinite and sylvite → muscovite (700–800 °C) → corundum and quartz (900 °C) [42] Transformation: muscovite → dehydroxylation (750–1000 °C) → lattice destruction (1050–1100 °C) → crystallisation of α-Al_2O_3, γ-Al_2O_3, leucite (>1050 °C) (references in [376,377]) Transformation: muscovite → dehydroxylation (600–900 °C) → crystal lattice destruction (700–1100 °C) [376,377]
Na-bearing oxides (Na_2MO_2, Na_2MO_4, $Na_2M_2O_4$)	Formation reaction: $M(s) + 2NaCl(g) + 2O_2(g) \rightarrow Na_2MO_4(s,l) + Cl_2(g)$ (M is mostly Fe, Cr and Ni) [65] Formation reaction: $M_2O_3(s) + 2NaCl(s,l) + 0.5O_2(g) \rightarrow Na_2M_2O_4(s,l) + Cl_2(g)$ (M is mostly Fe, Cr and Ni) [65] Formation reaction: $0.5M_2O_3(s) + 2NaCl(s,l) + 1.25O_2(g) \rightarrow Na_2MO_4(s,l) + Cl_2(g)$ (M is mostly Fe, Cr and Ni) [65] Formation reaction: $M_2O_3(s) + 4NaCl(g) + 2.5O_2(g) \rightarrow 2Na_2MO_4(s,l) + 2Cl_2(g)$ (M is mostly Fe, Cr and Ni) [65] Formation reaction: $MO(s) + Na_2O(s,l) \rightarrow Na_2O.MO(s,l)$ (M is mostly Fe, Cr and Ni) [65]
Na (elemental form)	Formation reaction: $NaCl(l) + 0.5H_2 \rightarrow Na(g) + HCl$ [387]
Na–Fe oxide ($Na_2Fe_2O_4$)	Formation reaction: $Na_2O + Fe_2O_3 \rightarrow Na_2Fe_2O_4$ [72]
Na–Fe sulphate ($Na_3Fe(SO_4)_3$)	Formation reaction: $3Na_2SO_4(s) + Fe_2O_3(s) + 3SO_2(g) \rightarrow 2Na_3Fe(SO_4)_3(s,l)$ [65]
Na hydroxide ($NaOH$)	Formation reaction: $Na(g) + OH(g) \rightarrow NaOH(g)$ [174] Formation reaction: $NaCl(g) + H_2O \rightarrow NaOH(g) + HCl(g)$ [174,387]
Na–Mg silicate ($Na(Mg_{0.5}Si_{0.5})O(Si_2O_6)$)	Formation: crystallisation at 530 °C [261]
Na oxide (Na_2O)	Formation reaction: $2Na(g) + 0.5O_2 \rightarrow Na_2O(l)$ [68]
Na silicate (Na_2SiO_3)	Formation reaction: $SiO_2 + 2NaCl(l) + H_2O \rightarrow Na_2SiO_3 + 2HCl$ [59,387] Formation reaction: $2SiO_2 + Na_2CO_3 \rightarrow Na_2O\cdot 2SiO_2 + CO_2$ [59,72]
Natrite (Na_2CO_3)	Formation reaction: $2NaOH(g) + CO_2(g) \rightarrow Na_2CO_3(l,g) + H_2O(g)$ [346]

Table 8 (*continued*)

Phase, mineral	Formation, transformation or reaction and reference used
Natrofairchildite($Na_2Ca(CO_3)_2$)	Transformation: decarbonation at 850 °C [219]
Nitrates	Transformation: decomposition at 200–550 °C [116], 200–700 °C [22]
Nitre (KNO_3)	Formation: crystallisation at < 250 °C [22] Transformation: decomposition at 200–700 °C [22]
NO_X	Formation reaction: $N + O_2 \rightarrow NO_X$ (NO, NO_2, N_2O) [353]
Oldhamite (CaS)	Formation: crystallisation at 500–815 °C [343]
Opal ($SiO_2{\cdot}nH_2O$) (see silica minerals)	Formation and transformation: crystallisation and recrystallization at < 300 °C) [376,377]
Orthoclase ($KAlSi_3O_8$)	Transformation: orthoclase → polymorphic transformation to sanidine (900 °C) → decomposition and formation of leucite, nepheline, amorphous SiO_2, sillimanite (900–1170 °C) (references in [376,377]) Transformation: polymorphic transformation to sanidine (900–1000 °C) [376,377]
Periclase (MgO)	Formation: crystallisation at 200–900 °C [389], $\geqslant$400 °C [310], $\geqslant$575 °C [336], 750–1150 °C [20], 815 °C [338], 816–1225 °C, [201], 1200–1600 °C [329], 1492–1541 °C [202] Formation: oxidation of organically bound Mg at 200–700 °C [389] Formation: from ankerite decarbonation at 500–800 °C, dolomite decarbonation at 500–900 °C [389] Formation: $MgCO_3 \rightarrow MgO + CO_2$ (references in [376,377]) Formation: melt crystallisation at 1492–1541 °C [202] Transformation: dissolution in melt at 1100–1600 °C [376,377]
Phosphates	Formation: melt crystallisation at 1064–1154 °C [202]
Pirssonite ($Na_2Ca(CO_3)_2.2H_2O$)	Transformation: dehydration at 200 °C [219]
Plagioclases (see albite and anorthite)	Formation: melt crystallisation at 1100–1300 °C [376,377] Transformation: dissolution in melt at 1100–1600 °C [376,377]
Polychlorinated dibenzo-p-dioxins (PCDD) and dibenzofurans (PCDF)	Formation: $4HCl + O_2 \rightarrow 2H_2O + 2Cl_2$ and Cl_2 + organic molecules → chlorinated molecules (PCDD/F) [211]
Portlandite ($Ca(OH)_2$)	Formation: hydroxylation of lime at $\leqslant$600 °C [376,377], 650 [390] Formation reaction: $CaO + H_2O \rightarrow Ca(OH)_2$ [12,36,48,390] Transformation: dexydroxylation to lime at 450 °C [129], 475–620 °C (references in [376,377]), 490–500 °C [219], 525–575 °C [283], 550 °C [390], >600 °C [14], 600–800 °C [376,377] Transformation: $Ca(OH)_2 \rightarrow CaO + H_2O$ (550 °C) [390] Transformation: $Ca(OH)_2(s) \rightarrow Ca(OH)_2(l) + CO_2(l) \rightarrow CaCO_3(s) + H_2O$ (portlandite dissolution and calcite formation) [49]
Proteins	Transformation: decomposition at 320–450 °C [254]
Pyrite (FeS_2)	Transformation: oxidation at 100–500 °C [376,377,389] Transformation: pyrite → hematite (400–700 °C in oxidising atmosphere), pyrite → pyrrhotite (325–750 °C in inert atmosphere) (references in [376,377])
Pyrrhotite ($Fe_{1-x}S$)	Transformation: to hematite at 600 °C (references in [376,377])
Quartz (SiO_2) (see silica minerals)	Formation: crystallisation at 400–850 °C [20], $\geqslant$400 °C [310], 500–815 °C [343], 630–1000 °C [333] Transformation: polymorphic of quartz, tridymite and cristobalite at 575–1500 °C [376,377] Transformation: dissolution in melt (1100–1600 °C) [376,377]
Rankinite ($Ca_3Si_2O_7$)	Formation: solid-state reaction at 700–1300 °C [376,377] Transformation: dissolution in melt at 1100–1600 °C [376,377]
Sanidine ($KAlSi_3O_8$)	Formation: crystallisation at $\geqslant$ 900 °C [331]
Serendibite ($CaMg_3O(Si_3O_9)$	Formation: crystallisation at 600 °C [261]
Siderite ($FeCO_3$)	Formation: carbonation of Fe oxyhydroxides at 200–400 °C [376,377] Transformation: siderite → wustite (350–610 °C, mostly 527 °C) → hematite plus maghemite (670 °C) → hematite (830 °C) (references in [376,377]) Transformation: decarbonation to hematite at 400–800 °C [376,377,389]
Silica (amorphous SiO_2)	Formation: at 200–1100 °C [376,377]
Silica minerals ($SiO_2{\cdot}nH_2O$, SiO_2)	Transformation: opal ($SiO_2{\cdot}nH_2O$) → α-cristobalite (65–300 °C), α-tridymite → β-tridymite (114 °C), α-cristobalite → β-cristobalite (200–270 °C), α-quartz → β-quartz (573 °C) → β-tridymite (867 °C) → β-cristobalite (1470 °C), β-quartz → β-cristobalite (1050 °C) (references in [376,377]) Transformation: dissolution in melt at 1100–1600 °C [376,377]
Sillimanite (Al_2SiO_5)	Formation: crystallisation at 600 °C [261]
S (organically bound and elemental S)	Transformation: oxidation to S oxide at 200–700 °C [376,377,389]
SO_X	Formation: from pyrite and marcasite oxidation at 100–500 °C; from organically bound S and elemental S at 200–700 °C and decomposition of sulphates at 300–1300 °C [376,377,389]
Sphalerite ((Zn,Fe)S)	Transformation: to ZnO at 850 °C (references in [376,377])
Spinel ($MgAl_2O_4$–$Mg(AlFe)_2O_4$)	Formation: solid-state reaction at 700–1200 °C [376,377] Transformation: dissolution in melt at 1100–1600 °C [376,377]
Srebrodolskite ($Ca_2Fe_2O_5$)	Formation reaction: $2CaO + Fe_2O_3 \rightarrow Ca_2Fe_2O_5$ ($\geqslant$575 °C) [336]
Sylvite (KCl)	Formation: crystallisation at 200–400 °C [59], $\geqslant$400 °C [310], 400–1000 °C [20], 500–815 °C [343], 600 °C [261] Formation reaction: $K + HCl(g) + O \rightarrow KCl + OH$ [174]

(*continued on next page*)

Table 8 (*continued*)

Phase, mineral	Formation, transformation or reaction and reference used
	Formation reaction: $KOH(g) + HCl(g) \rightarrow KCl(g,l) + H_2O(g)$ [346]
Thenardite (Na_2SO_4)	Formation: suphation of Na_2O originated from organic matter at 200–800 °C [389] Formation reaction: $2NaCl(s) + SO_2(g) + O_2(g) \rightarrow Na_2SO_4(s) + Cl_2(g)$ [65,260] Formation reaction: $2NaCl(s,g,l) + SO_2(g) + 0.5O_2(g) + H_2O(g) \rightarrow Na_2SO_4(s,g,l) + 2HCl(g)$ [56,65,132,176,199,235,260,281,387] Formation reaction: $4NaCl(s,g) + 2SO_2(g) + O_2(g) + 2H_2O(g) \rightarrow 2Na_2SO_4(s,g) + 4HCl(g)$ [208,311] Formation reaction: $2NaOH(g) + SO_2(g) + 0.5O_2(g) \rightarrow Na_2SO_4(g,l,s) + H_2O(g)$ [235,387] Transformation: desulphation at 800–1100 °C [389]
Tridymite (SiO_2) (see silica minerals)	Formation: crystallisation at 1100–1500 °C [376,377], 1125–1325 °C [201] Formation: melt crystallisation at 1100–1500 °C [376,377] Formation: polymorphic transformation of crystobalite → tridymite at 1125–1325 °C [201] Transformation: dissolution in melt at 1100–1600 °C [376,377]
Vivianite ($Fe_3(PO_4)_2.8H_2O$)	Transformation: dehydration (250–300 °C) → decomposition (500 °C) (references in [376,377])
Water–gas shift reaction	$CO + H_2O \rightarrow CO_2 + H_2$ [388]
Whitlockite ($Ca_9Fe(PO_4)_7$)	Formation: crystallisation at 630–1000 °C [333]
Wollastonite ($CaSiO_3$)	Formation: crystallisation at 400–1300 °C [376,377], 900–1100 °C [327], 1163–1253 °C [202] Formation: solid-state reaction at 400–1300 °C [376,377] Formation: melt crystallisation at 1163–1253 °C [202] Formation reaction: $SiO_2(s) + CaCl_2(l) + H_2O(g) \rightarrow CaSiO_3(s) + 2HCl(g)$ [311] Formation reaction: $SiO_2(s) + CaCl_2(l) + 0.5O_2(g) \rightarrow CaSiO_3(s) + Cl_2(g)$ [311] Formation reaction: $SiO_2(s) + CaO(s) \rightarrow CaSiO_3(s)$ [346] Transformation: dissolution in melt at 1100–1600 °C [376,377]
Zeolites ($(Ca,Sr,Ba,Na_2,K_2)Al_2Si_{2-10}O_{8-24}\cdot 2-8H_2O$)	Transformation: zeolites → loss of zeolitic water (80–450 °C) → reversible transition (400–670 °C) → destruction (700–860 °C) → formation of sintered amorphous phase (900–940 °C) → solid-solution formation, mullite-type nucleation (1185 °C) (references in [376,377])

based on proved, improved or new approaches and methods are required to reduce uncertainties. There are thus ample opportunities for new research in this area.

The major tasks of the present work are: to compile and systematize a reliable database; to describe the basic findings and clarify some of the problems; to supply additional results; and to explain some of the advantages and challenges related to origin, composition, properties and combustion behaviour of biomass varieties specified in different types and sub-types. The present overview includes a critical review of publications and own investigations as an attempt will be undertaken to address the following objectives:

(1) Characterization of the composition and properties of biomass fuels and their solid combustion products.
(2) Elucidation of the phase-mineral transformations and chemical interactions of OM and IM during biomass combustion up to 1500 °C.
(3) Clarification of the ash fusion behaviour of biomass.
(4) Explanation of the ash formation mechanisms of biomass types and sub-types during combustion.
(5) Indication of some potential technological and environmental risks connected with combustion of biomass types and sub-types and application of their BAs.

The present work is the first part of this overview and comprises points 1 and 2, while the investigation on points 3–5 will be reported in the second part.

2. Materials, methods and data used

The results used in this overview were obtained from: (1) reference peer-reviewed data and investigations; and (2) own new data and studies. For better differentiation, they are referred to as: (1) “reference investigations”; and (2) “present study” throughout the text, respectively. The chemical ash composition of biomass groups and sub-groups is given in Table 6 (based on [1,3]). The phases and minerals identified or assumed (with some uncertain identification) in BA include approximately 291 species listed in Table 7 using mostly peer-reviewed investigations and own data ([2,3] and references therein) plus some supplementary reference data [219,261,348,357,386]. An attempt was undertaken to systematize the possible physico-chemical formations, transformations and reactions (Table 8) during biomass combustion, as well as transport and storage of BA based on numerous references and huge information ([12,14,16,20,22,24,36,42,48,49,54,56,59,65,66,68,72,75,79,85,97,102,116,129,131–133,144,146,156,159,165,168,174,176,185,188,189,199,201,202,208–211,219,220,233,235,253,254,260,261,281,283,285,296,308,310,311,319,327,329,331–333,336,338,343,344,346,347,350,353,355,367,369,376,377,387–391], and references in [376,377]). Additionally, the melting point (MP) temperatures of many inorganic phases and minerals identified or assumed in biomass and BA are given in Table 9 based also on reference data [14,20,22,27,32,38,39,42,51,65,72,97,102,114,129,131,133,165,179,185,186,206,229,250,260,302,311,327,333,344,346,348,356,368,377,392–395].

Eight biomass samples were collected and studied for additional clarification of the chemical and phase composition of biomass and BA (Tables 10 and 11 based on [1–3] and present data), as well as behaviour of biomass during combustion in the present work. They include beech wood chips (BC), corn cobs (CC), marine macroalgae (MM), weathered plum pits (PP), rice husks (RH), switchgrass (SG), sunflower shells (SS) and walnut shells (WS). The majority of investigations up to now have been concentrated dominantly on woody biomass and wheat straw as solid biofuels. Most of these eight samples are herbaceous and agricultural residues and algae (sea lettuces) and much less is known about them. The selection of these samples is also based on their highly variable: (1) structural composition; and especially (2) inorganic chemical composition (Table 10 and Fig. 1). Another big advantage of these samples for comparative investigations (Fig. 1) is that they belong to: (1) different organic structural types (“CHL”, “LCH” and “HCL”); (2) all inorganic chemical types (“S”, “C”, “K”, and “CK” types) and different sub-types; and (3) all inorganic acid tenden-

Table 9
Melting point (MP) temperatures of inorganic phases and minerals identified or assumed (with uncertain identification) in biomass and biomass ash, °C.

Phase, mineral	Chemical formula	MP	Reference used
Silicates			
Akermanite	$Ca_2MgSi_2O_7$	1554	[393]
Albite	$NaAlSi_3O_8$	1118	[393]
Amorphous silica	SiO_2	1713	[393]
Amphibole	$NaCa_2(Mg,Fe,Al)_5(Si,Al)_8O_{22}(OH)_2$	1030–1140	[393]
Andalusite	Al_2SiO_5	1810	[393]
Anorthite	$CaAl_2Si_2O_8$	1553	[393]
Biotite	$K(Mg,Fe)_3AlSi_3O_{10}(OH,F)_2$	$\sim$1200	[393]
Ca–Mg silicates		1392–1554	[393]
Ca silicate hydrate	$CaO{\cdot}SiO_2{\cdot}H_2O$	$\sim$1540–1544[a]	[327,393]
Ca silicates	$CaSiO_4$, $CaSi_2O_5$, $Ca_4Si_2O_8$, $Ca_8Si_5O_{18}$, others	$\sim$1540–1544	[327,393]
Cd silicate	$CdSiO_3$	1785	[392]
Chlorite	$(Mg,Fe)_5Al_2Si_3O_{10}(OH)_8$	$\sim$1200	[393]
Clay minerals		1000–1810	[393]
Cristobalite	SiO_2	1713	[393]
Diopside	$CaMgSi_2O_6$ or $CaMg(SiO_3)_2$	1392	[393]
Enstatite	$MgSiO_3$	1557	[393]
Fayalite	Fe_2SiO_4	1205	[393]
Feldspars	$NaAlSi_3O_8$–$CaAl_2Si_2O_8$, $KAlSi_3O_8$	1118–1553	[393]
Forsterite	Mg_2SiO_4	1890	[393]
Gehlenite	$Ca_2Al_2SiO_7$	1590	[393]
Hydromica	Illite and hydromuscovite	1000–1300	[393]
Illite	$(KH_2O)Al_2(AlSi)Si_3O_{10}(OH)_2$	1200–1300	[393]
Kalsilite-kaliophilite	$KAlSiO_4$	1684–1750	[229,393]
K aluminosilicate		$\sim$695	[129]
Kaolinite	$Al_2Si_2O_5(OH)_4$	1650–1810	[393]
K–Ca silicates	K_2CaSiO_4, $K_4CaSi_3O_9$, others	720–850	[20,129,348]
K feldspars	$KAlSi_3O_8$	1170	[393]
K–Mg silicate		$\sim$685	[129]
K–Na silicates (eutectics)		540–1170	[32,38,39,102,129,250,356]
K silicates (eutectics)	$K_2O.4SiO_2$, $K_2Si_4O_9$, $K_6Si_2O_7$ others	600–980	[22,27,38,39,51,72,97,102,114,131,185,186,302,344,346]
Larnite	Ca_2SiO_4	2130	[185,186,392]
Leucite	$KAlSi_2O_6$	1686	[393]
Melilite (akermanite–gehlenite)	$Ca_2MgSi_2O_7$–$Ca_2Al_2SiO_7$	1554–1590	[393]
Metakaolinite	$Al_2Si_2O_5$	1650–1810	[393]
Mg silicate		1557–1890	[393]
Microcline	$KAlSi_3O_8$	1170	[393]
Montmorillonite	$(Na,Ca)_{0.3}(Al,Mg,Fe)_2Si_4O_{10}(OH)_2{\cdot}xH_2O$	1000–1300	[377,393]
Mullite	$Al_6Si_2O_{13}$	1810	[393]
Muscovite	$KAl_2AlSi_3O_{10}(OH,F)_2$	$\sim$1200	[393]
Na silicates (eutectics)	$Na_2O{\cdot}2SiO_2$	$\geqslant$874	[72]
Na silicate (water glass)	$Na_2Si_3O_7$ or Na_2SiO_3	1088	[392]
Nepheline	$(Na,K)AlSiO_4$	1526	[393]
Opal	$SiO_2{\cdot}nH_2O$	1713[a]	[393]
Orthoclase	$KAlSi_3O_8$	1170	[393]
Plagioclases	$NaAlSi_3O_8$–$CaAl_2Si_2O_8$	1118–1553	[393]
Quartz	SiO_2	1713	[393]
Sanidine	$KAlSi_3O_8$ or $(K,Na)(Si,Al)_4O_8$	1170	[393]
Silica	SiO_2	1713	[393]
Sillimanite	Al_2SiO_5	1810	[393]
Tridymite	SiO_2	1713	[393]
Wollastonite	α-$Ca_3Si_3O_9$ or α-$CaSiO_3$	1540–1544	[327,393]
Zeolites	$(Ca,Sr,Ba,Na_2,K_2)Al_2Si_{2-10}O_{8-24}{\cdot}2\text{–}8H_2O$	896–1185	[393]
Zircon	$ZrSiO_4$	2552	[393]
Oxides and hydroxides			
Alumina	γ-Al_2O_3	2050	[393]
Anatase	TiO_2	1827	[393]
Brookite	TiO_2	1827	[393]
Brucite	$Mg(OH)_2$	2800[a]	[393]
Bunsenite	NiO	1955	[392]
Ca–Al oxides	$Ca_3Al_2O_3$, $Ca_3Al_2O_6$	1535	[392]
Ca–Fe oxide	$Ca_XFe_YO_Z$	1225–1325	[393]
Ca–Fe oxide	$CaO{\cdot}Fe_2O_3$	1225–1250	[393]
Ca–Fe oxide	$2CaO{\cdot}Fe_2O_3$	1300–1325	[393]
Corundum	Al_2O_3	2050	[393]
Cr-Fe oxide	$(Cr,Fe)_2O_3$	1597–1990	[392,393]
Cuprite	Cu_2O	1236	[392]
Eskolaite	Cr_2O_3	1990	[392]
Gibbsite	$Al(OH)_3$	2050[a]	[393]
Goethite	α-FeOOH	1567[a]	[393]
Hausmannite	Mn_3O_4	1565	[392]
Hematite	α-Fe_2O_3	1567–1594	[392,393]
K–Fe oxide	$K_2Fe_2O_4$	$\geqslant$1135	[72,102]
K hydroxide	KOH	380–406	[114,392]

(*continued on next page*)

Table 9 (*continued*)

Phase, mineral	Chemical formula	MP	Reference used
K–Na–Fe oxide	$K(Na)_2Fe_2O_4$	⩾1135	[72]
Lime	CaO	2570–2597	[368,393]
Macedonite	$PbTiO_3$	1170	[392]
Maghemite	γ-Fe_2O_3	1567–1597	[393]
Magnetite	$FeFe_2O_4$	1592–1597	[392,393]
Manganosite	MnO	1875	[392]
Massicot (litharge)	PbO	886	[392]
Molybdite	MoO_3	795	[393]
Na–Fe oxide	$Na_2Fe_2O_4$	⩾1135	[72]
Na hydroxide	$NaOH$	318	[392]
Na oxide	Na_2O	1132	[392]
Periclase	MgO	2800	[393]
Portlandite	$Ca(OH)_2$	2570–2597[a]	[368,393]
Rutile	TiO_2	1827	[393]
Senarmontite	Sb_2O_3	642–656	[392,393]
Spinel	$MgAl_2O_4$	2135	[393]
Srebrodolskite	$Ca_2Fe_2O_5$	1450	[392]
Valentinite	Sb_2O_3	642–655	[393]
Wustite	FeO	1370–1378	[392,393]
Zincite	ZnO	1975	[392]
Zn ferrite	$(Zn,Fe)Fe_2O_4$	~1590	[392]
Zn-Ti oxide	$Zn_XTi_YO_4$	~1549	[392]
Phosphates			
Apatite	$Ca(PO_4)_3(Cl,F,OH,CO_3)$	1270–1660	[393]
Berlinite	$AlPO_4$	2000	[392]
Ca–K phosphates	With 40–60% K_2O	590	[348]
Carbonateapatite	$Ca(PO_4)_3(CO_3)$ or $Ca_5(PO_4)_3(CO_3)$	1470	[393]
Chloroapatite	$Ca(PO_4)_3(Cl)$ or $Ca_5(PO_4)_3(Cl)$	1580	[393]
Chloro–fluoro-apatite	$Ca(PO_4)_3(Cl,F)$ or $Ca_5(PO_4)_3(Cl,F)$	1270	[393]
Evansite	$Al_3(PO_4)(OH)_6.6(H_2O)$	>1502	[393]
Fluoroapatite	$Ca(PO_4)_3(F)$ or $Ca_5(PO_4)_3(F)$	1660	[393]
Hydroxylapatite	$Ca(PO_4)_3(OH)$, $Ca_5(PO_4)_3(OH)$ or $Ca_{10}(PO_4)_6(OH)_2$	1400[a]	[393]
K–Ca phosphate	$KCa(PO_4)$	1560	[229]
K phosphate	KPO_3	1325–1620	[368]
K phosphate	K_2PO_4	~800	[179,333]
K phosphate mixture	KPO_3–$K_4P_2O_7$	⩾610	[368]
Mg phosphate		~1348	[392]
Sulphates, sulphides, sulphosalts, sulphites and thiosulphates			
Anglesite	$PbSO_4$	1170	[392]
Anhydrite	$CaSO_4$	1450[a]	[393]
Arcanite	K_2SO_4	1067–1100	[20,114,133,165,185,186,377,206,229,393]
Barite	$BaSO_4$	1580–2400[a]	[392,393]
Bassanite	$CaSO_4.0.5H_2O$	1450[a]	[393]
Ca sulphate		1450[a]	[393]
Chalcocite	Cu_2S	1130	[393]
Chalcopyrite	$CuFeS_2$	800–1027	[393]
Cu sulphate	$CuSO_4$	200	[392]
Galena	PbS	1097	[393]
Gypsum	$CaSO_4 \cdot 2H_2O$	1450[a]	[393]
K–Al sulphate	$K_3Al(SO_4)_3$	690–800	[42]
Kieserite (dehydrated)	$MgSO_4$	1130	[392]
K–Na sulphate–chloride mixture		515	[311]
K sulphide	K_2S	835	[392]
Mn sulphate	$MnSO_4$	700	[392]
Molybdenite	MoS_2	730	[393]
Orpiment	As_2S_3	310	[393]
Pyrite	FeS_2	743	[392]
Pyrrhotite	$Fe_{1-x}S$	1027–1175	[392,393]
Realgar	AsS	320	[393]
Stibnite (antimonite)	Sb_2S_3	546	[393]
Thenardite	Na_2SO_4	884	[393]
Troilite	FeS	1175	[393]
Zn sulphide		1775	[392]
Carbonates and bicarbonates			
Fairchildite–butschliite	$K_2Ca(CO_3)_2$	815	[185,186]
K carbonate (potash)	K_2CO_3	788–904	[14,133,344,356,392]
Natrite	Na_2CO_3	850	[392]
Chlorides, chlorites and chlorates			
Bischofite	$MgCl_2 \cdot 6(H_2O)$	714[a]	[393]
Ca chloride	$CaCl_2$	772	[392]
Calomel	Hg_2Cl_2	543	[393]
Cd chloride	$CdCl_2$	569	[392]
Chlorargyrite	$AgCl$	455	[393]

Table 9 (*continued*)

Phase, mineral	Chemical formula	MP	Reference used
Cotunnite	$PbCl_2$	501	[392]
Cr chloride	$CrCl_2$	815–845	[65,392]
Cr chloride	$CrCl_3$	631–947	[65,392]
Cu chloride	CuCl	451	[392]
Cu chloride	$CuCl_2$	630	[392]
Halite	NaCl	801	[65,185,186,393]
K halite	$K_{0.2}Na_{0.8}Cl$ or $K_{0.4}Na_{0.6}Cl$	770–801	[393]
K–Na–Fe chlorides mixtures (eutectics)	KCl–NaCl–$FeCl_2$	340–390	[260]
Mn chloride	$MnCl_2$	650	[392]
Molysite	$FeCl_3$	300–308	[65,392,393]
Na chloride–sulphate mixture (eutectics)	NaCl–Na_2SO_4	$\geqslant$628	[394]
Ni chloride	$NiCl_2$	1009	[392]
Rokühnite	$FeCl_2$	677	[65,392]
Sb chloride	$SbCl_3$	73	[392]
Sb chloride	$SbCl_5$	4	[392]
Sylvite	KCl	770–790	[20,51,65,114,133,185,186,392,393]
Zn chloride	$ZnCl_2$	317–318	[368,392]
Nitrates			
Nitratine (nitratite)	$NaNO_3$	370	[393]
Nitre (niter)	KNO_3	~330	[395]
Elemental forms			
Elemental Ag	Ag	961	[393]
Elemental Al	Al	660	[392]
Elemental Au	Au	1063	[393]
Elemental Cr	Cr	1857	[392]
Elemental Cu	Cu	1083	[392]
Elemental Fe	Fe	1536	[392]
Elemental Hg	Hg	−39	[393]
Elemental Mn	Mn	1244	[392]
Elemental Ni	Ni	1453	[392]
Elemental Pb	Pb	327	[392]
Elemental Pt	Pt	1769–1774	[392,393]
Elemental S	S	112	[393]
Elemental Si	Si	1420	[393]
Elemental Sb	Sb	631	[392]
Elemental Zn	Zn	420	[392]
Graphite	C	3527	[393]
Glass	Various elements	$\geqslant$874	[72]
Other inorganic phases			
Fluorite	CaF_2	1378	[393]

[a] After decomposition.

cies (high, medium and low); that have been specified recently for biomass and BA [1–3]. Additionally, five samples from them belong to the low acid "K" and "CK" types and sub-types (Fig. 1), which are among the most problematic biomass resources from technological and environmental points of view [2–4]. Finally, the composition of these eight biomass samples differs widely in comparison with coals (Tables 6, 10 and 11 and Figs. 1 and 2). The samples collected were between 2 and 5 kg in weight and they were air dried under ambient conditions during a period of over 12 months. After that, visible contaminants such as sand, soil or shell particles were eliminated manually from RH and MM. Then the samples were cut/crushed (CC, PP, WS) and ground (BC, CC, MM, PP, RH, SS, SG, WS) to a particle size of <500 μm (BC, MM, RH, SG, SS) or <1000 μm (CC, PP, WS). Finally, they were investigated using light microscopy, powder X-ray diffraction (XRD), scanning electron microscopy (SEM), differential-thermal (DTA), thermo-gravimetric (TGA) and chemical analyses, as well as some leaching, precipitation, ashing and other procedures.

An ordinary stereomicroscope under transmitted and reflected light was used for optical observations. XRD patterns of finely ground samples were recorded by D2 Phaser Bruker AXS and DRON 3 M diffractometers, and collected at 10–70° 2θ using Cu and Co Kα radiations, respectively. The investigation by SEM was carried out on a JEOL JSM 6390 microscope equipped with an Oxford INCA energy dispersive X-ray analyser (EDX). The high-temperature ashes (HTAs) of biomass samples were produced in an electric oven (Carbolite) with static air at 500 ± 10 °C for 2 h with a heating and cooling rate of about 5 °C min^{-1}. The above temperature and holding time were selected as the lowest ones for gentle and successful incineration of biomass prior to intensive decomposition ($\geqslant$500 °C) of some carbonates and sulphates which are typical minerals for many biomass varieties and their ashes. This argument has not been well recognised in the literature and standards or procedures worldwide for the determination of ash yield (or content) of biomass by using higher combustion temperatures than 500 °C.

The thermal experiments include a gradual heating of HTAs produced at 500 °C/2 h via 200 ± 5 °C intervals in the electric oven under atmosphere of static air. The heating was conducted at 700, 900, 1100, 1300 and 1500 °C or up to the fluid ash-fusion temperatures of the samples (excluding only RH), namely 1100 °C (CC, SG), 1300 °C (BC, MM, PP, SS, WS) and 1500 °C (RH). The sample RH has a fluid ash-fusion temperature higher than 1500 °C. Initial portions of HTA samples (0.1–0.9 g) spread out in a layer (about 1–3 mm thickness) at the bottom of ceramic crucibles (5 × 3 cm in diameter and 3.5 cm height) were heated up to the respective temperature for each experiment. The heating and cooling rate was about 10 °C min^{-1}. A holding time at the fixed temperature was 1 h and

Table 10
Data for eight biomass samples (air-dried basis), wt.% (indicated otherwise).

Characteristic	Rice husks	Switchgrass	Corn cobs	Plum pits (weathered)	Marine macroalgae	Beech wood chips	Walnut shells	Sunflower shells
Code	RH	SG	CC	PP	MM	BC	WS	SS
Organic type	CHL	CHL	CHL	LCH	HCL	CHL	LCH	CHL
Inorganic type	S	S	K	CK	K	C	CK	K
Inorganic sub-type	S-HA	S-MA	K-LA	CK-LA	K-LA	C-LA	CK-LA	K-LA
Source	Kovachevo, Bulgaria	Mead, Nebraska, USA	Debnevo, Bulgaria	Debnevo, Bulgaria	Tsarevo, Bulgaria	JRS Rosenberg, Germany	Debnevo, Bulgaria	Billa Sofia, Bulgaria
Collection time	08.2007	2003	08.2008	08.2008	08.2009	01.2009	08.2008	08.2008
Note	Cleaned from sand and soil grains	Two mixed harvests (50:50 vol%)		Weathered for 1 year	Cleaned from sand and shell grains	Produced size is 1–4 mm		
Size reduction (mm)	<0.5	<0.5	<1	<1	<0.5	<0.5	<1	<0.5
VM (db)	62.4	80.4	81.1	81.4	47.4	81.6	60.5	76.1
FC (db)	19.1	14.5	16.8	17.9	24.4	17.1	38.6	20.9
A (db)	18.5	5.1	2.1	0.7	28.2	1.3	0.9	3.0
Sum	100.0	100.0	100.0	100.0	100.0	100.0	100.0	100.0
Bulk density (loose) (kg m^{-3})	451	263	412	889	954	454	833	250
Bulk density (shaken) (kg m^{-3})	476	286	435	1000	1250	479	883	275
pH of leachate (solid–liquid = 1:10 mass ratio)	6.66	5.20	5.32	5.57	6.75	5.15	5.28	5.12
Electrical conductivity of leachate (mS/cm)	2.12	1.63	1.60	0.67	19.81	0.70	0.88	3.47
DWR	1.5	7.8	0.8	0.3	15.1	1.4	0.9	2.9
DTA 1 exopeak (°C)	338	340	335	351	334	349	343	324
DTA 2 exopeak (°C)	440	453	453	485	520	425	445	434
DTA 1 exopeak (mm)	44	59	26	42	22	44	38	32
DTA 2 exopeak (mm)	41	53	45	43.5	43	55	50	57
DTA 1/2 exopeaks ratio	1.07	1.11	0.58	0.97	0.51	0.80	0.76	0.56
Initial smoke (°C)	282	265	272	215	278	275	285	222
Ash (500 °C/2 h)	18.50	5.14	2.14	0.66	28.24	1.31	0.90	2.97
Ash (700 °C/1 h)	17.48	4.23	1.70	0.52	23.58	0.94	0.77	2.36
Ash (900 °C/1 h)	17.41	4.17	1.47	0.51	20.50	0.86	0.57	1.95
Ash (1100 °C/1 h)	17.37	4.14	1.44	0.50	17.17	0.84	0.52	1.86
Ash (1300 °C/1 h)	17.37			0.47	11.69	0.80	0.51	1.67
Ash (1500 °C/1 h)	17.22							
Fluid AFT observed (°C)	>1500	⩽1100	⩽1100	⩽1300	⩽1300	⩽1300	⩽1300	⩽1300
Fluid AFT by DTA (°C)	>1500	1193	1235	1233	1240	1300	1230	1236
Ash (500 °C/2 h) bulk density (loose) (kg m^{-3})	270	80	200	130	430	170	150	120
HTA (500 °C/2 h)								
SiO_2	89.86	62.90	36.67	12.01	5.60	5.48	2.84	1.45
CaO	1.40	7.69	2.12	43.95	22.06	62.58	38.11	15.57
K_2O	4.16	18.77	47.57	16.29	7.56	18.00	49.33	49.84
P_2O_5	0.60	2.44	4.82	10.17	0.97	2.49	2.37	6.54
Al_2O_3	1.04	0.89	0.81	2.57	0.98	0.49	0.52	0.12
MgO	0.49	4.20	1.97	4.18	7.69	7.49	3.80	11.87
Fe_2O_3	0.41	0.42	1.50	1.75	0.69	0.36	0.40	1.32
SO_3	1.31	2.17	3.44	7.72	28.49	0.77	2.03	11.39
Na_2O	0.23	0.11	0.28	0.79	14.07	0.11	0.12	0.22
TiO_2	0.02	0.04	0.06	0.16	0.03	0.03	0.05	0.01
Cl_2O	0.21	0.23	0.69	0.27	11.84	0.09	0.38	1.60
MnO	0.27	0.14	0.07	0.14	0.02	2.11	0.05	0.07
Sum	100.00	100.00	100.00	100.00	100.00	100.00	100.00	100.00
DAI	10.85	1.81	0.65	0.21	0.27	0.07	0.04	0.03

Table 10 (*continued*)

Characteristic	Rice husks	Switchgrass	Corn cobs	Plum pits (weathered)	Marine macroalgae	Beech wood chips	Walnut shells	Sunflower shells
Reference data ([1,2] and references therein)								
VM (db)	62.8	80.4	81.2	80.8	50.5	82.0	59.3	76.0
FC (db)	19.2	14.5	16.8	17.8	25.9	17.2	37.9	20.9
A (db)	18.0	5.1	2.0	1.4	23.6	0.8	2.8	3.1
Sum	100.0	100.0	100.0	100.0	100.0	100.0	100.0	100.0
C (daf)	49.3	49.6	47.8	49.9	41.7	47.2	49.8	50.4
O (daf)	43.6	43.4	45.6	42.4	44.3	46.6	42.4	42.9
H (daf)	6.1	6.1	5.9	6.7	6.0	6.1	6.2	5.5
N (daf)	0.8	0.7	0.5	0.9	2.1	0.1	1.4	1.1
S (daf)	0.08	0.11	0.01	0.08	2.51	0.01	0.09	0.03
Cl (daf)	0.12	0.08	0.23	0.01	3.34	0.01	0.15	0.10
Sum	100.00	99.99	100.04	99.99	99.95	100.02	100.04	100.03
Cel (daf)	43.8	48.7	48.1	23.7	28.5	45.2	28.1	56.5
Hem (daf)	31.6	38.4	37.2	22.0	65.5	32.7	26.6	28.0
Lig (daf)	24.6	12.9	14.7	54.3	6.0	22.1	45.3	15.5
Sum	100.0	100.0	100.0	100.0	100.0	100.0	100.0	100.0
Ext (daf)	6.6	8.0	7.0	5.4	15.1	1.1	2.7	2.6

Abbreviations: A, ash yield; AFT, ash-fusion temperature; Cel, cellulose; daf, dry ash-free basis; DAI, detrital/authigenic index (Si + Al + Fe + Na + Ti oxides/Ca + Mg + Mn + K + P + S + Cl oxides); db, dry basis; DTA, differential-thermal analysis; DWR, dry water-soluble residue; Ext, extractives; FC, fixed carbon; Hem, hemicellulose; HTA, high-temperature ash; Lig, lignin; VM, volatile matter.

then gradual cooling to ambient temperature was carried out. The holding time used is based on the former investigations [20,376,377,396,397] that found a time interval of ⩾30 min to be entirely sufficient to achieve equilibrium in the system. The prolonged holding time and slow cooling rate used were selected in order to accomplish a high degree of crystallinity for better XRD detections in the HTAs produced. Breaking of the ceramic crucibles and gentle handpicking under a binocular microscope were applied to separate the slag formed from the fused material at the maximum temperatures. Despite that, a few fine ceramic particles from the crucibles were observed microscopically as contaminants in BC, MM, PP and SS slags. These contaminants were identified as mullite, plagioclase and quartz, and probably some leucite by XRD for these four samples heated at 1300 °C. Additionally, DTA and TGA analyses were conducted using a Stanton Redcroft STA 760 apparatus. These experiments were carried out for 10–20 mg of biomass samples and their HTAs produced at 500 °C/2 h. The samples were gradually heated in corundum crucibles from ambient temperature to 1400 °C under oxidising conditions with a flow rate of air of 30 ml min^{-1} and a heating rate of 10 °C min^{-1}. The thermally treated HTAs are defined below as ashes and slags.

Dry, water-soluble residues (DWRs) were isolated from the biomass samples by evaporation and precipitation of the water-soluble solutions leached. The leachates from this extraction procedure were generated from 10 g of biomass samples placed in glass containers with 100 ml of distilled water and soaked for 24 h at ambient temperature. The suspensions were periodically stirred and finally decanted and filtered. The pH and electrical conductivity were measured in the generated water solutions by a bench pH-mV-conductivity meter PC 5000L (VWR International Ltd). Then the leachates were placed in a drying oven at 80 °C for evaporation and crystallisation giving DWRs. These leaching and precipitation procedures are similar to those applied for coals [398,399] and refuse-derived fuels [52].

The contents of elements in BAs (500 °C/2 h) were determined by inductively coupled plasma-mass spectrometry (ICP-MS), laser ablation ICP-MS (LA-ICP-MS) and SEM-EDX. The ICP-MS and LA-ICP-MS investigations were carried out, respectively, following:

(1) Acid digestion of the samples by HCl, HNO_3 and HF and subsequent measurement of the solutions (for Mn) by Perkin Elmer ELAN DRC-e mass spectrometer; and
(2) Preparation of discs after fusion of the samples with $Li_2B_4O_7$ at 1000 °C and subsequent measurement of the glass discs (for Al, Ca, Fe, K, Mg, Na, P, Si and Ti) by the above apparatus combined with New Wave UP193FX excimer laser ablation system. NIST SRM glasses 610 and 612 were used as external calibration standards.

The contents of S and Cl in the above ashes were determined by SEM-EDX of carbon coated powder material. The elemental spectrum of an area has been taken for all finely ground samples under identical conditions (area of 160 × 250 μm, magnification of 370× and accelerating voltage of 15 kV) using internal standards.

3. Results and discussion

3.1. General considerations about composition of biomass and biomass ash

The chemical and phase-mineral composition of biomass [1,2] and BA [1,3] has been characterised in detail recently and only some summarized data (Tables 2–7) and general comments are given herein.

Table 11
Phases and minerals identified in eight biomass samples and their high-temperature ashes (HTAs) produced at different combustion temperatures (°C).

Phase, mineral	Formula	Biomass	HTA-500	HTA-700	HTA-900	HTA-1100	HTA-1300	HTA-1500
Silicates								
Cristobalite (Cr)	SiO_2		●	●	●	●	●	●
Kalsilite (Ks)	$KAlSiO_4$		●	●	●	●		
K feldspars (KF)	$KAlSi_3O_8$		●					
Leucite (Le)	$KAlSi_2O_6$		●	●	●	●	●	
Opal (Op)	$SiO_2{\cdot}nH_2O$	●						
Plagioclases (Pl)	$NaAlSi_3O_8$–$CaAl_2Si_2O_8$		●	●?	●?	●		
Quartz (Q)	SiO_2		●	●	●	●	●	●
Tridymite (Tr)	SiO_2				●	●	●	●
Oxides and hydroxides								
Lime (L)	CaO			●	●	●		
Periclase (Peri)	MgO		●	●	●	●		
Portlandite (Port)	$Ca(OH)_2$		●	●	●	●	●	
Phosphates								
Apatite (Ap)	$Ca(PO_4)_3(Cl,F,OH,CO_3)$		●	●	●	●	●	
Whitlockite (Wl)	$Ca_3(PO_4)_2$		●	●	●			
Sulphates								
Anhydrite (A)	$CaSO_4$		●	●	●	●		
Arcanite (Arc)	K_2SO_4	●	●	●	●	●		
Gypsum (G)	$CaSO_4.2H_2O$	●?	●					
Picromerite (Pm)	$K_2Mg(SO_4)_2.6H_2O$		●					
Carbonates and bicarbonates								
Butschliite (Bu)	$K_2Ca(CO_3)_2$		●	●	●			
Dolomite (D)	$CaMg(CO_3)_2$		●?					
Fairchildite (F)	$K_2Ca(CO_3)_2$		●	●	●			
Calcite (Cc)	$CaCO_3$	●	●	●	●	●	●	
Kalicinite (K)	$KHCO_3$	●	●	●	●	●		
Magnesite rich in Fe (MFe)	$(Mg,Fe)CO_3$	●?						
Natrite (N)	Na_2CO_3		●					
Natrofairchildite (NF)	$Na_2Ca(CO_3)_2$		●					
Chlorides								
Halite (Ha)	NaCl	●	●	●	●			
Sylvite (Sy)	KCl	●	●	●	●			
Nitrates								
Ca nitrate hydrate (CaNH)	$Ca(NO_3)_2.2H_2O$	●						
Nitrocalcite (NCc)	$Ca(NO_3)_2.4H_2O$	●						
Other inorganic phases								
Inorganic amorphous material (non-glass and glass) (IAM)		●	●	●	●	●	●	●
Glass				●	●	●	●	●
Organic phases								
Char			●	●	●	●?	●?	●?
Organic matter (cellulose, hemicellulose, lignin) (OM)		●						
Organic minerals								
Weddelite (Wd)	$Ca(CO_2)_2.(H_2O)_2$	●						
Whewellite (Wh)	$Ca(CO_2)_2{\cdot}H_2O$	●						

Biomass is a contemporaneous (non-fossil) and complex biogenic organic–inorganic solid product generated by natural and anthropogenic (technogenic) processes, and comprises: (1) natural constituents originated from growing land- and water-based vegetation via photosynthesis or generated via animal and human food digestion; and (2) technogenic products derived via processing of the above natural constituents. The overall classification of biomass varieties as fuel resources can be divided preliminary and roughly into several groups and sub-groups according to their biological diversity, source and origin (Table 1). Biomass, similar to solid fossil fuels, is a complex heterogeneous mixture of OM (structural ingredients and organic minerals) and, to a lesser extent, IM (minerals, mineraloids and amorphous material), containing various intimately associated solid and fluid phases with different contents and origin. The main structural organic components in biomass are cellulose, hemicellulose and lignin and these matrices contain in addition various major, minor or accessory organic and inorganic phases (Table 2). The phases in biomass originate from natural (authigenic and detrital) and technogenic processes during pre-syngenesis, syngenesis, epigenesis and post-epigenesis of biomass according to the main formation process and place, time and mechanism of phase formation (Table 3).

BA is the solid residue that results from the combustion of biomass and includes: (1) laboratory produced low-temperature ash (LTA) in oxygen plasma at 100–250 °C; (2) laboratory generated HTA in air normally above 500 °C and at regulated temperatures; (3) industrially produced bottom ash (from dry-ash discharge boilers) or slag (from melt discharge boilers); and (4) industrially generated fly ash (from flue gas discharge systems); as the last two ash types are produced in combustion installations at temperatures commonly between 800 and 1600 °C. The laboratory HTAs and industrial ashes are formed under different conditions; however, they show similar ash formation mechanisms and phase-mineral transformations, despite some peculiarities, as described for coal ashes [377].

BA is a complex inorganic–organic mixture with polycomponent, heterogeneous and variable composition and particle morphology, and contains intimately associated solid, liquid and gaseous phases

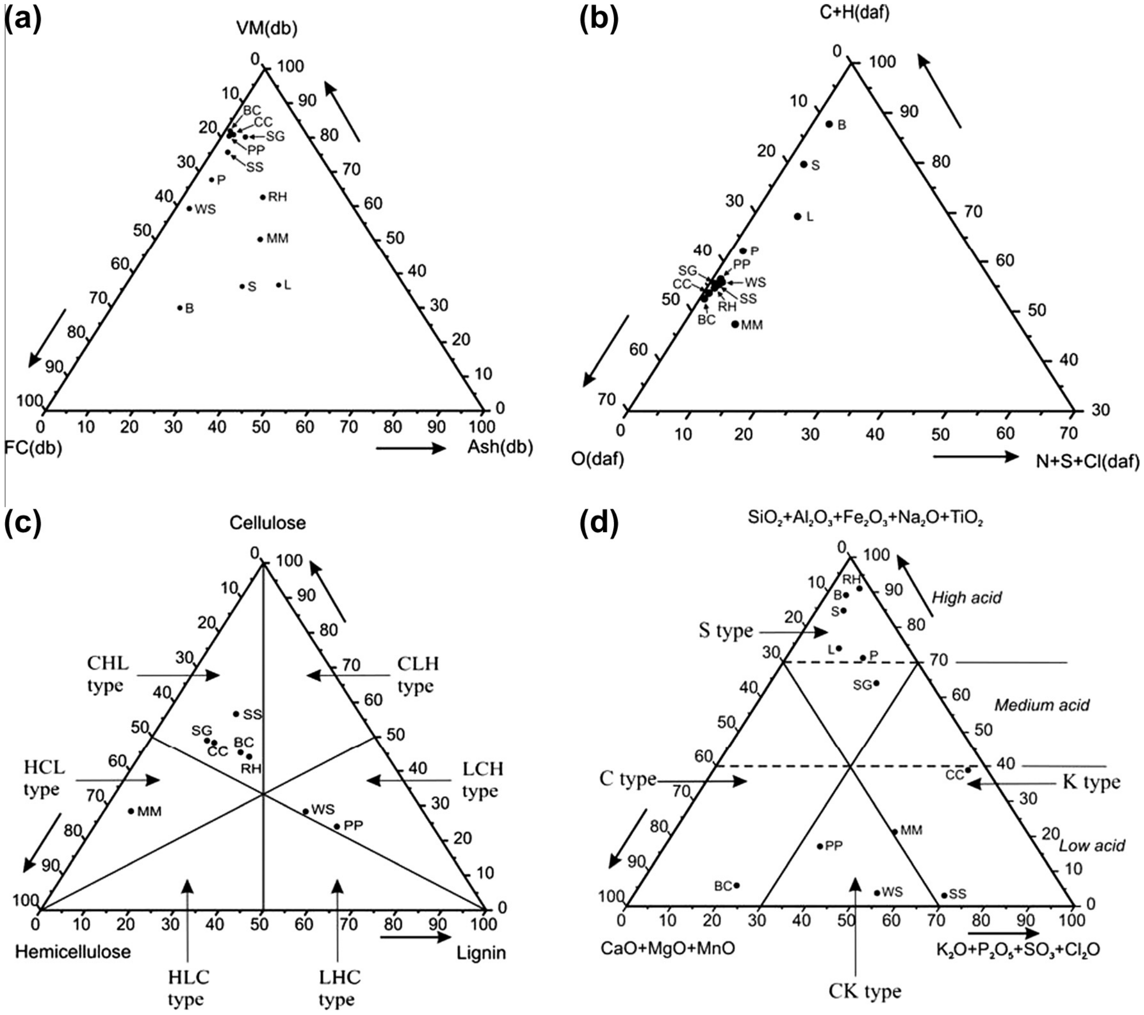

Fig. 1. Positions of eight biomass varieties in some classification systems based on data from: (a) proximate; (b) ultimate; (c) structural; and (d) ash analyses, wt.%. Abbreviations: B, bituminous coal; BC, beech wood chips; CC, corn cobs; daf, dry, ash-free basis; db, dry basis; FC, fixed carbon; L, lignite; MM, marine macroalgae; P, peat; PP, plum pits; RH, rice husks; S, sub-bituminous coal; SG, switchgrass; SS, sunflower shells; VM, volatile matter; WS, walnut shells.

(Table 4) with different contents and origin (Table 5). The composition of BA depends on many factors including: (1) biomass resource (type of biomass, plant species or part of plants, growing processes and conditions, age of the plants, fertiliser and pesticide doses used, harvesting time, collection technique, transport, storage, pollution, processing, others); (2) biomass combustion (fuel preparation, combustion technology and conditions, collection and cleaning equipment); and (3) transport and storage of BA. Therefore, BAs have highly variable chemical and phase-mineral composition and properties and these characteristics are more changeable and differ significantly in comparison with those of coal ashes (Tables 6 and 7 and Figs. 1 and 2).

The chemical composition of BA comprises: (1) major (>1%); (2) minor (1–0.1%); and (3) trace (<0.1%) elements; according to their elemental concentrations, where the major and minor elements are mostly expressed as oxides (Table 6). The oxide contents in BA are normally $SiO_2 > CaO > K_2O > P_2O_5 > Al_2O_3 > MgO > Fe_2O_3 > SO_3 > Na_2O > MnO > TiO_2$ (based on mean values in Table 6). BA from natural biomass is commonly enriched in Mn > K > P > Cl > Ca > Na > Mg and depleted in Al > Ti > Fe > Si > S in comparison with coal ash. The bulk chemical composition of biomass and BA is an important characteristic; however, it is insufficient for a reliable explanation of elemental behaviour during biomass combustion. The abundance, origin and performance of modes of element occurrence (minerals and phases) in biomass and BA are needed to fully understand this elemental behaviour.

The phase-mineral composition of BA includes: (1) mostly IM composed of non-crystalline (amorphous) and crystalline to semi-crystalline (mineral) constituents; (2) subordinately OM consisting of char and organic minerals; and (3) some fluid matter comprising moisture and gas and gas–liquid inclusions associated with both IM and OM (Tables 4 and 7).

The phases and minerals in BA can be divided into: (1) forming (>10%); (2) major (1–10%); (3) minor (0.1–1%); and (4) accessory (<0.1%); based on their contents (Table 7). The forming and major species identified in BAs normally include glass, sylvite, calcite, leucite, K–Ca silicate, char, feldspars, quartz, anhydrite, ankerite, kaolinite, siderite, cristobalite, arcanite, hematite, illite, lime, fairchildite, hydroxylapatite, merwinite, periclase, glaserite, larnite and portlandite. The extremely large variations of phase-mineral composition of BAs are mostly due to the highly variable contents of bulk IM and different genetic classes of IM in diverse biomass varieties [3].

BA is composed of original (primary) or newly formed (secondary and tertiary) inorganic and organic solid phases generated from natural (authigenic and detrital) and technogenic inorganic, organic and fluid matter during biomass combustion. Therefore, the phases and minerals in BA can be classified by origin as: (1) pri-

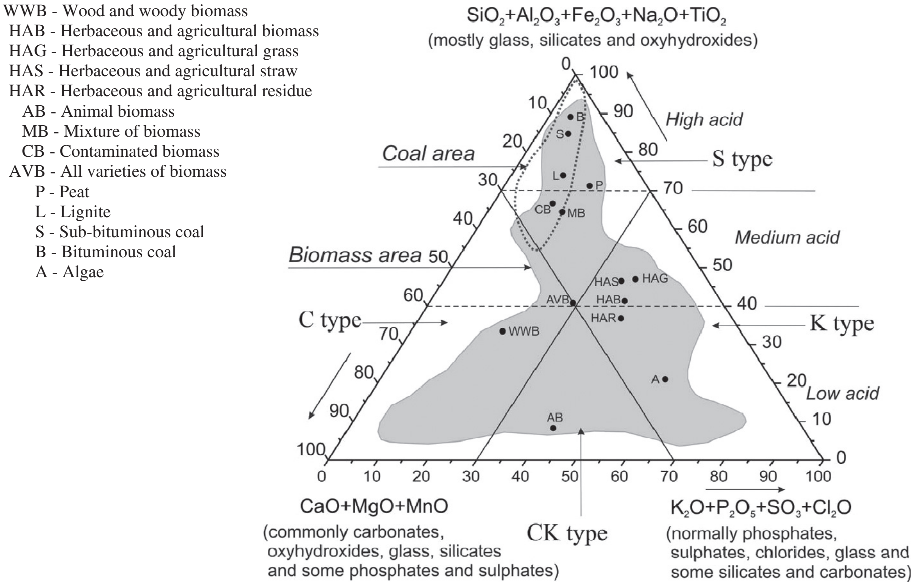

Fig. 2. Position areas of 86 biomass varieties and 38 solid fossil fuels in the chemical classification system of biomass ash, wt.%.

mary, namely pre-existing or original minerals and phases in biomass that have undergone no phase transformations during combustion (mostly refractory silicates, oxyhydroxides and phosphates); (2) secondary such as new phases formed during combustion process (species from all mineral classes plus glass and char); and (3) tertiary, namely new minerals or phases formed during transport and storage of BA (mainly carbonates and hydroxides) (Tables 5 and 7).

The phases and minerals identified in BA include approximately 291 species (Table 7) in contrast to 188 species found in coal ash [383]. Most of the minerals and phases identified in coal ashes were also found in BAs [3]. However, many mineral species among Ca–K–Mn silicates, Ca–Al–Mn oxides, K–Na–Ca chlorides and K–Ca–Mg–Na carbonates, sulphates and phosphates were normally not identified in coal ashes. The reason for that could be the enrichment of elements such as Ca, Cl, K, Mg, Mn, Na and P in BAs compared to coal ashes. In contrast, typical Si-, Al-, Fe- and Ti-bearing minerals of coal ashes (quartz, clay and mica minerals, mullite, feldspars, Fe oxides and rutile), were not characteristic of many BAs probably due to limited contents of these elements in BAs [1,3].

It was emphasised that there is a big advantage if the biomass and BA classification systems are based on: (1) the identification and implementation of significant relationships between elemental concentrations; (2) combined chemical and phase-mineral associations; and especially (3) on an application approach for specification of the phases in biomass and BAs based on their origin. In this case the reasons for different problems or benefits during biomass processing can be systematically identified and explained [4].

3.2. General observations about behaviour of biomass during combustion

Summarized data from references and own studies concerning: (1) composition and characteristics of biomass and BA (Tables 1–6); (2) phases and minerals identified in BAs (Table 7); (3) melting point (MP) temperatures of inorganic phases and minerals identified or assumed in biomass and BA (Table 9); (4) processes responsible for ash formation (Table 5); and (5) physico-chemical formations, transformations and reactions during biomass combustion (Table 8); are given systematically herein. This information provides a sound foundation for the database that can be used for an initial and reliable characterization of biomass during combustion.

The reference investigations show that many findings about the behaviour of various components during thermo-chemical conversion of biomass are based only on theoretical thermodynamic, equilibrium and stoichiometric calculating tools (modelling) of chemical databases and programs such as ChemApp, ChemSage, ChemSheet, DICTRA, FACT-SAGE, FACT-Win, GFEDBASE, HSC Chemistry, JANAF, MINGTSYS, MTDATA, SGTE, SOLGASMIX, Thermo-Calc and others [32,59,83,97,98,127,129,142,148,174,177,207,209,214,223,225,232,235,271,301,314,341,366,368,369,371]. The equilibrium calculation is used to determine thermodynamically stable chemical and physical forms (mineral species and phases) in the system during heating. For that purpose, parameters such as the elemental composition of the fuel and air, temperature and pressure have been entered in the system. The calculations are performed by minimization of the total Gibb's free energy for the system under a mass balance constraint. Although the equilibrium analysis is a useful tool to predict the stable species during the thermo-chemical process, there are numerous very serious disadvantages and limitations of the method and they include important critical assumptions and decisions before and during the actual calculation such as:

- Accuracy and consistency of the thermodynamic data for the phases and species involved (problems with input of elements, stoichiometric compounds, isomorphism and variable composition of phases and minerals, polymorphic minerals, unreacted original phases, post-combustion phase formations, others).
- Temperature must be high enough or the residence time for species should be long enough to reach the thermodynamic equilibrium in the system.
- Assumption that all elements are available for reaction (perfect mixing).
- Kinetic limitations are ignored.
- Gas phase is considered ideal.
- All condensed phases are pure.
- No organic association of elements was included.

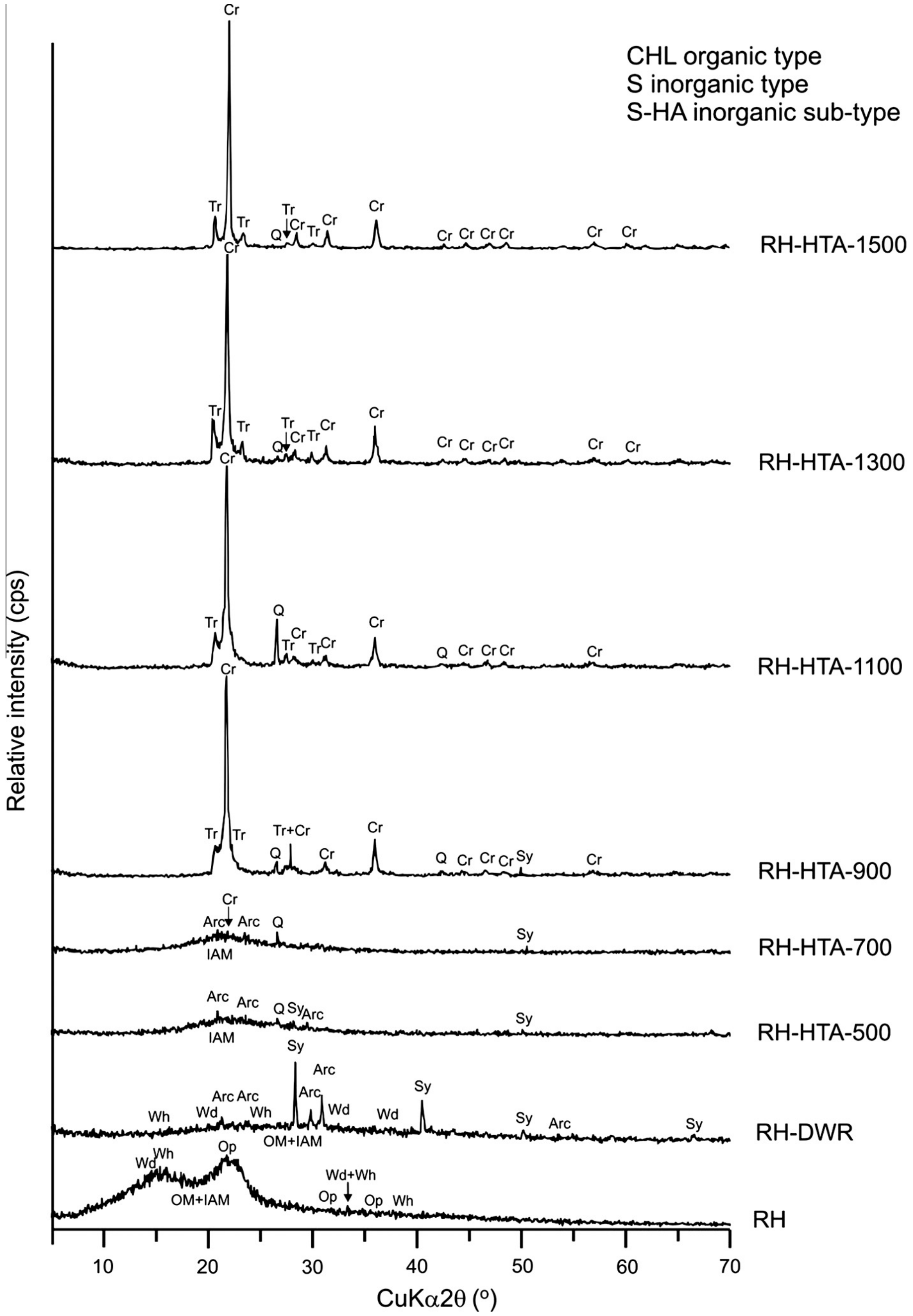

Fig. 3. XRD patterns of rice husks (RH), dry water-soluble residue (DWR) from RH and high-temperature ashes (HTAs) of RH generated at 500 °C/2 h, 700 °C/1 h, 900 °C/1 h, 1100 °C/1 h, 1300 °C/1 h and 1500 °C/1 h. Abbreviations: Arc, arcanite (K_2SO_4); Cps, counts per second; Cr, cristobalite (SiO_2); IAM, inorganic amorphous material (non-glass and glass); OM, organic matter; Op, opal ($SiO_2 \cdot nH_2O$); Q, quartz (SiO_2); Sy, sylvite (KCl); Tr, tridymite (SiO_2); Wd, weddelite ($Ca(CO_2)_2(H_2O)_2$); Wh, whewellite ($Ca(CO_2)_2 \cdot H_2O$).

- Complications with liquid, condensed and glass phase determinations and overestimated formation of gaseous and liquid phases; and finally
- Difficulties when the calculation results are compared with those of real combustion, gasification or pyrolysis systems.

Most of the above listed limitations and problems have been mentioned or explained elsewhere [59,83,174,225,235,314,368]. Therefore, these indirect investigations may be quite unrealistic for actual predictions of phases in a multicomponent system under non-equilibrium conditions and many of these studies demonstrate undoubtedly very serious prediction problems (see for example [369] among others). Such equilibrium and stoichiometric calculations can be used only to provide a preliminary prediction. Finally, this subsidiary procedure cannot replace the most important and real approach, namely direct (input, output) phase studies of the systems.

The reference investigations also show that TGA data alone for biomass are frequently used to evaluate the combustion behaviour of OM and this is a serious omission. Such data without parallel DTA and other phase investigations cannot be applied to describe the actual thermal behaviour of OM because some reasons for weight losses in the system remain unspecified. For instance, the weight losses related to combustion of OM (exothermic effects) also associate with: (1) decomposition, dehydration and dehydroxylation of certain carbonates, sulphates, hydroxides and silicates

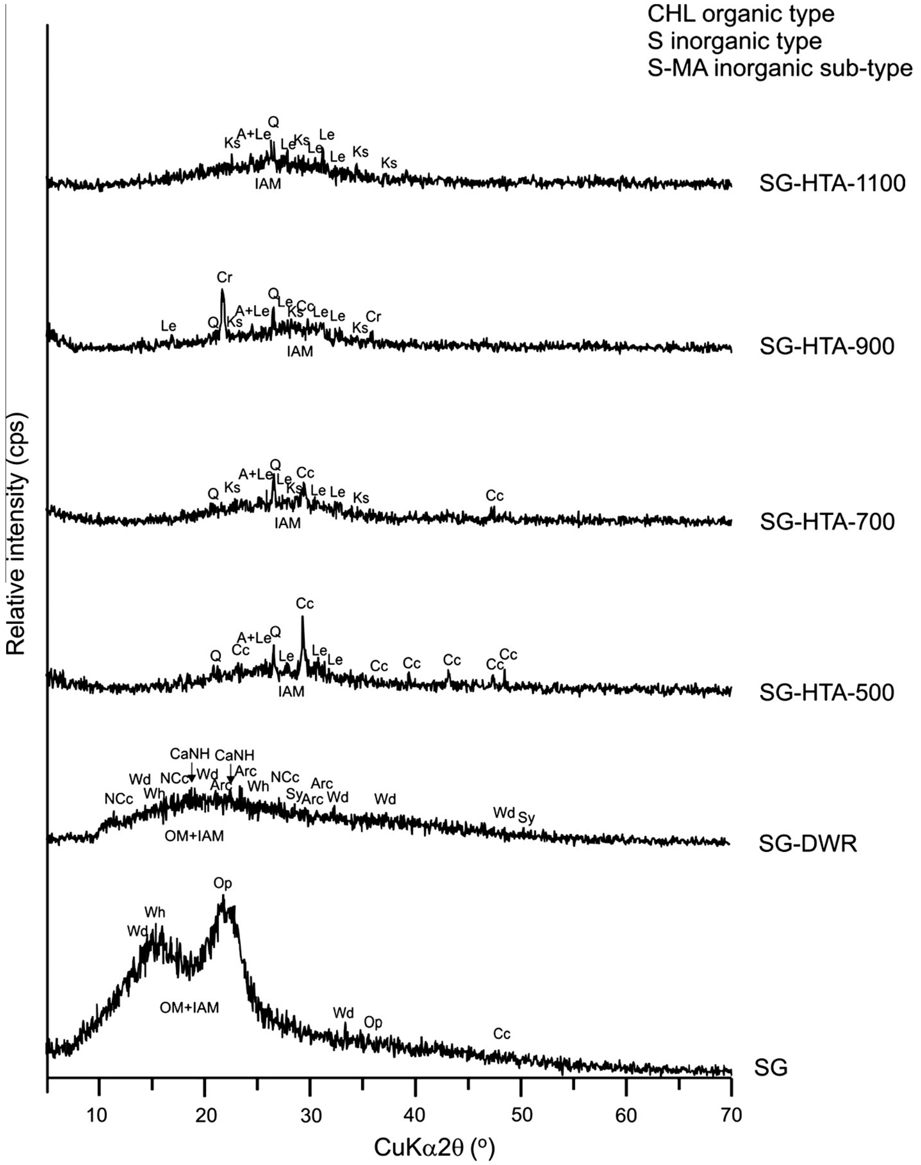

Fig. 4. XRD patterns of switchgrass (SG), dry water-soluble residue (DWR) from SG and high-temperature ashes (HTAs) of SG generated at 500 °C/2 h, 700 °C/1 h, 900 °C/1 h and 1100 °C/1 h. Abbreviations: A, anhydrite ($CaSO_4$); Arc, arcanite (K_2SO_4); CaNH, Ca nitrate hydrate ($Ca(NO_3)_2.2H_2O$); Cc, calcite ($CaCO_3$); Cps, counts per second; Cr, cristobalite (SiO_2); IAM, inorganic amorphous material (non-glass and glass); Ks, kalsilite ($KAlSiO_4$); Le, leucite($KAlSi_2O_6$); NCc, nitrocalcite ($Ca(NO_3)_2.4H_2O$); OM, organic matter; Op, opal ($SiO_2{\cdot}nH_2O$); Q, quartz (SiO_2); Sy, sylvite (KCl); Wd, weddelite ($Ca(CO_2)_2.(H_2O)_2$); Wh, whewellite ($Ca(CO_2)_2{\cdot}H_2O$).

(endothermic reactions); (2) oxidation of sulphides and hydration and hydroxylation of some oxides (exothermic effects); and (3) melt evaporation (endothermic reactions); which can occur in the same temperature interval as for OM burning.

The present study explains the behaviour of OM and IM and ash formation for eight biomass varieties during their combustion at different temperatures. The XRD patterns of these biomass samples and their water-soluble residues, as well as biomass ashes (500 °C) thermally treated up to 1500 °C are illustrated in Figs. 3–10. The DTA-TGA profiles of the biomass samples and their ashes (500 °C) heated up to 1400 °C are shown in Figs. 11–18. The chemical composition of the eight biomass HTAs (500 °C) and the phases and minerals identified in them (500–1500 °C) are given in Tables 10 and 11, respectively. It can be seen that their chemical composition is highly variable and numerous original (primary) and newly formed (secondary and tertiary) minerals or phases occur in HTAs as their origin is related to various organic and inorganic species identified in biomass (see below). Some processes such as: (1) fragmentation (disintegration) of particles (500 °C); (2) initial (700–900 °C), significant (700–1100 °C) and intensive (700–1300 °C) agglomeration or occasionally swelling of particles; (3) initial (700 °C), extensive (900–1100 °C) and complete (1100–1500 °C) fusion of particles or minerals with different melting points; (4) various new phase crystallizations (500–1500 °C); and (5) melt/glass formation (700–1500 °C); were observed microscopically in BAs.

It was found that the DTA-TGA profiles of the biomass varieties studied (Figs. 11–18 with index (a)) show very similar combustion behaviour for OM despite their highly variable phase (structural components) and chemical composition. For example, the samples reveal common and similar transformations such as:

(1) Loss of adsorbed water (endothermic effects at 57–92 °C accompanied by some mass losses).

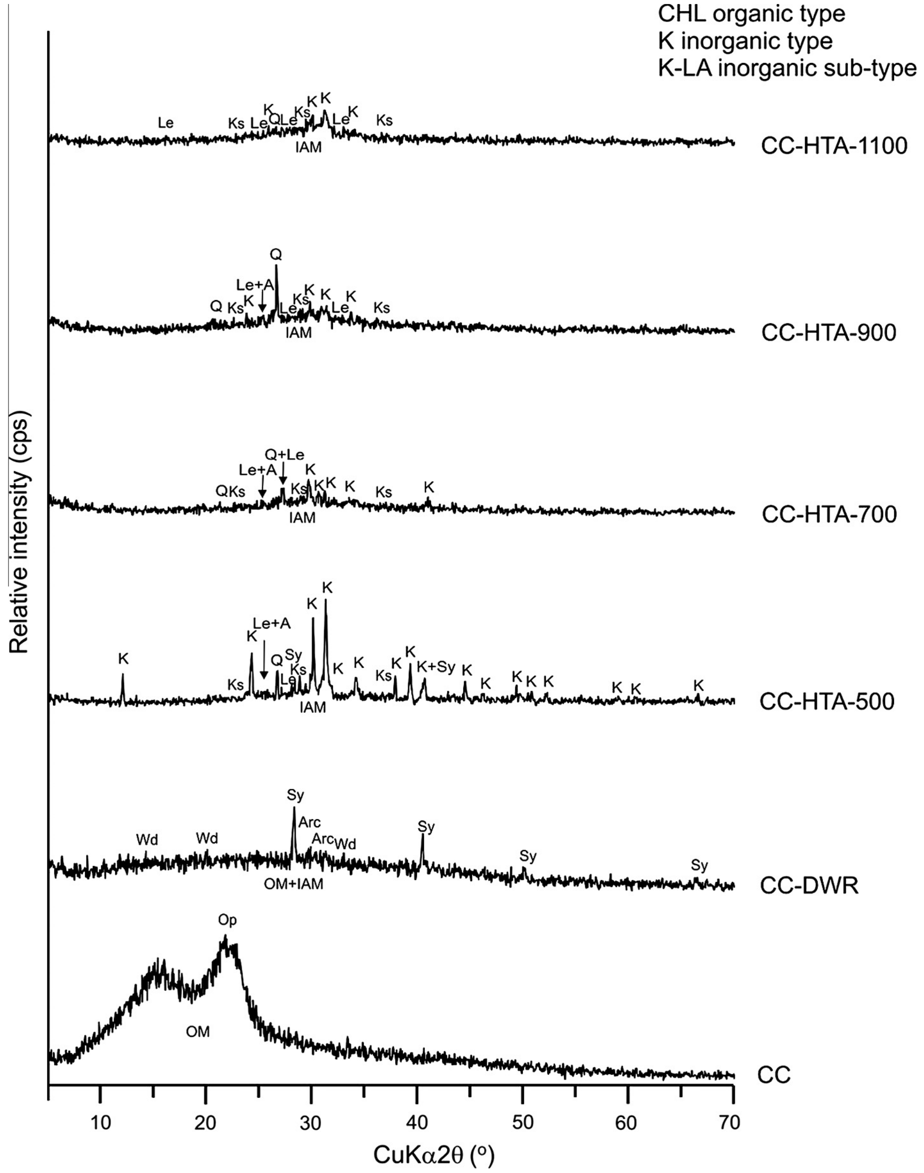

Fig. 5. XRD patterns of corn cobs (CC), dry water-soluble residue (DWR) from CC and high-temperature ashes (HTAs) of CC generated at 500 °C/2 h, 700 °C/1 h, 900 °C/1 h and 1100 °C/1 h. Abbreviations: A, anhydrite ($CaSO_4$); Arc, arcanite (K_2SO_4); Cps, counts per second; IAM, inorganic amorphous material (non-glass and glass); K, kalicinite ($KHCO_3$); Ks, kalsilite ($KAlSiO_4$); Le, leucite($KAlSi_2O_6$); OM, organic matter; Op, opal ($SiO_2{\cdot}nH_2O$); Q, quartz (SiO_2); Sy, sylvite (KCl); Wd, weddelite ($Ca(CO_2)_2(H_2O)_2$).

(2) OM combustion (exothermic effects between 200 and 650 °C accompanied by intensive mass losses).
(3) Burning of some residual char (exothermic effects commonly between 650 and 850 °C accompanied by some mass losses).
(4) Complex phase transformations related to decomposition of various carbonates, sulphates and phosphates, formation of silicates, polymorphic transformations, melting of phases and other processes up to 1300–1400 °C accompanied or not by mass loss.

In contrast to biomass samples, the DTA-TGA profiles of BAs produced at 500 °C (Figs. 11–18 with index (b)) show very distinct and complex transformation behaviour due to their highly variable inorganic composition (Tables 10 and 11). For instance, the samples reveal:

(1) Loss of adsorbed water (endothermic effects at 69–129 °C accompanied by some mass losses).
(2) Burning of the residual char (exothermic effects mainly between 300 and 850 °C accompanied by some mass losses).
(3) Calcite decomposition (endothermic reactions at 538–896 °C accompanied by intensive mass losses).

Different phase transformations and mineral crystallizations related to OM, silica minerals, leucite, lime, periclase, portlandite, anhydrite, arcanite, calcite, whitlockite, apatite, glass and other phases and minerals in BAs can be seen on XRD patterns with increasing ashing temperatures (Figs. 3–10). It should be noted that the detection of most phase transformations (especially for IM) are impossible only by DTA-TGA investigations of biomass. Their identifications also require an incineration of OM at low temperatures (500 °C in the present study) and the subsequent investigation of ash residue by DTA-TGA and other methods at higher temperatures (up to 1500 °C in the present study). Furthermore, some future investigations of biomass LTA can extract information

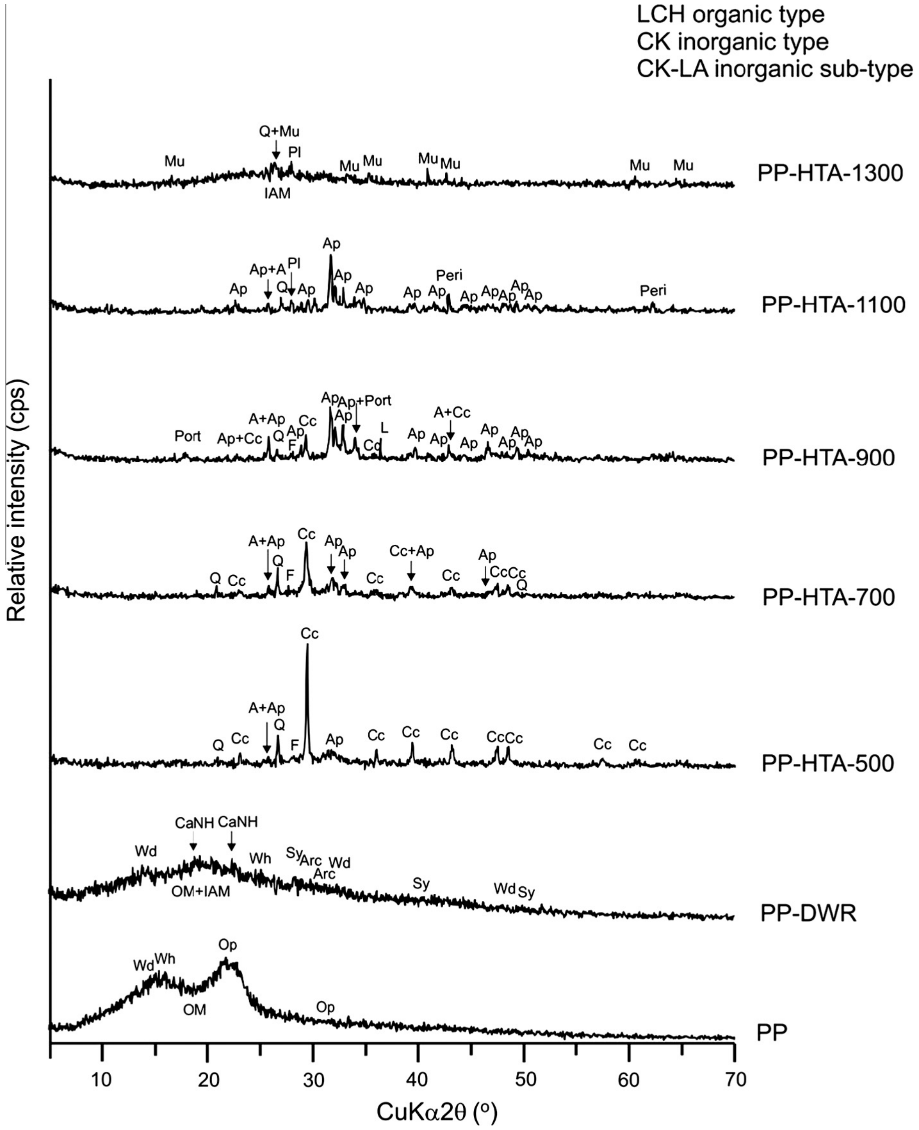

Fig. 6. XRD patterns of plum pits (PP), dry water-soluble residue (DWR) from PP and high-temperature ashes (HTAs) of PP generated at 500 °C/2 h, 700 °C/1 h, 900 °C/1 h, 1100 °C/1 h and 1300 °C/1 h. Abbreviations: A, anhydrite ($CaSO_4$); Ap, apatite ($Ca(PO_4)_3(Cl,F,OH)$); Arc, arcanite (K_2SO_4); CaNH, Ca nitrate hydrate ($Ca(NO_3)_2.2H_2O$); Cc, calcite ($CaCO_3$); Cps, counts per second; F, fairchildite ($K_2Ca(CO_3)_2$); IAM, inorganic amorphous material (non-glass and glass); L, lime (CaO); Mu, mullite ($Al_6Si_2O_{13}$); OM, organic matter; Op, opal ($SiO_2{\cdot}nH_2O$); Peri, periclase (MgO); Pl, plagioclases ($NaAlSi_3O_8$–$CaAl_2Si_2O_8$); Port, portlandite ($Ca(OH)_2$); Q, quartz (SiO_2); Sy, sylvite (KCl); Wd, weddelite ($Ca(CO_2)_2.(H_2O)_2$); Wh, whewellite ($Ca(CO_2)_2{\cdot}H_2O$). The occurrence of Q, Mu and Pl in the sample PP-HTA-1300 is a result of contamination from the broken ceramic crucible.

of some inorganic phase transformations even for the temperature interval between 200 and 500 °C.

The combustion temperature has a leading effect on the ash yield and qualitative and quantitative composition of ashes produced from different biomass varieties. For example, the reference investigations show that ash yields determined at 1000–1300 °C are 10–70% lower than those produced by LTA at 100–150 °C or HTA at 500–575 °C ([3] and references therein). The present study (Table 10) confirmed the above observations and reveals that the ash yields determined at 1100–1500 °C are 7–59% lower than those produced at 500 °C, namely MM (59%) > SS (44%) > WS (43%) > BC (39%) > CC (33%) > PP (29%) > SG (19%) > RH (7%). This order shows that minimum losses occur for the biomass varieties highly (RH, SG) and significantly (CC and PP) enriched in silica and silicates while maximum losses are typical for biomass varieties abundant commonly in Ca, Cl, Fe, K, Mg, Na, P, S, chlorides, sulphates, carbonates and phosphates (Table 10, Figs. 3–10 and [3]). These weight losses for biomass are normally higher than for coal and such differences are a result of some more intensive phase transformations (loss of adsorbed and combined water, combustion of volatile matter, decomposition of less stable minerals) and probably higher volatilization behaviour of certain mobile elements (Br, C, Cl, H, Hg, K, N, Se, S and other trace elements) from biomass phases in the higher temperature ranges [3,376,377].

The reference investigations also reveal that the particle size ([3] and references therein) and morphology (Table 4) of BAs are highly variable. For example, the size of biomass fly ash particles varies from 10–50 nm to more than 1–2 mm, but these powder materials are commonly very fine as their median size is predominantly below 10–100 μm. It was also found that the alkali chlorides and sulphates and some trace elements (for example, Pb and Zn) were normally enriched in the finest fly ash fraction (<1 μm) originated from volatilized elements that nucleate to form new particles or condense on existing particles during the flue gas cooling. On the other hand, the coarser ash fraction (>1 μm) is dominated by components containing non-volatile elements such as Ca, Si, Mg, Al, Fe, P and Mn that

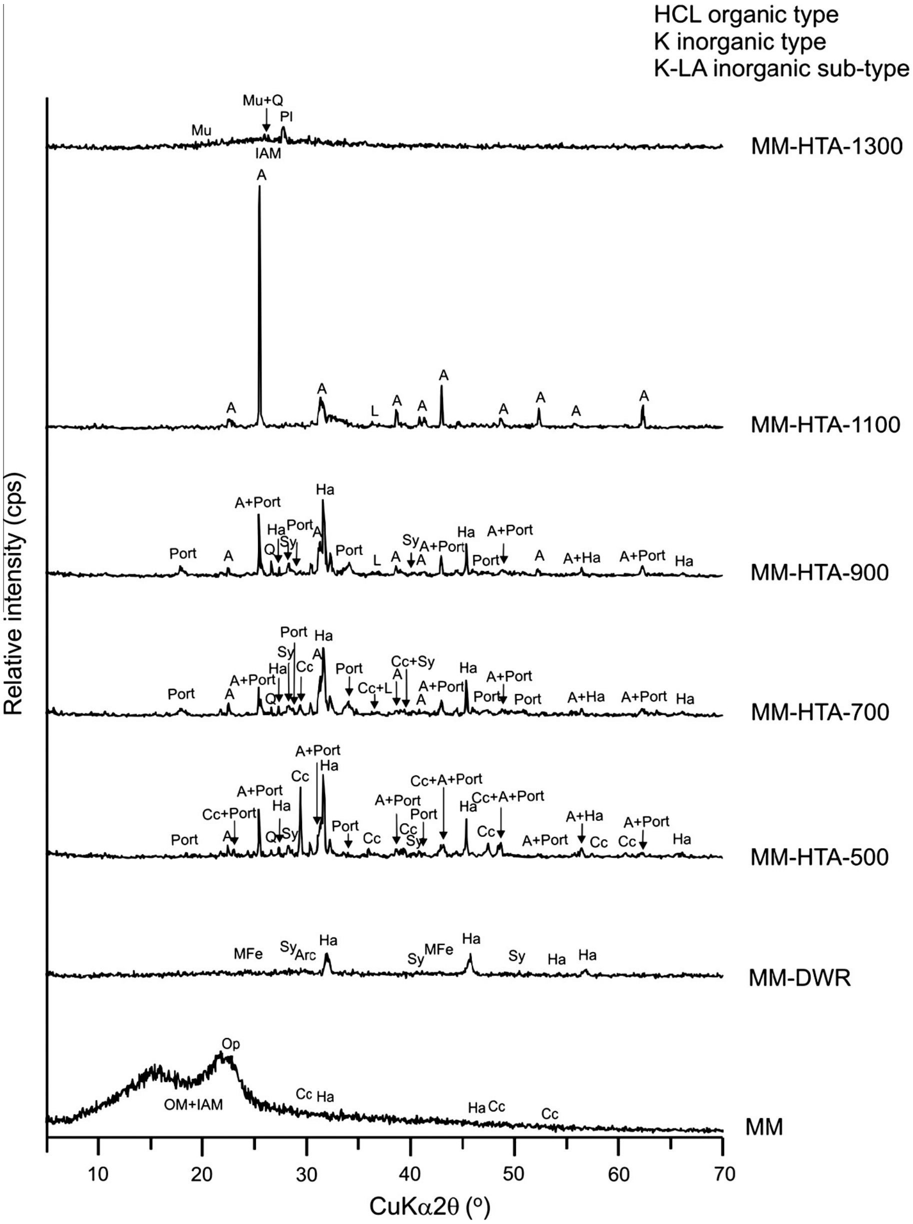

Fig. 7. XRD patterns of marine macroalgae (MM), dry water-soluble residue (DWR) from MM and high-temperature ashes (HTAs) of MM generated at 500 °C/2 h, 700 °C/1 h, 900 °C/1 h, 1100 °C/1 h and 1300 °C/1 h. Abbreviations: A, anhydrite ($CaSO_4$); Cc, calcite ($CaCO_3$); Cps, counts per second; Ha, halite (NaCl); IAM, inorganic amorphous material (non-glass and glass); L, lime (CaO); MFe, magnesite rich in Fe ($(Mg,Fe)CO_3$); Mu, mullite ($Al_6Si_2O_{13}$); OM, organic matter; Op, opal ($SiO_2{\cdot}nH_2O$); Pl, plagioclases ($NaAlSi_3O_8$–$CaAl_2Si_2O_8$); Port, portlandite ($Ca(OH)_2$); Q, quartz (SiO_2); Sy, sylvite (KCl). The occurrence of Q, Mu and Pl in the sample MM-HTA-1300 is a result of contamination from the broken ceramic crucible.

have remained in the solid and/or liquid phases during the combustion process. It was also identified that Ca-bearing minerals seemed to be commonly enriched in the size range 1–50 μm, while Si-bearing minerals were normally found in the largest particles (>10–50 μm) ([3] and references therein).

The present study demonstrates some important combustion trends. It was found that OM of different biomass varieties tends to show similar combustion behaviour, whereas IM of these biomass varieties has a tendency to reveal variable performance during burning. These preliminary observations also indicate that the thermal behaviour of IM and ash formation mechanisms of different BAs tend to be: (1) diverse between the inorganic “S”, “C”, “K” and “CK” types; and (2) similar within the inorganic types and subtypes; specified recently [1–3]. These very interesting observations will be discussed in detail in Part II of the present work.

3.3. Behaviour of organic matter during biomass combustion

3.3.1. Cellulose, hemicellulose and lignin

The reference investigations and numerous data collected for transformation of cellulose, hemicellulose and lignin during thermal treatment of biomass in oxidising and inert atmosphere are listed in Table 8. It should be noted that their transformation includes mostly decomposition (degradation) and subsequent oxidation due to the very high oxygen contents in natural biomass, namely 21–49% on dry, ash-free basis (daf) [1] in contrast to coal, normally 4–20% daf basis [400]. Therefore, the TGA, DTA and differential thermo-gravimetric curves observed for biomass have similar decomposition steps and mechanisms under both oxidising (air) and inert (N_2, Ar) atmosphere [164,207,209,347]. For example, it was emphasised that only the combustion stage is faster under

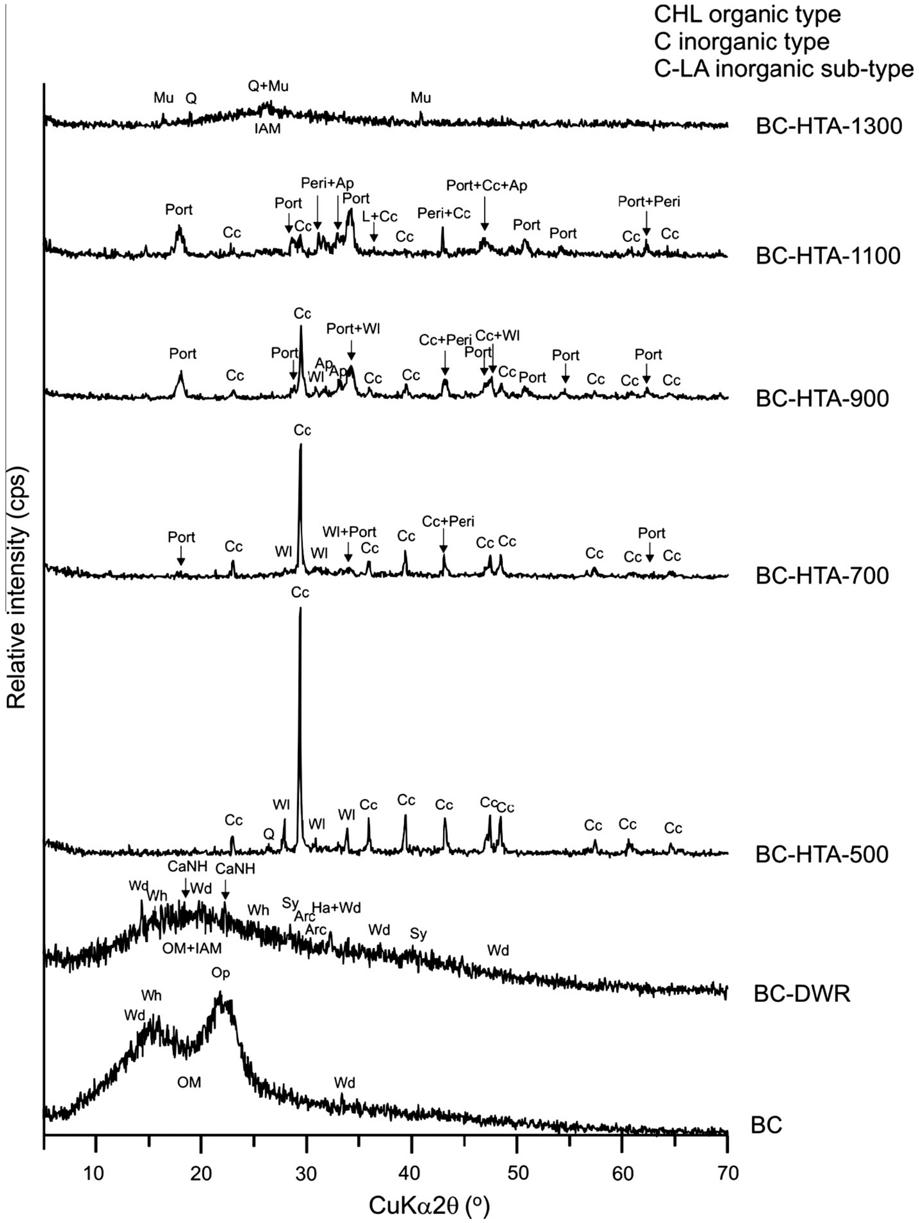

Fig. 8. XRD patterns of beech wood chips (BC), dry water-soluble residue (DWR) from BC and high-temperature ashes (HTAs) of BC generated at 500 °C/2 h, 700 °C/1 h, 900 °C/1 h, 1100 °C/1 h and 1300 °C/1 h. Abbreviations: Ap, apatite ($Ca(PO_4)_3(Cl,F,OH)$); Arc, arcanite (K_2SO_4); CaNH, Ca nitrate hydrate ($Ca(NO_3)_2{\cdot}2H_2O$); Cc, calcite ($CaCO_3$); Cps, counts per second; Ha, halite (NaCl); IAM, inorganic amorphous material (non-glass and glass); L, lime (CaO); Mu, mullite ($Al_6Si_2O_{13}$); OM, organic matter; Op, opal ($SiO_2{\cdot}nH_2O$); Peri, periclase (MgO); Port, portlandite ($Ca(OH)_2$); Q, quartz (SiO_2); Sy, sylvite (KCl); Wd, weddelite ($Ca(CO_2)_2{\cdot}(H_2O)_2$); Wh, whewellite ($Ca(CO_2)_2{\cdot}H_2O$); Wl, whitlockite ($Ca_3(PO_4)_2$). The occurrence of Q and Mu in the sample BC-HTA-1300 is a result of contamination from the broken ceramic crucible.

air than under inert atmosphere [164]. Hence, many findings related to the biomass combustion behaviour are also applicable for biomass pyrolysis, gasification and liquefaction. It is generally accepted that the biomass combustion process takes place in two steps: (1) combustion of cellulose and hemicellulose at 250–350 °C, which is greater for annual species (with lower lignin content); and (2) combustion process of lignin at 350–500 °C, which is greater for perennial species (with higher lignin content) [24]. Further, the DTA shoulder of the major combustion reaction for biomass is usually considered to arise from hemicellulose decomposition at lower temperatures, while the main peak at higher temperatures is considered to be mainly due to cellulose degradation [209]. However, the present study does not support the above observations and reveals that such simplified generalisations for the thermal behaviour of structural components of biomass cannot be applied universally for all biomass varieties.

The summarized reference data in the present study (Table 8) clearly show that the minimum, maximum and peak temperatures for decomposition/oxidation of the specific structural components are less informative. For example, these data reveal highly variable and even abnormal decomposition temperature ranges, namely: (1) 150–350 °C for hemicellulose; (2) 240–500 °C for cellulose; and (3) 160–900 °C for lignin. Thus, it is impossible to identify some highly definitive or even characteristic transformation temperatures for the specific structural components because such temperatures are strongly dependent on the biomass varieties studied. Therefore, the present observations are somehow not in accordance with widely accepted statements in the literature about

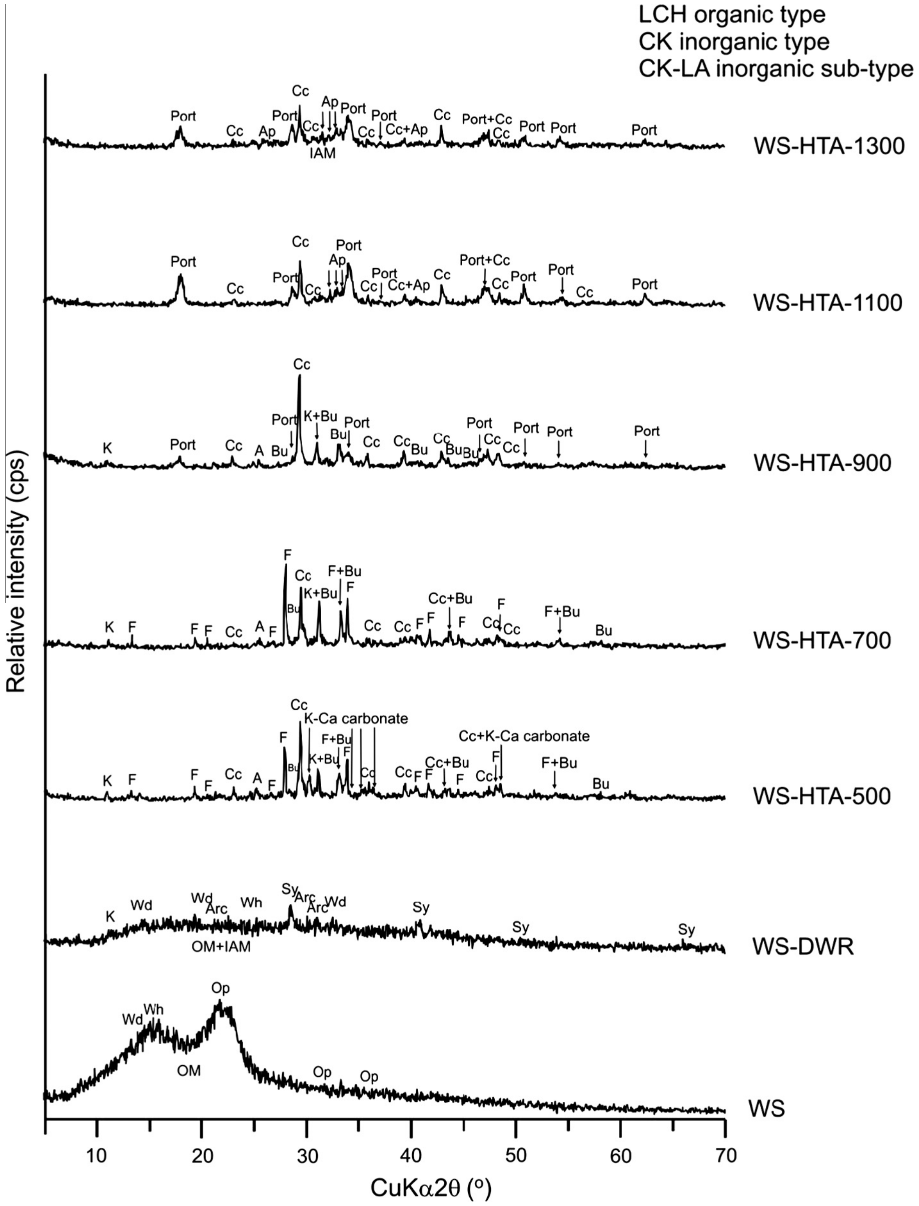

Fig. 9. XRD patterns of walnut shells (WS), dry water-soluble residue (DWR) from WS and high-temperature ashes (HTAs) of WS generated at 500 °C/2 h, 700 °C/1 h, 900 °C/1 h, 1100 °C/1 h and 1300 °C/1 h. Abbreviations: A, anhydrite ($CaSO_4$); Ap, apatite ($Ca(PO_4)_3(Cl,F,OH)$); Arc, arcanite (K_2SO_4); Bu, butschliite ($K_2Ca(CO_3)_2$); Cc, calcite ($CaCO_3$); Cps, counts per second; F, fairchildite ($K_2Ca(CO_3)_2$); IAM, inorganic amorphous material (non-glass and glass); K, kalicinite ($KHCO_3$); OM, organic matter; Op, opal ($SiO_2{\cdot}nH_2O$); Port, portlandite ($Ca(OH)_2$); Sy, sylvite (KCl); Wd, weddelite ($Ca(CO_2)_2{\cdot}(H_2O)_2$); Wh, whewellite ($Ca(CO_2)_2{\cdot}H_2O$).

some typical thermal transformations of specific structural components and they require more detailed considerations.

The present study of DTA profiles for eight biomass varieties (Figs. 11–18 with index (a)) show that the OM oxidation is characterised by large exothermic effects mostly between 200 and 650 °C and represented as two consecutive peaks with maximums at 324–351 °C and 425–520 °C. These two consecutive peaks have changeable heights as the first peak can be higher (RH and SG) or lower (BC, CC, MM, PP, SS and WS as PP peaks are almost equal) in heights. This observation indicates the greater reactivity of RH, SG and PP samples in comparison with other biomass varieties. The two major exothermic reactions are accompanied by two intensive mass losses according to TGA curves in Figs. 11–18 (with index (a)). It should also be stated that the DTA and TGA profiles are similar for all biomass samples despite their different organic types ("CHL", "LCH" and "HCL" in Fig. 1c) and highly variable contents of structural components (Table 10). The only exclusion is the algae sample (MM) having also an additional third and small exothermic peak with maximum at 782 °C and accompanied by some weight loss (Fig. 15a). This last very interesting observation is related to oxidation of some capsulated residual char (see below).

Several initial steps were undertaken for clarification of the thermal behaviour of individual structural components, namely: (1) the first and second exothermic peak temperatures from DTA; and (2) the first and second exothermic peak heights from DTA and the ratio between them; for the eight biomass samples were measured and calculated (Table 10). The results obtained were subjected to a correlation test to calculate correlation coefficient values (R^2) of these three parameters (Table 12) with contents of cellulose, hemicellulose and lignin plus many other characteristics listed in Table 10. Surprisingly, it was found that the above three parameters do not show very strong correlations with the structural components. The only exclusions are: (1) the significant positive correlation between lignin and the first exothermic peak

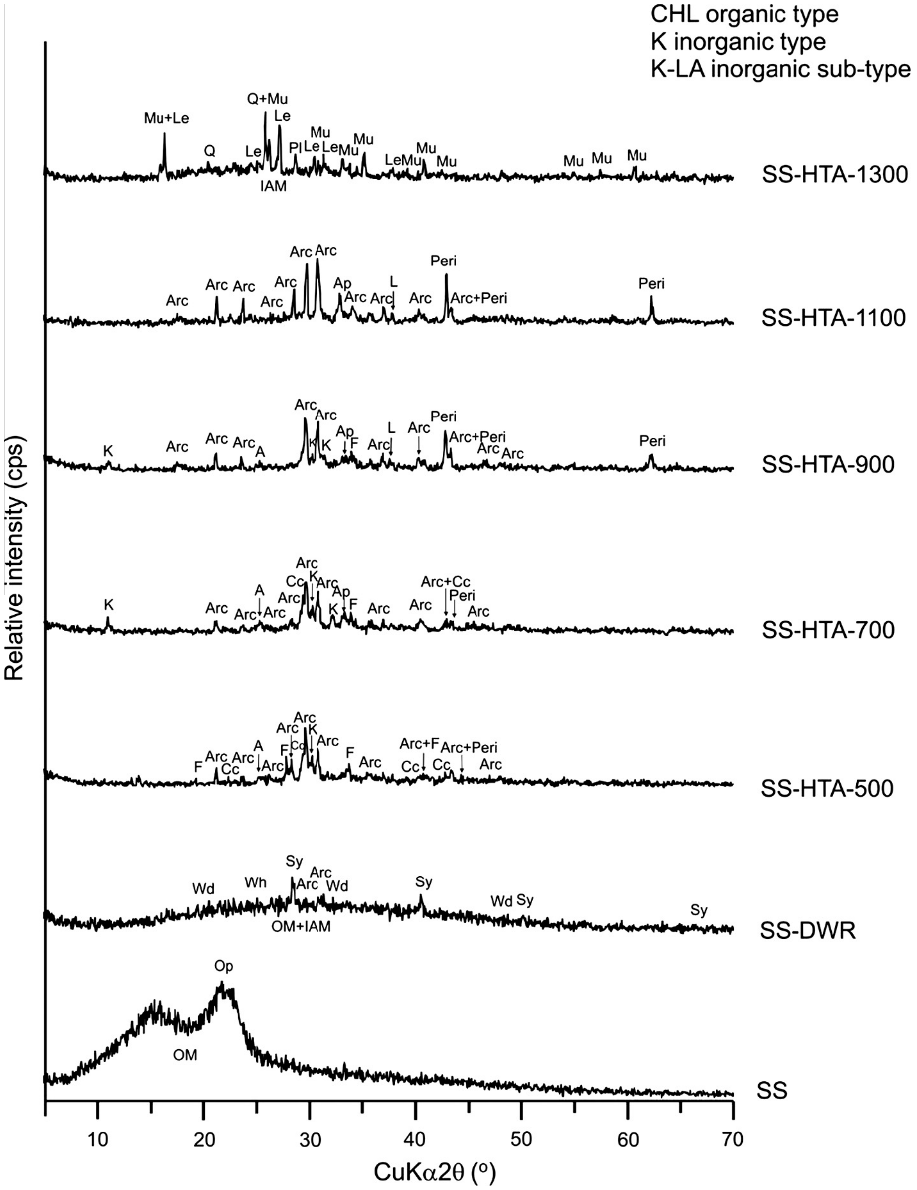

Fig. 10. XRD patterns of sunflower shells (SS), dry water-soluble residue (DWR) from SS and high-temperature ashes (HTAs) of SS generated at 500 °C/2 h, 700 °C/1 h, 900 °C/1 h, 1100 °C/1 h and 1300 °C/1 h. Abbreviations: A, anhydrite ($CaSO_4$); Ap, apatite ($Ca(PO_4)_3(Cl,F,OH)$); Arc, arcanite (K_2SO_4); Cc, calcite ($CaCO_3$); Cps, counts per second; F, fairchildite ($K_2Ca(CO_3)_2$); IAM, inorganic amorphous material (non-glass and glass); K, kalicinite ($KHCO_3$); L, lime (CaO); Le, leucite($KAlSi_2O_6$); Mu, mullite ($Al_6Si_2O_{13}$); OM, organic matter; Op, opal ($SiO_2{\cdot}nH_2O$); Peri, periclase (MgO); Pl, plagioclases ($NaAlSi_3O_8$–$CaAl_2Si_2O_8$); Q, quartz (SiO_2); Sy, sylvite (KCl); Wd, weddelite ($Ca(CO_2)_2{\cdot}(H_2O)_2$); Wh, whewellite ($Ca(CO_2)_2{\cdot}H_2O$). The occurrence of Q, Mu, Pl and probably some Le in the sample SS-HTA-1300 is a result of contamination from the broken ceramic crucible.

temperature; (2) the significant positive correlation between hemicellulose and the second exothermic peak temperature; and (3) the significant negative correlation between cellulose and the second exothermic peak temperature ($R^2 = \pm 0.66$). Furthermore, other characteristics associated with OM of biomass (volatile matter, extractives, H, S, Cl, N, C, even water-soluble salts) commonly show even stronger correlations with the exothermic peak temperatures and peak heights ratios than the structural components (Table 12). Hence, both major exothermic temperatures (associated with the greatest mass losses) and the exothermic peak heights ratios for OM do not correlate strongly and definitely to the contents, distribution and decomposition/oxidation stages of specific structural components in biomass as it has been widely described in literature [16,24,88,92,117,138,144,146,162,189,204,207,209,233,238,240,254,268,274,285,296,299,307,308,319,332,339,342,350]. The present results emphasise that these two consecutive exothermic peaks accompanied by the greatest mass losses are simply due to the two stage combustion behaviour of OM, namely burning of volatile matter and char, respectively, as it has been mentioned elsewhere [8,39,45,72,75,126,163,164,286,330,338,347,367]. It is interesting also to note that the initial smoke observed during heating of biomass samples in air (215–285 °C) fits with the beginning of the first combustion stage for all samples (Table 10 and Figs. 11–18 with index (a)). Therefore, the proportions among structural components in biomass seem to have limited significance during the combustion process and the two stage combustion behaviour of OM with increasing of temperature is basically related to: (1) devolatilization and burning of combustible volatile matter; and subsequently (2) char formation and combustion; simultaneously from the three structural components of the bulk OM with some temperature fluctuations depending on the content and distribution of cellulose, hemicellulose and lignin in the specific biomass varieties. Hence,

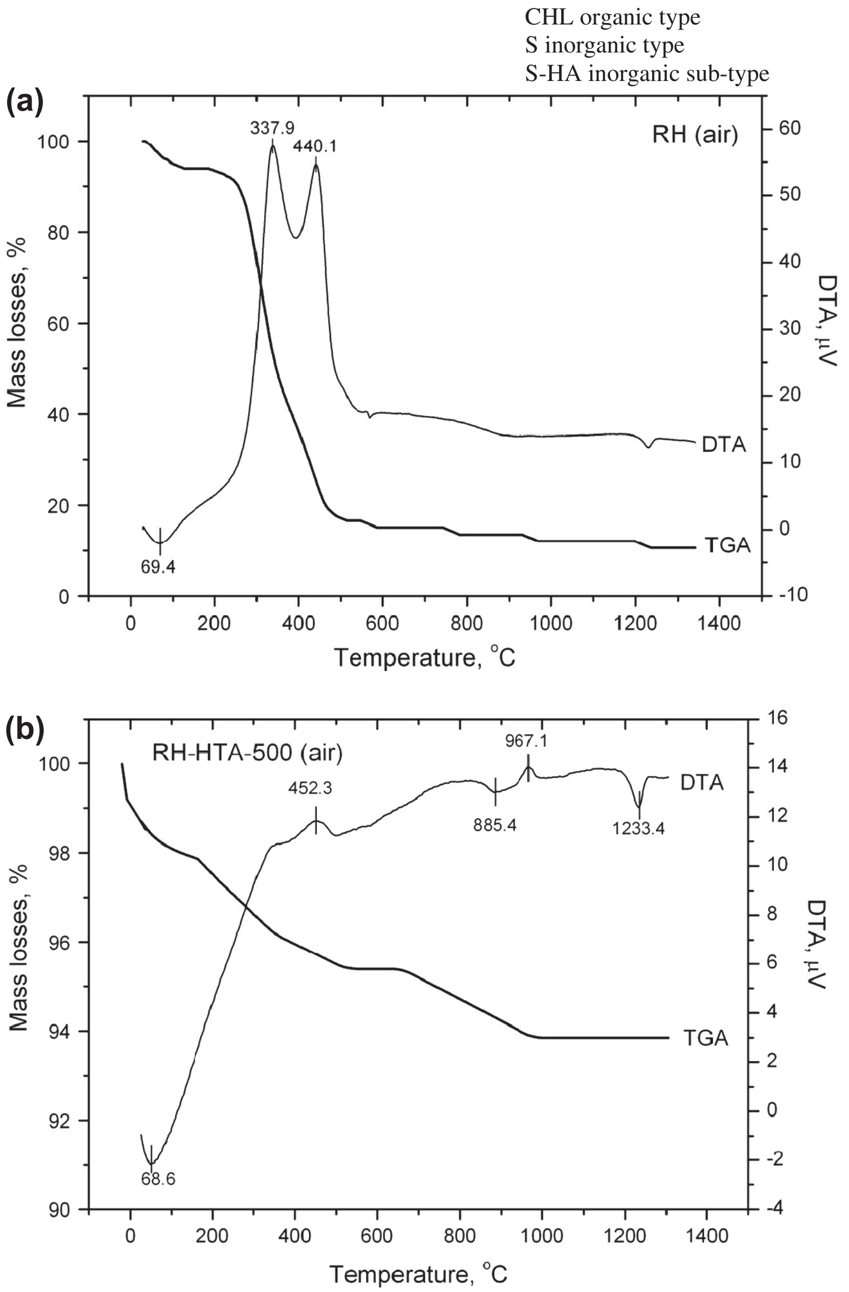

Fig. 11. DTA and TGA profiles of: (a) rice husks (RH); and (b) high-temperature ash (HTA) of RH generated at 500 °C/2 h.

the ill-defined structure, variable composition, different impurities and changeable properties of cellulose, hemicellulose and lignin in biomass varieties [1–3] reflect directly on their variable and less predictable thermo-chemical conversion behaviour.

The present study of TGA profiles for eight biomass varieties (Figs. 11–18 with index (a)) show that the OM oxidation is represented by intensive mass losses accompanying the large exothermic effects between 200 and 650 °C with two consecutive peaks at 324–351 °C and 425–520 °C. These mass losses of OM include one major stage with two sub-stages separated by a shoulder which correspond to the above described exothermic temperatures. Additionally, these two combustion stages, which are significantly independent from the distribution of structural components, are also confirmed by the disappearance of the first characteristic exothermic peak (related to combustible volatile matter) for some BAs produced at 500 °C (Figs. 11–14 with index (b)). Hence, the data from DTA of BA and TGA of biomass and BA also confirmed the above two stage combustion behaviour of bulk OM. Finally, it should be stated that similar observations are also characteristic of lignites and sub-bituminous and bituminous coals [376,377], as well as refuse derived fuels from municipal solid wastes [52]; however, the role of volatile matter combustion is much more typical of natural biomass than other solid fuels.

As mentioned above, only the algae sample (MM) has an additional third and small exothermic peak between 740 and 830 °C (maximum at 782 °C) accompanied by some mass loss and related to oxidation of some residual char (Fig. 15a). Therefore, some supplementary optical observations were conducted for algae ashes produced at 500, 700 and 900 °C in the present study. A few individual char components were recognised by light microscopy as black particles encapsulated by coarse sized chloride aggregates built up of cubic crystals in the ashes obtained at 500 and 700 °C.

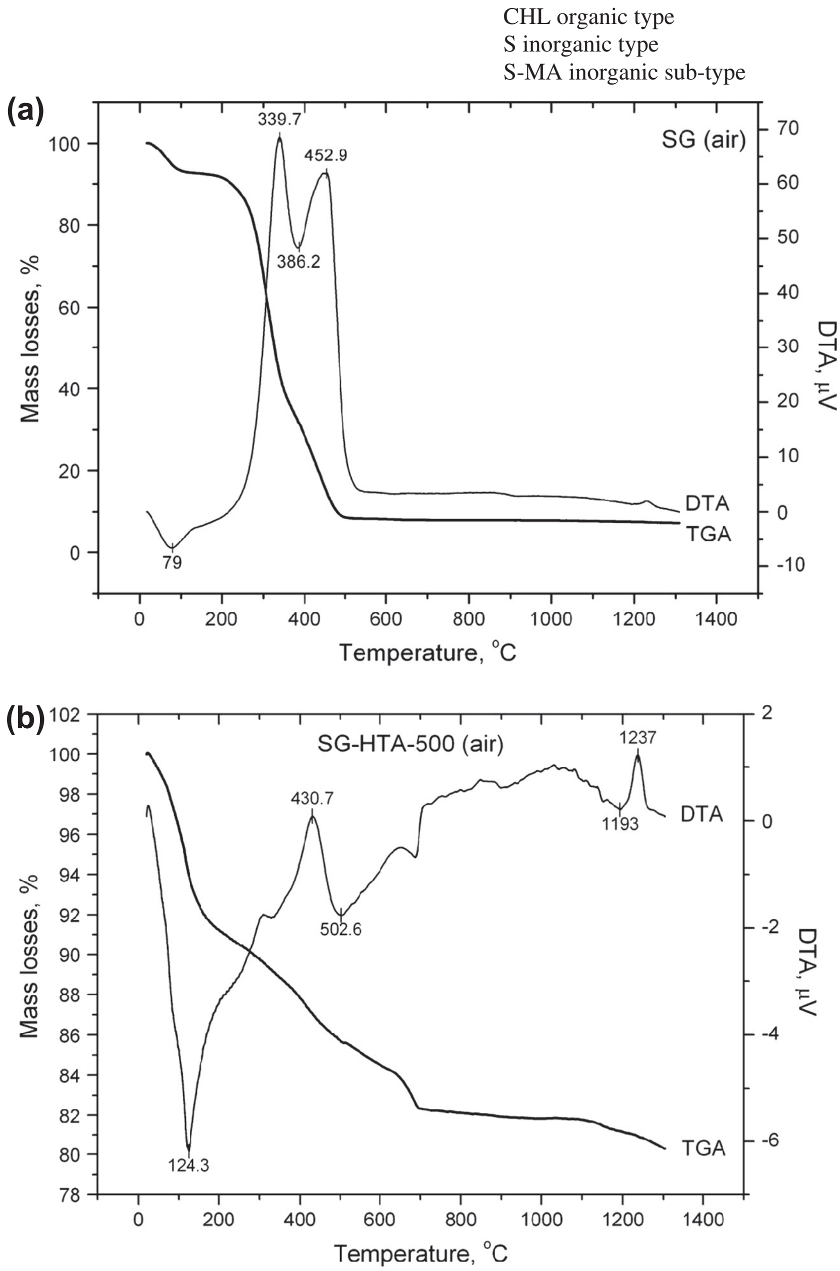

Fig. 12. DTA and TGA profiles of: (a) switchgrass (SG); and (b) high-temperature ash (HTA) of SG generated at 500 °C/2 h.

It can be seen that MM ash is highly enriched in Cl, Na and K represented by halite and sylvite (Tables 10 and 11 and Fig. 7). It is well known that the melting points of these minerals are in the temperature interval 770–801 °C (Table 9). It can also be seen that the DTA profile of MM ash produced at 500 °C (Fig. 15b) shows: (1) an endothermic peak at 538 °C (with some mass loss) corresponding to calcite decomposition (see Fig. 7 for calcite transformation); (2) an endothermic peak at 745 °C (with some mass loss) consistent with eutectic melting of a halite-sylvite mixture; and (3) an exothermic peak at 792 °C (followed by intensive mass loss) due to oxidation of unburned char. Hence, the combustion of the encapsulated residual char after 782–792 °C follows closely melting of the chloride matrix because the chloride melt allows oxygen diffusion and combustion of this unburned char. The reference investigations show that the existence of two char combustion stages (with two exothermic peaks) was not related to the occurrence of two specific types of chars with a different nature because any structure evolution of the char was not found [367]. On the other hand, the oxidation of lignin derived char at higher temperatures (600–900 °C) has been described for some lignin rich biomass varieties (pure lignin, wood stems, barks and shoots, and switchgrass) [146,233,319,347]. However, this is not the case herein because it is well known that marine macroalgae normally do not contain lignin [254] or contain quite limited amount of this component [401]. Finally, the above combustion mechanism for some residual char encapsulated in chlorides can also be valid for char entrapped by certain carbonates, sulphates, phosphates and silicates and its subsequent burning at higher temperatures (see Section 3.3.2).

It is widely accepted that the gases released from the thermal decomposition of structural components include dominantly CO_2, CO, H_2O, H_2 and methane (CH_4), and to a lesser extent, N_2, NO_X, SO_X, ethane (C_2H_2), ethene (C_2H_6) and others [85,233,307,350,353,391]. Additionally, it was found that hemicellulose had

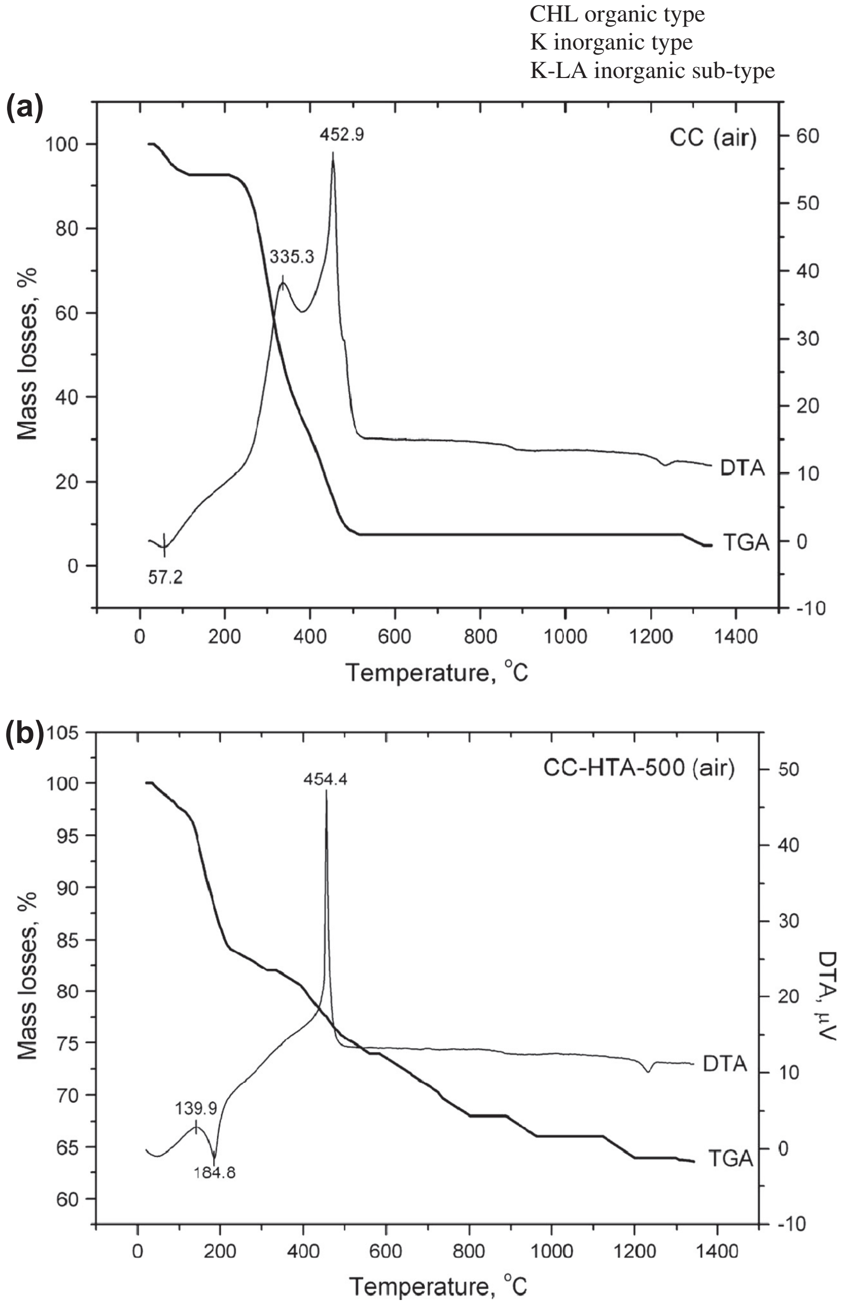

Fig. 13. DTA and TGA profiles of: (a) corn cobs (CC); and (b) high-temperature ash (HTA) of CC generated at 500 °C/2 h.

higher CO_2 yield, cellulose generated higher CO yield, and lignin owned higher H_2 and CH_4 yield [233]. As a result of biomass combustion, volatilization of elements forming OM (C, H, N, S, O) or inorganic elements associated with OM (Ca, Mg, K, Na and, to a lesser extent, P, Si, Fe, Al, Mn, Ti and others) as covalently or ionically bound elements, organic-metal components, adsorbed ions or metal ions in ion-exchanged forms bound to specific functional groups [2] occurs mainly in the temperature interval between 200 and 850 °C. These elements can: (1) escape the system as volatile components; (2) form discrete inorganic phases in ash; (3) react with each other; and (4) react with original or newly formed IM of biomass and ash [3]; which is similar to coal [376,377].

It is also well known that the combination of high O and VM contents in biomass indicates a potential for creating large amounts of inorganic vapours during combustion [39]. For example, the highly variable volatilisation of elements (Table 13) during biomass combustion have been summarized recently ([3] and references therein). These data show that elements with the highest volatilization potential (13–99% based on mean values) are: Hg > (Cd, Sb, Se, V) > Br > Cr > Pb > Zn > Cl > As > S > K > Na.

3.3.2. Char and other organic phases

The char and other organic phases identified in BA are listed in Table 7 and described earlier [3]. Shortly, the reference investigations ([3] and references therein) show that these organic phases include mostly secondary semi-coked and coked char particles and associated with them other minor organic phases in BA originated from incomplete biomass combustion. Additionally, the presence of some technogenic organic phases in semi-biomass as impurities (additives or contaminants) generated from processing

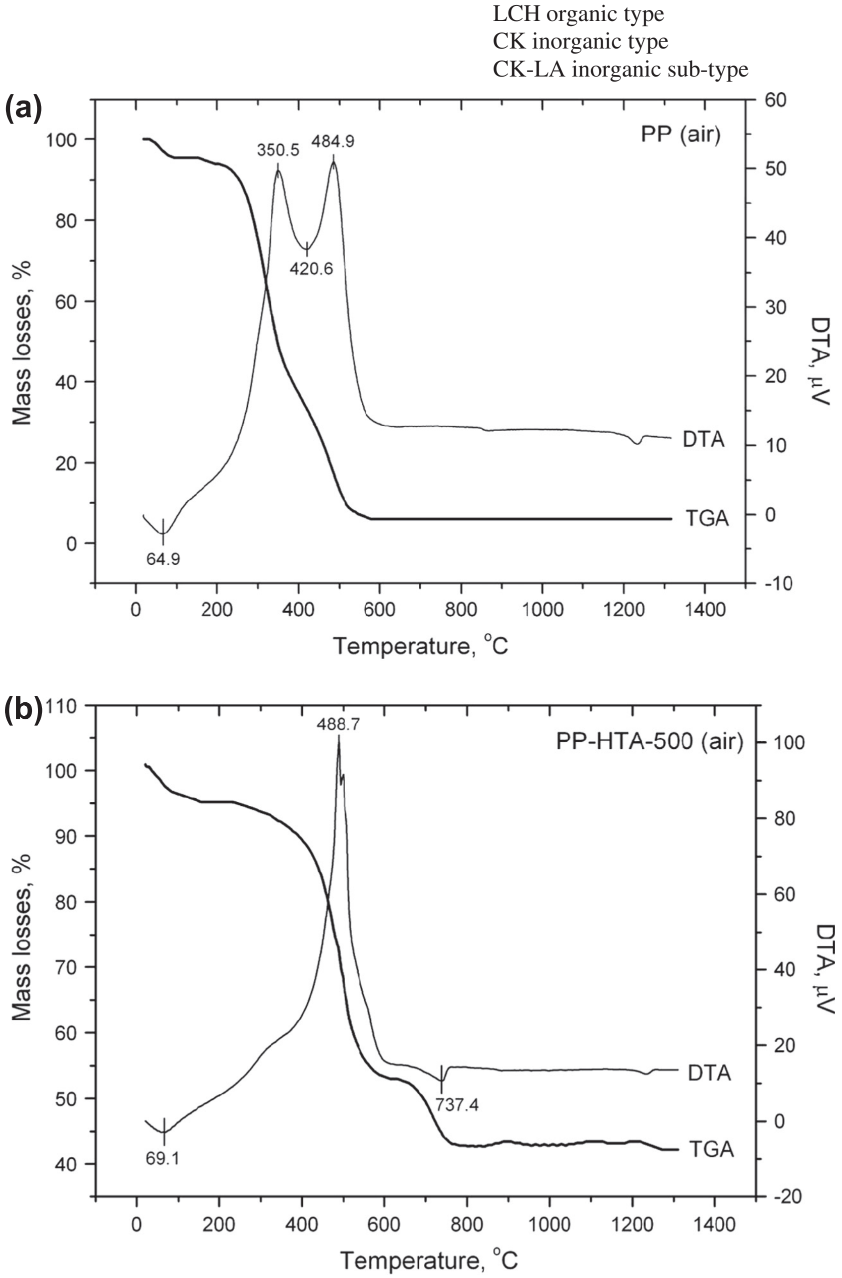

Fig. 14. DTA and TGA profiles of: (a) plum pits (PP); and (b) high-temperature ash (HTA) of PP generated at 500 °C/2 h.

of natural biomass can also occur in BA. The char contents in BA are highly variable (up to 79%); however, the most common values are in the range 1–20%. The char particles have various morphologies (Table 4), but the original textures and structures of biomass are often maintained in char particles. It was found that the coarser grain fractions of BA normally contain increased amounts of unburned matter. An association of organic pollutant species (polychlorinated dioxins and furans and polycyclic aromatic hydrocarbons) with char when the unburned organic levels in BA are high is possible. The formation of some Na cyanate is also plausible during biomass combustion; however, such cyanate is only stable under reducing environments and decomposes to other alkali salts and gaseous N compounds under oxidising conditions ([3] and references therein).

The present study of eight biomass varieties and their HTAs confirmed some of the above observations. For example, discrete char components were recognised by light microscopy as individual black particles (with signs of some original biomass textures and structures) in the ashes obtained at 500 °C (BC, CC, MM, PP, RH, SG, SS, WS), 700 °C (CC, MM), 900 °C (CC, MM) and occasionally even higher temperatures. The burning of this residual organic material mostly proceeds between 300 and 967 °C (Figs. 11–18 with index (b)), which is similar to the temperature interval (370–950 °C) described in the literature (Table 8). For instance, the present study shows that the possible combustion temperatures of residual char can be the exothermic peaks accompanied by mass losses at:

- 300, 450 and 794 °C (for BC ash in Fig. 16b);
- 307, 380, 603, 792 and 1110 °C (for MM ash in Fig. 15b);
- 330, 500, 600, 723, 838, 940 and 1207 °C (for WS ash in Fig. 17b);

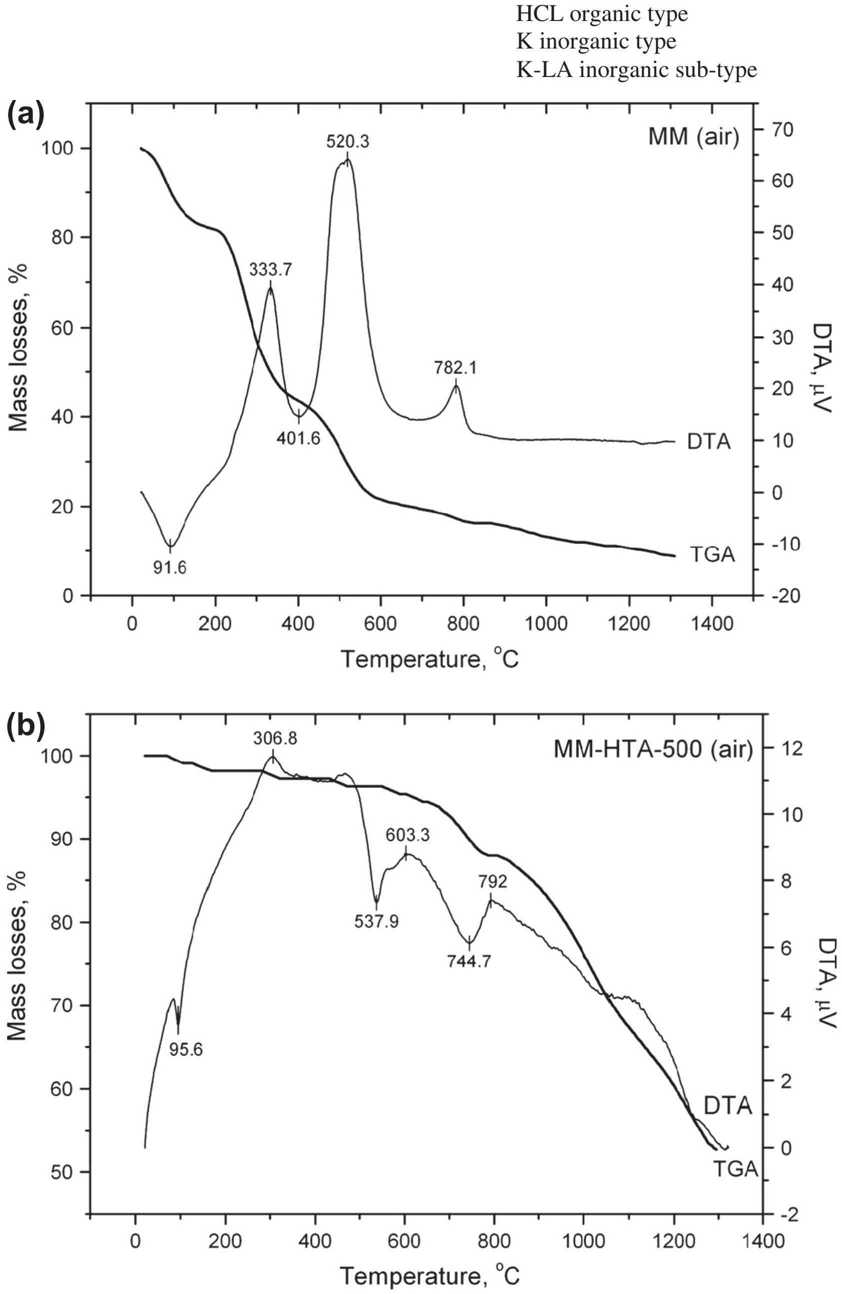

Fig. 15. DTA and TGA profiles of: (a) marine macroalgae (MM); and (b) high-temperature ash (HTA) of MM generated at 500 °C/2 h.

- 363, 570, 813 and 1250 °C (for SS ash in Fig. 18b);
- 431, 1030 and 1237 °C (for SG ash in Fig. 12b);
- 452 and 967 °C (for RH ash in Fig. 11b);
- 454 °C (for CC ash in Fig. 13b);
- 489–510 °C (for PP ash as a double peak in Fig. 14b).

Additionally, a few individual char particles encapsulated by large chloride, carbonate, sulphate and silicate aggregates in the ashes obtained at 500–900 °C and even higher temperatures were also observed microscopically. Hence, the above pointed combustion mechanism for some residual char encapsulated in chlorides (see Section 3.3.1) can also be valid for char entrapped by other mineral classes and its subsequent burning at higher temperatures. For example, the formation of some secondary chlorides, carbonates, sulphates, phosphates and silicates (Table 11) occurs simultaneously with the formation and combustion of char. Therefore, some of them can capsulate the char (as char covered by mineral layers or included in mineral matrix), thus limiting the oxygen diffusion to the OM. In this case the combustion of the encapsulated residual char may follow closely the decomposition, recrystallization or melting of the outer mineral layers or matrices to allow some oxygen diffusion and allowing char burnout. For instance, the below listed possible combustion temperatures of the residual char are based on: (1) the exothermic effects accompanied by mass losses in Figs. 11–18 (with index (b)); (2) the endothermic reactions in Figs. 11–18 (with index (b)); and (3) the mineral transformations in Figs. 3–10. These temperatures are:

- 500 °C and 600 °C, following some portlandite–lime crystallizations at 386–542 °C (for WS in Fig. 17b and SS in Fig. 18b);

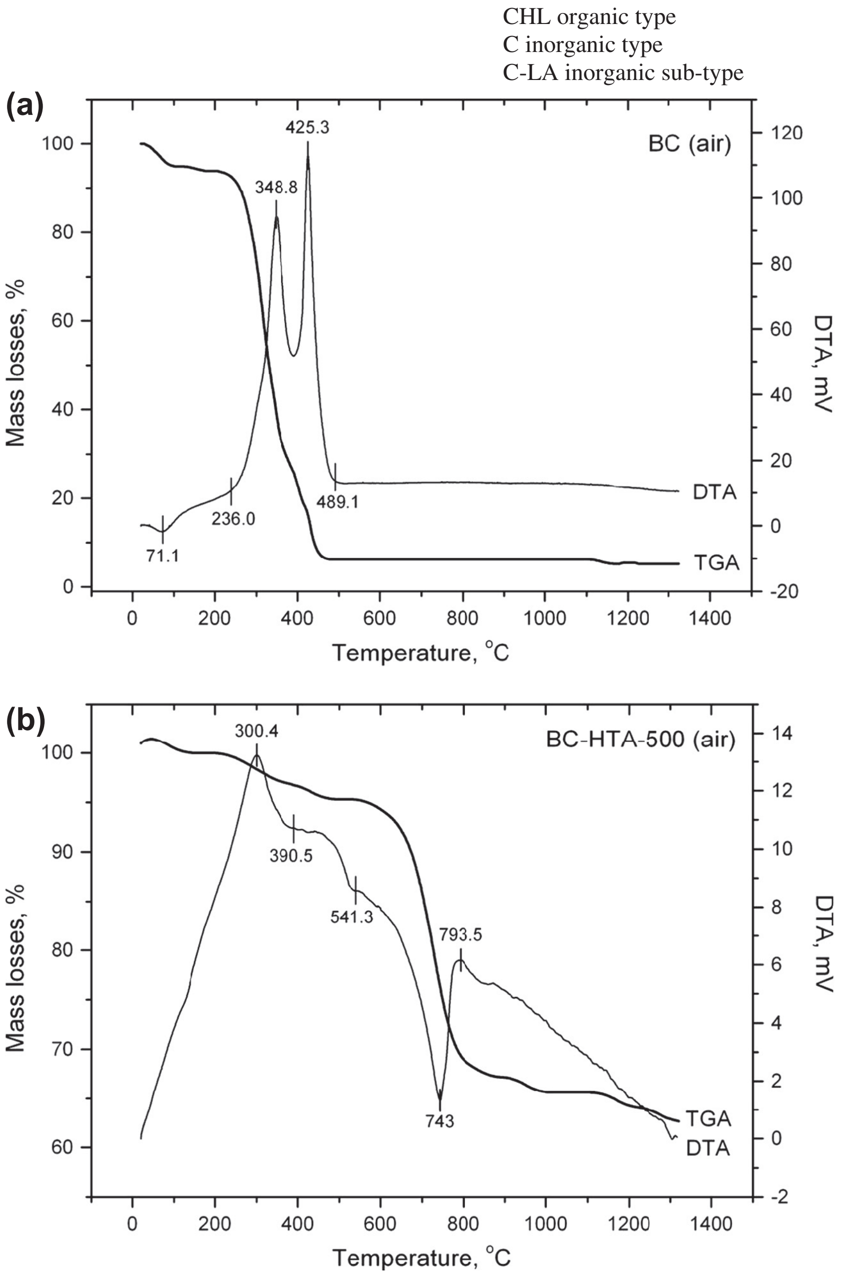

Fig. 16. DTA and TGA profiles of: (a) beech wood chips (BC); and (b) high-temperature ash (HTA) of BC generated at 500 °C/2 h.

- 603 °C, 794 °C, 813 °C and 940 °C, respectively after calcite decomposition at 538 °C (for MM in Fig. 15b), 743 °C (for BC in Fig. 16b), 740 °C (for SS in Fig. 18b) and 896 °C (for WS in Fig. 17b);
- 723 °C and 838 °C, following some decomposition of K (dehydrogened kalicinite), K–Ca (butschliite, fairchildite) and Na–Ca (natrofairchildite) carbonates at 706 °C and 777 °C (for WS in Fig. 17b);
- 782–792 °C, after melting of chlorides at 745 °C (for MM in Fig. 15b);
- 967 °C and 1030 °C, following crystallisation of amorphous silica to cristobalite at 885 °C (for RH in Fig. 11b) and 900 °C (for SG in Fig. 12b), respectively;
- 1207 °C, after anhydrite decomposition at 1170 °C (for WS in Fig. 17b);
- 1237 °C, following ash melting at 1193 °C (for SG in Fig. 12b); and
- 1250 °C, after arcanite decomposition and ash melting at 1236 °C (for SS in Fig. 18b).

It should be stated that the intensive formation of some newly formed minerals and low-temperature and less viscous melts also provides some contribution to increased char components in ashes produced from low-rank coals. For instance, films of anhydrite, calcite, lime and glass were observed to encapsulate unburned char particles, thus preventing oxygen diffusion and complete combustion of OM in lignites [384]. Furthermore, the processes related to formation of secondary carbonates, chlorides, phosphates and low-temperature melts for possible char encapsulating are much more characteristic of BAs than coal ashes [3].

3.3.3. Organic minerals

The organic minerals identified in BA are listed in Table 7 and described earlier [3]. Oxalates are minerals, but they are assigned

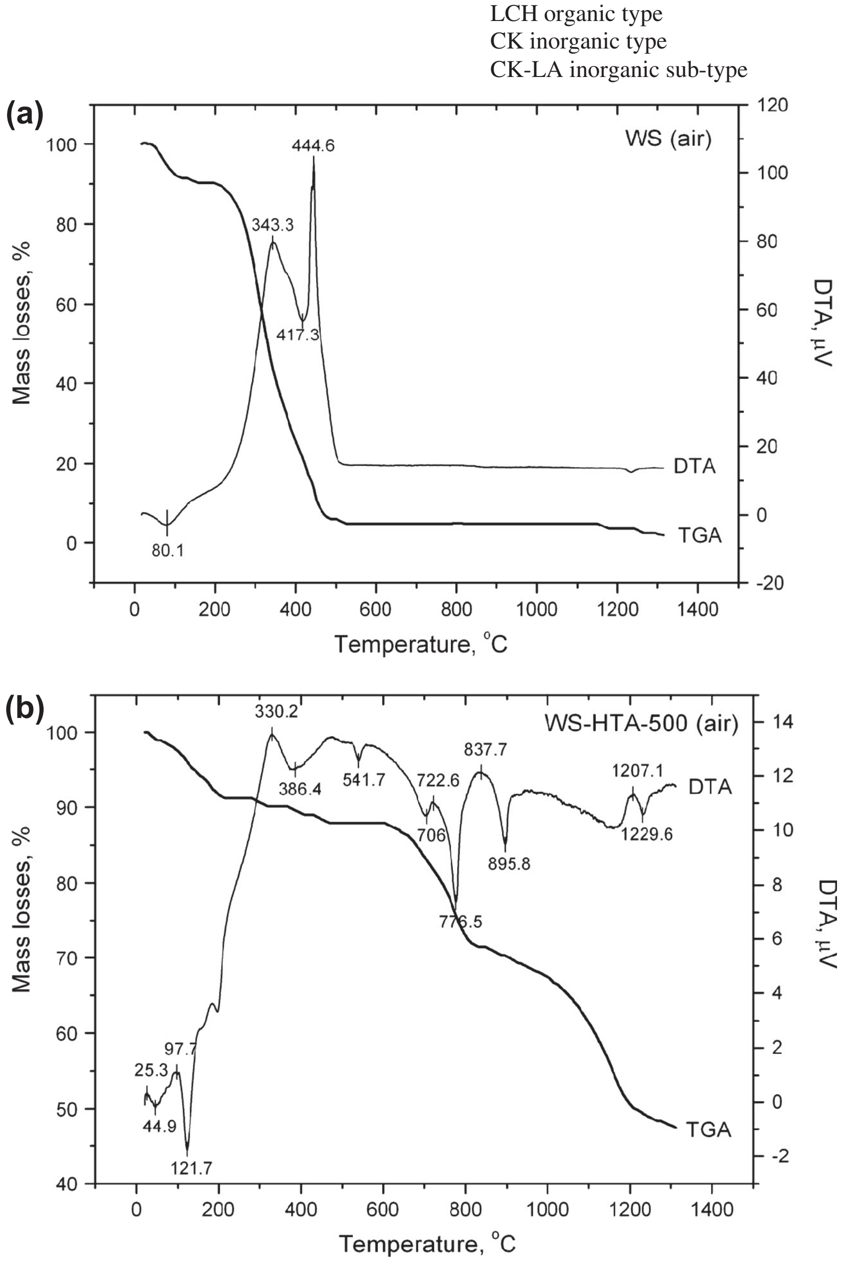

Fig. 17. DTA and TGA profiles of: (a) walnut shells (WS); and (b) high-temperature ash (HTA) of WS generated at 500 °C/2 h.

to a special group because they are organic species, which is one of the exceptions in a mineralogical sense. Shortly, the reference investigations ([3] and references therein) show that weddelite (Ca oxalate dihydrate), whewellite (Ca oxalate monohydrate) and dehydrated whewellite were identified only in LTA of biomass. They can be secondary, tertiary and probably primary accessory phases in BA (Table 7). For instance, oxalates are typical authigenic minerals in plants because they originate from syngenetic and epigenetic evaporation and precipitation of mineralized aqueous solution enriched in different cations and oxalate anion. Hence, some oxalates may be primary phases in BA due to their possible presence as unchanged relics despite their relatively low to moderate decomposition temperatures (up to 700 °C in Table 8) during heating. Additionally, the occurrence of some technogenic oxalates in semi-biomass as impurities generated from processing of natural biomass may also be primary as a result of their presence as unaltered minerals in BA. However, the secondary and tertiary oxalates of Ca, K, Mg, Mn and Na are probably dominant in BA and these newly formed phases may be a result of decomposition of OM under some unstable and lower temperature conditions in the system during biomass combustion ([3] and references therein).

The present study of eight biomass varieties and their HTAs confirmed some of the above observations. For example, oxalates were not found in BAs produced at 500 °C and higher temperatures (Table 11). It is well known that the transformation of Ca oxalates includes: (1) dehydration at 170–200 °C; and (2) decomposition and carbonation at 300–500 °C (occasionally up to 700 °C) with formation of more stable calcite (Table 8). Therefore, significant parts of calcite identified in many ashes produced at 500 °C (SG, PP, WS, SS, and especially BC in Figs. 4, 6 and 8–10) may originate from such characteristic minerals of biomass.

CHL organic type
K inorganic type
K-LA inorganic sub-type

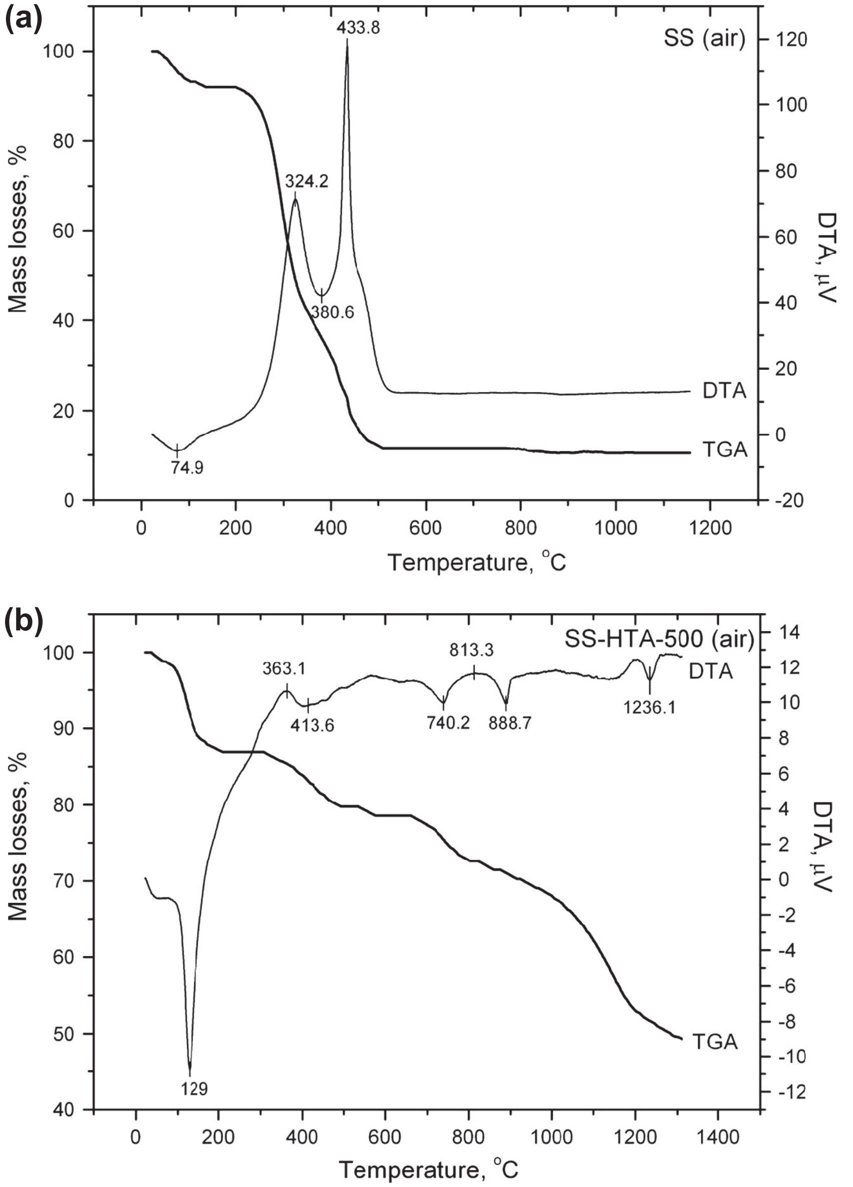

Fig. 18. DTA and TGA profiles of: (a) sunflower shells (SS); and (b) high-temperature ash (HTA) of SS generated at 500 °C/2 h.

3.4. Behaviour of inorganic matter during biomass combustion

3.4.1. Silicates

The numerous silicates identified in BA are listed in Table 7 and described earlier [3]. Shortly, the reference investigations ([3] and references therein) show that silicates can be mostly secondary, to a lesser extent primary, and occasionally tertiary phases in BA (Table 7). These minerals have both detrital and authigenic occurrence in/on plants because: (1) quartz, cristobalite, feldspars, clay and mica minerals plus other silicates such as pyroxenes, olivines, chlorites and amphiboles are typical soil minerals and they can have some detrital uptake from the soil during plant growth; and (2) opal is a characteristic authigenic mineral in plants and originates from syngenetic and epigenetic evaporation and precipitation of water, namely mineralized aqueous solution enriched in noncharged silicic acid. Hence, some silicates can be primary phases in BA due to their possible presence as unchanged relics having relatively high decomposition (Table 8) and/or melting (Table 9) temperatures during heating. For example, MPs of silicates are commonly more than 1100 °C (Table 9). Additionally, some technogenic silicate impurities as fillers, additives or contaminants (clay minerals, zeolites, talc and other silicates) in semi-biomass generated from processing of natural biomass can also be primary as a result of their occurrence as unaltered minerals in BA. However, the secondary silicates are dominant in BA (Table 7) and these newly formed phases originate from the alteration of pre-existing silicates, melt crystallisation and mostly from the complex reactions among silica and oxyhydroxides of Al, Ba, Ca, Cd, Fe, K, Mg, Mn, Na, Sr and Ti generated commonly from the decomposition of OM, oxalates, carbonates, phosphates, sulphates, chlorides and nitrates during biomass combustion (Table 8). For instance, crystallisation of various newly formed silicates (grains and crystals

Table 12

Significant positive (+) and negative (−) correlation coefficient values (R^2) at 95% confidence levels (bold font),[a] and insignificant (normal font) R^2 values for some characteristics of eight biomass samples.

Characteristic	Correlation coefficient value with:
First exothermic peak temperature from DTA	(+) **H(0.89) CaO(0.68) Lig(0.66) TiO_2(0.63)** Al_2O_3(0.58) MnO(0.48) VM(0.26) P_2O_5(0.14) C(0.10) O(0.10) (−) Cel(0.57) MgO(0.41) SO_3(0.41) K_2O(0.38) EC (0.37) N(0.37) Cl_2O(0.34) DWR(0.33) A(0.32) Hem(0.32) Cl(0.28) Ext(0.25) Na_2O(0.23) S(0.23) Fe_2O_3(0.14) pH(0.12) SiO_2(0.03) FC(0.02)
Second exothermic peak temperature from DTA	(+) **Ext(0.85) Na_2O(0.84) S(0.83) SO_3(0.82) Cl(0.81) Cl_2O(0.80) EC (0.78) N(0.72) DWR(0.70) Hem(0.66)** A(0.60) pH(0.58) Al_2O_3(0.54) TiO_2(0.38) H(0.33) Fe_2O_3(0.26) FC(0.07) P_2O_5(0.07) MgO(0.02) (−) **C(0.68) Cel(0.66)** VM(0.52) MnO(0.45) K_2O(0.40) SiO_2(0.20) O(0.19) Lig(0.06) CaO(0.05)
Ratio between first and second exothermic peak heights from DTA	(+) **SiO_2(0.67)** H(0.57) C(0.51) Al_2O_3(0.43) Lig(0.37) VM(0.29) TiO_2(0.27) MnO(0.10) pH(0.01) (−) SO_3(0.60) Cl_2O(0.56) MgO(0.55) EC(0.52) Cl(0.51) K_2O(0.50) Na_2O(0.48) S(0.46) Hem(0.42) N(0.42) Fe_2O_3(0.31) FC(0.30) DWR(0.27) O(0.27) Ext(0.17) A(0.14) Cel(0.05) P_2O_5(0.04) CaO(0.03)

Abbreviations: A, ash yield; Cel, cellulose; DTA, differential-thermal analysis; DWR, dry water-soluble residue; EC, electrical conductivity; Ext, extractives; FC, fixed carbon; Hem, hemicellulose; Lig, lignin; VM, volatile matter.

[a] The significant R^2 values at 95% confidence level are $\geqslant 0.63$ and $\leqslant -0.63$ for 8 variables.

Table 13

Mean and range values of elements volatilized during biomass combustion, wt.%.

Element	Mean	Minimum	Maximum	Samples
Hg	99	95	100	5
Cd	95			1
Sb	95			1
Se	95			1
V	95			1
Br	85	80	90	2
Cr	75	70	80	2
Pb	71	40	100	5
Zn	70	3	95	7
Cl	66	15	100	9
As	58	25	90	2
S	57	7	90	15
K	36	5	90	8
Na	13	2	24	2

with size between 1 μm and 1 mm) within the glass and wollastonite matrices was observed in BAs. The origin of these secondary silicates in BA is similar to that in coal ash and their formation mechanisms have been described in detail earlier ([376,377] and references therein). A special case in some BAs is the significant formation of certain secondary K, Na, K–Na, K–Ca and K–Mg silicates having very low eutectic MPs at 540–980 °C (Table 9) and such phases can be the reason for low-temperature formation of melt/glass in BAs. Finally, the tertiary silicates may include minerals containing water molecules and/or hydroxyl groups such as Ca silicate hydrate, afwillite, serandite, zeolites (faujasite, gismondite, makatite, paranatrolite) and amphiboles (riebeckite, tremolite), as well as some chlorite, clay and mica minerals (Table 7), which can be a result of hydration and hydroxylation of other less stable silicates by water and moisture in the air during transport and storage of BA ([3] and references therein).

The present study of eight biomass varieties and their HTAs confirmed most of the above observations. The silica minerals are among the most appropriate examples for explanation of the thermal behaviour of silicates during biomass combustion. The RH ash contains about 90% SiO_2 (Table 10) and the thermal behaviour of this sample is illustrated in Figs. 3 and 11. The phase transformation of original authigenic opal and amorphous silica present in biomass includes their crystallisation/recrystallization to more stable secondary: (1) quartz (500–1500 °C); (2) cristobalite (700–1500 °C, especially above 900 °C); and tridymite (900–1500 °C) in HTA (Fig. 3). The DTA-TGA profile of RH HTA (Fig. 11b) also shows some less intensive but indicative phase transformations with increasing of temperatures such as: (1) quartz polymorphic transformation (small endothermic peaks about 570 °C, also observed in Fig. 11a); (2) combustion of residual char (exothermic peaks at 452 and 967 °C accompanied by mass losses); (3) cristobalite crystallisation (endothermic peak at 885 °C); and (4) tridymite formation (endothermic peak at 1233 °C). Similar polymorphic transformations of silica minerals have been described elsewhere (Table 8). The newly formed silica minerals are stable and inert over a large temperature range, namely 500–1500 °C (Table 11 and Figs. 3–8) due to their high melting temperatures (Table 9) and limited reactions with other minor components in the RH ash system. In contrast, the dissolution of silica minerals in the active melts at 1100 and 1300 °C for other HTAs can be seen on XRD patterns (Figs. 4–6). Instead of solid-state transformations the secondary silica minerals can also be a result of some melt crystallisation at 1100–1300 °C for the same samples (Figs. 4–6). Finally, primary quartz probably also occurs in some HTAs (Figs. 3–8) due to detrital origin of this mineral in biomass. Feldspars (plagioclases and K feldspars) are stable minerals in HTAs produced at 500–1100 °C (Table 11 and Fig. 6) and their formation is listed in Table 8. It should be stated that the origin and behaviour of primary and secondary feldspars in HTAs is similar to that of quartz (Tables 7 and 8). It is well known that some biomass feedstock can be enriched in soil contaminants including quartz, feldspars and clay and mica minerals. In this case numerous interactions take place between the authigenic and detrial phases in the fuel above 500–900 °C resulted in a complex formation of various secondary silicates with different (refractory or fluxing) behaviour during combustion (Tables 8 and 9).

The present study (Table 11 and Figs. 4 and 5) also shows the occurrence of some very interesting newly formed K aluminosilicates in HTAs, namely leucite ($KAlSi_2O_6$) and kalsilite ($KAlSiO_4$, polymorphous with kaliophilite), produced from SG and CC samples enriched in SiO_2 (37–63%). It is well known that these K-rich and Na- and Si-deficient minerals are typical of some volcanic rocks and they are incompatible with quartz because they react with silica to form more stable K feldspars [402]. It can be seen (Table 11 and Figs. 4 and 5) that these secondary K silicates (unusual minerals for coal ash) are stable from 500 °C to 1100 °C (kalsilite) or 1300 °C (leucite) and their formation mechanisms include reactions between K compounds (K_2O, KCl, KOH, K_2CO_3, K_2SO_4) and Si and Al oxides (Table 8). It seems that these K silicates can be a result of both solid-state reactions (preferably at 500–900 °C) and melt crystallisation (dominantly 1100–1300 °C). Their coexistence with quartz in some HTAs is probably due to the occurrence of detrital and coarse grained quartz (less active) relics with primary origin in these samples before the ash melting.

The reference investigations and present study reveal that numerous silicates can occur in BAs (Table 7). However, these minerals are not typical of all BAs (in contrast to coal ashes) because they do not play significant to major roles in every biomass combustion product. In comparison with coal ashes, there are BAs within medium acid and especially low acid types and sub-types (Fig. 2) where silicates play, respectively, subordinate to almost insignificant roles in contrast to other mineral classes during ash formation (see Part II).

3.4.2. Oxides and hydroxides

The various oxides and hydroxides found in BA are listed in Table 7 and described earlier [3]. Shortly, the reference investigations ([3] and references therein) show that oxides and hydroxides can be mostly secondary, to a lesser extent primary, and occasionally tertiary (especially hydroxides) phases in BA (Table 7), which is identical to silicates. These minerals have commonly detrital and occasionally authigenic accessory occurrence in/on plants because: (1) Fe, Al and Ti oxyhydroxides are typical soil minerals and they can have some relatively low detrital uptake from the soil during plant growth; and (2) some authigenic hydroxides in plants may originate from syngenetic and epigenetic evaporation and precipitation of mineralized aqueous solution enriched in different cations and hydroxide anion. Hence, some oxyhydroxides can be primary phases in BA due to their possible presence as unchanged relics having relatively high decomposition (Table 8) and/or melting (Table 9) temperatures during heating. For example, MPs of oxides are normally much more than 1200 °C (Table 9). Additionally, the occurrence of some technogenic Fe-, Al-, Mg-, Ca- and Ti-bearing oxyhydroxides in semi-biomass as impurities (additives or contaminants) generated from processing of natural biomass can also be primary as a result of their presence as unaltered minerals in BA. However, the secondary oxyhydroxides (especially oxides) of Al, Ca, Cd, Cr, Cu, Fe, K, Mg, Mn, Na, Ni, Pb, Pd, Sn, Ti and Zn (Table 7) are dominant in BA and these newly formed phases originate mostly from the decomposition and oxidation of OM, oxalates, carbonates, phosphates, sulphates, chlorides and nitrates, and, to a lesser extent, melt crystallisation during biomass combustion (Table 8). A special case in some BAs (especially from semi-biomass) is the possible formation of certain secondary K, Mo, Pb and Sb oxyhydroxides having very low eutectic MPs at 380–886 °C (Table 9) and such phases can be a reason for a low-temperature formation of melt/glass in BAs. Finally, the tertiary oxyhydroxides may include minerals containing mainly hydroxyl groups and water molecules (for example, brucite, gibbsite, goethite, hematite, hydrocalumite, maghemite, portlandite, and Cu, K, Na and Zn hydroxides in Table 7), which can be a result of hydration and hydroxylation of other less stable oxides by water and moisture in the air during transport and storage of BA ([3] and references therein). The origin of such secondary and tertiary oxyhydroxides in BA is similar to that in coal ash and their formation mechanisms have been described in detail earlier excluding the phases containing some trace elements ([376,377] and references therein). It should be stated that the specification of the origin for hydroxides in BAs (similar to carbonates, see Section 3.4.5) is not an easy task and some additional investigations are required for that purpose.

The present study of eight biomass varieties and their HTAs confirmed many of the above observations. The oxides of Ca (lime) and Mg (periclase) and hydroxides of Ca (portlandite) and Mg (brucite) are among the most suitable examples for explanation of the thermal behaviour of oxyhydroxides during biomass combustion (Table 7). It can be seen that some HTAs (BC, MM, PP, SS and WS in Table 10) contain high contents of CaO (16–63%) and MgO (4–12%) and the thermal behaviour of these samples is illustrated in Figs. 6–10 and 14–18. The phase transformation of original phases containing alkaline-earth elements (OM, oxalates, carbonates, phosphates and sulphates) in the biomass varieties studied includes their decomposition and crystallisation/recrystallization to newly formed (secondary and tertiary): (1) periclase (500–1100 °C); (2) portlandite (500–1300 °C); and (3) lime (700–1100 °C); in HTAs (Table 11 and Figs. 6–10). For example, the formation of lime from: (1) calcite decomposition at 538 °C (for MM in Figs. 7 and 15b), 743 °C (for BC in Figs. 8 and 16b), 740 °C (for SS in Figs. 10 and 18b) and 896 °C (for WS in Figs. 9 and 17b); and (2) from anhydrite decomposition at 1170 °C (for WS in Figs. 9 and 17b) and 1250 °C (for MM in Figs. 7 and 15b); can be seen on DTA-TGA profiles and supported by XRD patterns. Similar transformation temperatures for the above minerals have also been given elsewhere (Table 8). On the other hand, the dissolution of Ca and Mg oxides in the melt at 1300 °C for some HTAs (Figs. 6–10); can be seen on XRD patterns. The formation of lime and periclase is definitely secondary, while the dominant portlandite crystallisation probably has a tertiary origin in BAs. It is well known that the dexydroxylation of portlandite occurs mostly at 450–620 °C and occasionally up to 800 °C (Table 8). Hence, portlandite identified in the HTAs enriched in Ca and produced at 900–1300 °C is a result of hydroxylation of lime by moisture in the air during cooling and storage of PP, MM, BC and WS ashes (Figs. 6–9). The secondary occurrence of stable portlanide is only possible for HTAs produced at 500 and 700 °C (Figs. 7 and 8) due to hydroxylation of lime (Table 8). The exothermic peaks between 300 and 600 °C due to residual char combustion (Figs. 14–17 with index (b)) could also be related to some transitional hydroxylation of lime, which is similarly an exothermic reaction. It is well known that the very active lime is unstable in air and moisture and its particles are transformed easily to less active portlandite and later to calcite. On the other hand, lime included in the glass matrix has different behaviour than that of individual lime particles. Similar processes are also characteristic of periclase and active Ca and Ca–Mg silicates [378]. Brucite was not identified in the present work; however, this mineral normally follows the behaviour of portlandite as its Mg analogue (see Table 8 and [376,377]).

The reference investigations and present study reveal that various oxides and hydroxides can occur in BAs (Table 7). However, these minerals are not characteristic of all BAs because they do not play significant to major roles in every biomass combustion product, for example ashes from high and medium acid types and sub-types (Fig. 2). In contrast to coal ashes, there are BAs within medium acid and especially low acid types and sub-types (Fig. 2) where oxyxhydroxides play, respectively, subordinate to major roles in comparison with other mineral classes during ash formation (see Part II).

3.4.3. Phosphates

The various phosphates found in BA are listed in Table 7 and described earlier [3]. Shortly, the reference investigations ([3] and references therein) show that phosphates can be mostly secondary, to a lesser extent primary, and occasionally tertiary phases in BA (Table 7), which is identical to silicates and oxyhydroxides. These minerals have both detrital and authigenic occurrence in/on plants because: (1) certain phosphates (such as the group of apatite) are typical soil minerals and they can have some relatively low detrital uptake from the soil during plant growth; and (2) phosphates are characteristic authigenic minerals in plants and animals and originate from syngenetic and epigenetic evaporation and precipitation of mineralized aqueous solution enriched in different cations and phosphate and hydrogen phosphate anions. Hence, some phosphates can be primary phases in BA due to their possible presence as unchanged relics having relatively high decomposition (Table 8) and/or melting (Table 9) temperatures during heating. For example, MPs of phosphates are normally higher than 1200 °C (Table 9). Additionally, the occurrence of some technogenic phosphates in plants from fertilisers and in semi-biomass as impurities (additives or contaminants) generated from processing of natural biomass can also be primary as a result of their presence as unaltered minerals in BA. However, the secondary phosphates of Al, Ca, Fe, K, Mg, Mn, Na and Zn (Table 7) are dominant in BA and these newly formed phases are attributed to interaction between oxides of the above-listed elements and P generated mostly from OM, as well as melt crystallisation and phosphate condensation during biomass combustion (Table 8). For example, evidence of apatite crystallisation within the Si–K glass formed from melt was observed in BA. The origin of the secondary phosphates is probably similar to that in coal ash and this has been suggested elsewhere [52,372,373,375]. Finally, the tertiary phosphates may include minerals containing water molecules and/or hydroxyl groups (for example, hydroxylapatite and K pyrophosphate hydrate in Table 7), which can be a result of hydration and hydroxylation of other less stable phosphates by water and moisture in the air during transport and storage of BA. The less stable pyrophosphates (Table 7) are not characteristic phases of BA in contrast to phosphates, and their accessory occurrence could be a result of some unstable conditions in the system during biomass combustion ([3] and references therein).

The present study of eight biomass varieties and their HTAs confirmed many of the above observations. Minerals such as phosphates of Ca (apatite and whitlockite) identified in HTAs (Table 11) are among the most suitable examples for explanation of the thermal behaviour of this mineral class during biomass combustion (Table 7). It can be seen that some HTAs (BC, CC, PP, SS, SG, WS in Table 10) contain high contents of P_2O_5 (2–10%) and the thermal behaviour of these samples is illustrated in Figs. 4–6, 8–10, 12–14 and 16–18. The phase transformation of original phases containing Ca and P (OM, oxalates, carbonates, phosphates and sulphates) in the biomass varieties studied includes their decomposition and crystallisation/recrystallization to newly formed secondary: (1) whitlockite (500–900 °C); and (2) apatite (500–1300 °C); in HTAs (Table 11 and Figs. 6 and 8–10). It can be seen that the most intensive formation of apatite occurs at 900–1100 °C (Figs. 6, 8 and 10) and the less stable whitlockite transforms to more stable apatite at 1100 °C (Fig. 8). On the other hand, the dissolution of apatite in the melt at 1300 °C for some HTAs (Figs. 6, 8 and 10); can also be seen on XRD patterns. Similar formation and transformation temperatures for apatite, whitlockite and other Ca phosphates have also been given elsewhere (Table 8). Hence, the formation of apatite and whitlockite is mostly secondary, while for some samples the primary occurrence of apatite is also possible (for example, PP in Fig. 6).

The reference investigations and present study reveal that various phosphates can occur in BAs (Table 7). These minerals are characteristic of BAs (in contrast to coal ashes) and play significant (high acid type in Fig. 2) to major roles (medium and low acid types and sub-types in Fig. 2) in almost all biomass combustion products in comparison with other mineral classes during ash formation (see Part II).

3.4.4. Sulphates, sulphides, sulphosalts, sulphites and thiosulphates

The various sulphates identified in BA are listed in Table 7 and described earlier [3]. Shortly, the reference investigations ([3] and references therein) show that sulphates can be mostly secondary, and to a lesser extent, tertiary and primary phases in BA (Table 7). Sulphates are highly mobile during weathering and they are not typical soil minerals. These minerals have authigenic occurrence in plants because they originate from syngenetic and epigenetic evaporation and precipitation of mineralized aqueous solution enriched in different cations and sulphate anion, as well as probably sulphide anion. Hence, some sulphates can be primary phases in BA due to their possible presence as unchanged relics having relatively moderate to high decomposition (Table 8) and/or melting (Table 9) temperatures during heating. For example, MPs of sulphates are commonly higher than 700–1000 °C (Table 9). Additionally, the occurrence of some technogenic Al, Ba, Ca, Cd, Cu, Fe, K, Na, Sr and Zn sulphates (Table 7) in plants from fertilisers and in semi-biomass as impurities (additives or contaminants) generated from processing of natural biomass can also be primary as a result of their presence as unaltered minerals in BA. However, the secondary sulphates of Al, Ca, K, Mg and Na (Table 7) are dominant in BA and these newly formed phases are commonly attributed to interaction between acidic SO_X (SO_2 and SO_3) gases and oxides of the above elements generated mostly from OM and carbonates during biomass combustion (Table 8). The origin of these secondary sulphates is similar to that in coal ash and their formation mechanisms have been described in detail earlier ([376,377] and references therein). Finally, the tertiary sulphates may include minerals containing water molecules and/or hydroxyl groups (for example, bassanite, chalcanthite, ettringite, gypsum, picromerite, syngenite in Table 7), which can be a result of hydration and hydroxylation of other less stable sulphates by water and moisture in the air during transport and storage of BA. The less stable sulphides, sulphosalts, sulphites and thiosulphates (Table 7) are not common phases of BA in contrast to sulphates, and their accessory occurrence can be a result of some reducing and unstable conditions in the system during biomass combustion. For example, this statement was evidenced by the association of sulphides with char in BA ([3] and references therein).

The present study of eight biomass varieties and their HTAs confirmed many of the above observations. Minerals such as sulphates of Ca (anhydrite, gypsum), K (arcanite) and K and Mg (picromerite) identified in HTAs (Table 11) are among the most appropriate examples for explanation of the thermal behaviour of this mineral class during biomass combustion (Table 7). It can be seen that some HTAs (MM, PP and SS in Table 10) contain high contents of SO_3 (8–28%) and the thermal behaviour of these samples is illustrated in Figs. 6, 7, 10, 14, 15 and 18. The phase transformation of original phases containing S and alkaline and alkaline-earth elements (OM, oxalates, carbonates, phosphates and sulphates) in the biomass varieties studied includes their decomposition and crystallisation/recrystallization to newly formed (secondary and tertiary) sulphates: (1) gypsum (500 °C); (2) picromerite (500 °C); (3) anhydrite (500–1100 °C); and (4) arcanite (500–1100 °C); in HTAs (Table 11 and Figs. 3–7, 9 and 10). On the other hand, the decomposition of: (1) anhydrite at 900–1100 °C (for CC in Fig. 5 and SS in Fig. 10), 1100–1300 °C (for PP in Fig. 6), 1170 °C (for WS in Figs. 9 and 17b) and 1250 °C (for MM in Figs. 7 and 15b); and (2) arcanite at 1236 °C (for SS in Figs. 10 and 18b); can be seen on DTA-TGA profiles and supported by XRD patterns. Similar formation and transformation temperatures for anhydrite and arcanite have also been given elsewhere (Table 8). Hence, the formation of anhydrite and arcanite is dominantly secondary, while the crystallisation of gypsum and picromerite commonly has a tertiary origin in BAs due to the hydration of secondary anhydrite–bassanite and langbeinite, respectively, by moisture in the air during cooling and storage of HTAs (Tables 7 and 11).

The reference investigations and present study reveal that various sulphates can occur in BAs (Table 7). However, these minerals are not typical of all BAs (in contrast to coal ashes) because they do not play significant to major roles in every biomass combustion product, for example ashes from high and medium acid types and sub-types (Fig. 2). On the other hand, there are BAs within medium acid and especially low acid types and sub-types (Fig. 2) where sulphates can play, respectively, subordinate to major roles in comparison with other mineral classes during ash formation (see Part II).

3.4.5. Carbonates and bicarbonates

The various carbonates plus some bicarbonates (or hydrogencarbonates) identified in BA are listed in Table 7 and described earlier [3]. Shortly, the reference investigations ([3] and references therein) show that carbonates and bicarbonates can be mostly secondary, to a lesser extent tertiary, and occasionally primary phases in BA, which is similar to sulphates. Carbonates (normally calcite, dolomite, ankerite and magnesite) have both detrital and authigenic occurrence in/on plants because these minerals are: (1) typical for some soils and they can have some relatively low detrital uptake from the soil during plant growth; and (2) characteristic authigenic minerals in plants and animals and originate from syngenetic and epigenetic evaporation and precipitation of mineralized aqueous solution enriched in different cations and carbonate, hydrocarbonate and hydrobicarbonate anions. Hence, some carbonates can be primary phases in BA due to their possible presence as unchanged relics despite their relatively moderate decomposition (Table 8) and/or melting (Table 9) temperatures during heating. For example, MPs of alkaline carbonates are commonly about 800–900 °C (Table 9). Additionally, the occurrence of some technogenic carbonates in semi-biomass as impurities (fillers, additives or contaminants) generated from processing of natural biomass can also be primary as a result of their presence as unaltered minerals in BA (Table 7). However, the secondary carbonates of Al, Ca, Cr, Fe, K, Mg, Na and Zn (Table 7) are normally dominant in BA and these newly formed phases originate mostly from the decomposition and oxidation of OM, oxalates and carbonates and subsequent carbonation (and recarbonation) of the secondary oxyhydroxides during biomass combustion (Table 8). On the other hand, tertiary carbonates can be formed from secondary Ca and Mg hydroxides during transport and storage of BA due to reactions of the former minerals with CO_2 occurring in air and water. For example, the tertiary calcite is a result of lime hydroxylation and subsequent portlandite carbonation during HTA storage. Finally, other tertiary carbonates may also include minerals containing water molecules and/or hydroxyl groups (for example, arterite, baylissite, hydrocalcite, hydrotalcite, hydrozincite, nesquehonite, paraalumohydrokalcit and pirssonite in Table 7), which can be a result of hydration and hydroxylation of other less stable carbonates by water and moisture in the air during transport and storage of BA ([3] and references therein). Hence, the origin of these secondary and tertiary carbonates in BA is similar to that in coal ash and their formation mechanisms have been described in detail for some carbonates ([376,377] and references therein).

The present study of eight biomass varieties and their HTAs confirmed most of the above observations. It can be seen that different Ca, Mg, K and Na carbonates were identified in HTAs (Table 11) and they are among the most appropriate examples for explanation of the thermal behaviour of this mineral class during biomass combustion (Table 7). It should be stated that the specification of the origin for carbonates in BAs (similar to hydroxides) is not an easy task and some additional investigations are required. The phase transformation of original phases containing C, Ca, Mg, K, Na and Fe (OM, oxalates, carbonates, phosphates and sulphates) in the biomass varieties studied includes their decomposition and crystallisation/recrystallization to newly formed secondary and tertiary: (1) dolomite, magnesite, natrite and natrofairchildite (500 °C); (2) butschliite and fairchildite (500–900 °C); (3) kalicinite (500–1100 °C); and (4) calcite (500–1300 °C); in HTAs (Table 11 and Figs. 4–10). On the other hand, the decomposition of: (1) calcite at 538 °C (for MM in Fig. 15b), 690 °C (for SG in Fig. 12b), 737 °C (for PP in Fig. 14b), 740 °C (for SS in Fig. 18b), 743 °C (for BC in Fig. 16b), and 896 °C (for WS in Fig. 17b); (2) dehydrogened kalicinite, butschliite, fairchildite and natrofairchildite at 706 °C and 777 °C (for WS in Fig. 17b) and fairchildite at 889 °C (for SS in Fig. 18b); can be seen on DTA-TGA profiles and supported by XRD patterns. Similar formation and transformation temperatures for Ca, K and Na carbonates have also been given elsewhere (Table 8). It is well known that the decomposition of carbonates occurs between 500 and 900 °C (Table 8). Hence, Ca, K and Na carbonates (calcite, kalicinite, butschliite, fairchildite and natrofairchildite) identified in the HTAs produced at 900, 1100 and 1300 °C are mostly tertiary in origin and they are a result of carbonation of secondary Ca-, K- and Na-oxyhydroxides by CO_2 in the air during storage of SG, CC, PP, BC, WS and SS ashes (Table 11 and Figs. 4–6 and 8–10). It should be noted that kalicinite ($KHCO_3$) has reversible transformation to KCO_3 at 100–200 °C (Table 8).

The reference investigations and present study reveal that various carbonates can occur in BAs (Table 7). These minerals are typical of BAs (in contrast to coal ashes) and play significant (high acid type in Fig. 2) to major roles (medium and low acid types and sub-types in Fig. 2) in almost all biomass combustion products in comparison with other mineral classes during ash formation (see Part II).

3.4.6. Chlorides, chlorites and chlorates

The various chlorides identified in BA are listed in Table 7 and described earlier [3]. Shortly, the reference investigations ([3] and references therein) show that chlorides can be mostly secondary, and to a lesser extent, tertiary and primary phases in BA, which is similar to sulphates and carbonates. Chlorides are highly mobile during weathering and they are not typical soil minerals, similar to sulphates. These minerals have authigenic occurrence in plants because they originate from syngenetic and epigenetic evaporation and precipitation of mineralized aqueous solution enriched in different cations and chloride anion. Hence, some chlorides can be primary phases in BA due to their possible presence as unchanged relics despite their relatively low to moderate decomposition (Table 8) and/or melting (Table 9) temperatures during heating. For example, MPs of chlorides are normally 300–800 °C (Table 9). Additionally, the occurrence of some technogenic chlorides in plants from fertilisers and in semi-biomass as impurities (additives or contaminants) generated from processing of natural biomass can also be primary as a result of their presence as unaltered minerals in BA (Table 7). The secondary chlorides of Bi, Ca, Cd, Cu, Fe, K, Na, Pb and Zn (Table 7) are dominant in BA and these newly formed phases are commonly attributed to interaction between Cl-containing gases and the above elements (generated mostly from OM) during biomass combustion (Table 8). The origin of these secondary chlorides is probably similar to that in coal ash [387]. The tertiary chlorides may include minerals containing mostly water molecules and/or hydroxyl groups (for example, Ca chlorite hydrate, Ca and Cu hydroxylchlorides and Zn chloride hydrate in Table 7), which can be a result of hydration and hydroxylation of other less stable chlorides by water and moisture in the air during transport and storage of BA. Finally, tertiary chlorides such as halite and sylvite and others (Table 7) may also include minerals precipitated from water solutions (enriched in Na and K cations and chloride anion) and generated during transport and storage of BA. The less stable chlorites and chlorates (Table 7) are not common phases of BA in contrast to chlorides, and their accessory occurrence can be a result of some unstable conditions in the system during biomass combustion. For example, potassium forms perchlorates during low-temperature oxidation (100–250 °C) and these compounds decompose and melt between 200–700 °C releasing Cl ([3] and references therein).

The present study of eight biomass varieties and their HTAs confirmed many of the above observations. Minerals such as chlorides of Na (halite) and K (sylvite) identified in HTAs (Table 11) are the most appropriate examples for explanation of the thermal behaviour of this mineral class during biomass combustion. It can be seen that the biomass varieties and their HTAs studied (Table 10) are enriched in Cl (especially MM sample) and the thermal behaviour of these samples is illustrated in Figs. 3–10. The phase transformation of original phases containing Cl and alkaline elements (OM, carbonates, phosphates, chlorides and sulphates) in the biomass varieties studied includes their decomposition and crystallisation/recrystallization to newly formed (secondary and tertiary) chlorides: (1) halite (500–900 °C); and (2) sylvite (500–900 °C); in HTAs (Table 11 and Figs. 3, 5 and 7). On the other hand, the melting of halite and sylvite mixture at 745 °C (for MM in Fig. 15b) can be seen on DTA-TGA profiles and supported by XRD patterns (Fig. 7). Similar formation and transformation temperatures for both chlorides have also been given elsewhere (Tables 8 and 9). Hence, the formation of halite and sylvite can be primary according to the XRD data of dry, water-soluble residues produced from all biomass samples (Figs. 3–10). However, these chlorides are dominantly secondary in HTAs (Tables 7 and 11 and Figs. 3, 5 and 7). It is well known that the melting of both chlorides is at 770–801 °C (Table 9) and their identifications in some HTAs produced at 900 °C (Table 11 and Figs. 3 and 7) is probably due to their occurrence inside some coarse-grained particles. It should be stated that the unusually high-temperature occurrences of portlandite, gypsum, calcite, kalicinite, halite, sylvite and char in some ashes could be explained by: (1) their presence in less altered cores of coarser-grained particles in HTAs; and (2) some salt condensation and reversible transformations of some intermediate and less stable secondary phases (oxides and some sulphates) to their more stable primary or tertiary mineral occurrences (hydroxides, carbonates and hydrated sulphates) during cooling of HTAs and especially their storage in time; as described earlier [376,377].

The reference investigations and present study reveal that various chlorides can occur in BAs (Table 7). These minerals are characteristic of BAs (in contrast to coal ashes) and play significant to major roles in almost all biomass combustion products (high, medium and low acid types and sub-types in Fig. 2) in comparison with other mineral classes during ash formation (see Part II).

3.4.7. Nitrates

The nitrates identified in BA are listed in Table 7 and described earlier [3]. Shortly, the reference investigations ([3] and references therein) show that nitrates can be secondary, and to a lesser extent, tertiary and primary phases in BA, which is similar to sulphates, carbonates and chlorides. However, the available information for them is very limited. Nitrates are highly mobile during weathering and they are not typical soil minerals, similar to sulphates and chlorides. These minerals have authigenic occurrence in plants because they originate from syngenetic and epigenetic evaporation and precipitation of mineralized aqueous solution enriched in different cations and nitrate anion. Hence, some nitrates can be primary phases in BA due to their possible presence as unchanged relics despite their relatively low to moderate decomposition (Table 8) and/or melting (Table 9) temperatures during heating. For example, the decomposition temperatures and MPs of some nitrates are normally at 300–700 °C (Table 9). Additionally, the occurrence of some technogenic nitrates in plants from fertilisers and in semi-biomass as impurities (additives or contaminants) generated from processing of natural biomass may also be primary as a result of their presence as unaltered minerals in BA (Table 7). Nitrates such as Ca nitrate hydrate, nitre and nitrocalcite were identified only in biomass and LTA (Table 7). The secondary K and Ca nitrates in BA can be attributed to interactions between acidic NO_X (NO and NO_2) gases and K and Ca (generated mostly from OM) during biomass combustion (Table 8). The origin of these secondary nitrates is probably similar to that in coal ash. For example, potassium forms nitrates during low-temperature oxidation (100–250 °C) and these compounds decompose between 200–700 °C releasing N. Finally, the tertiary nitrates include minerals containing water molecules (Ca nitrate hydrate and nitrocalcite in Table 7), which can be a result of: (1) hydration of other less stable nitrates by water and moisture in the air; and (2) minerals precipitated from water solutions (enriched in Ca and K cations and nitrate anion); and generated during transport and storage of BA ([3] and references therein).

The present study shows that some of the biomass varieties studied (Table 10) are enriched in N (1.1–2.1% for SS, WS and MM samples); however, the occurrence of nitrates was not identified in BAs produced at 500 °C and higher temperatures (Table 11). The reason for that can be: (1) the highly volatile behaviour of N during combustion; (2) the respective low N contents in BAs; and (3) the relatively low detection capability of XRD.

The reference investigations reveal that some nitrates may occur in BAs (Table 7). However, it seems that these minerals could be typical only of some lower temperature BAs produced from N-enriched solid biofuels and could have a significant role (medium and especially low acid types and sub-types in Fig. 2) in certain cases during ash formation (see Part II).

3.4.8. Glass

Glass in BA has been described earlier [3]. Shortly, the reference investigations ([3] and references therein) show that glass is mostly secondary and, to a lesser extent primary, and occasionally tertiary phase in BA (Table 7), which is identical to silicates, oxyhydroxides and phosphates. The secondary amorphous phase resulted from fusion of inorganic material in biomass and rapid cooling of the melt produced during combustion. Some unchanged glass particles may also be primary in BA if there is pre-existing detrital (from volcanic rocks in soil and their uptake) and technogenic (impurities from additives or contaminants) occurrence of glass with relatively high melting temperatures in biomass and semi-biomass, respectively. It was found that glass in BA contains primarily Si, K, Ca and Na, and, to a lesser extent, Mg, S, P, Fe, Mn and Al. It forms rock-like, ribbon-like, hair-like and other morphological types (Table 4). Glass agglomerates also occur in BA, composed of different sintered or semi-melted ash particles bound by glassy materials. It was identified that some high silica BAs generated from rice straw and some grasses can produce highly vesicular glass products from bubble formation and expansion. These products occasionally form hollow spherical particles of 5–10 μm in diameter, which entrap gases. This is similar to coal ash cenospheres. In contrast to silica enriched BA, high Ca wood BA normally produces massive glass beads without quench crystals and vesicles. Some limited tertiary glass can be formed during weathering of BAs. The explanations above are identical or similar to those identified for various glass types and morphologies in coal ash ([3] and references therein).

The present study of eight biomass varieties and their HTAs confirmed most of the above observations. It was found microscopically that the glass formation occurs over a wide temperature range (700–1500 °C) as a result of initial (700 °C), significant (900–1100 °C) and complete (1100–1300 °C, excluding the RH sample) fusion of BAs. The thermal behaviour of these samples is also illustrated by DTA-TGA profiles and XRD patterns (Figs. 3–18). The glass material plus some poorly crystallised (cryptocrystalline) structures of inorganic matter (see Section 3.4.9) in HTAs are produced at 500–1500 °C. The former product is the most characteristic of ashes produced at higher temperatures (900–1500 °C), while the latter product is more typical of ashes generated at lower temperatures (500–700 °C). These both newly formed materials can be seen microscopically and also appear as amorphous halo with maximums in the range of 10–50° (2θ for CuKα radiation) on the base line of the XRD patterns (Figs. 3–10). Glass is the most abundant in ashes (slags) produced at the highest temperatures

Table 14

Systematization of the physico-chemical transformations during combustion of eight biomass samples with increasing of temperature.

Temperature	Transformation
⩽500 °C	Combustion of organic matter (cellulose, hemicellulose and lignin) Crystallization of secondary and recrystallization of primary silicates (opal, quartz, cristobalite, kalsilite, leucite, K feldspars, plagioclases) Crystallization of secondary (periclase, portlandite) and tertiary (portlandite from lime) oxyhydroxides Crystallization of secondary and recrystallization of primary sulphates (gypsum, anhydrite, arcanite) and formation of tertiary sulphates (gypsum and picromerite due to hydration of anhydrite and K–Mg sulphate) Crystallization of secondary phosphates (apatite and whitlockite) Crystallization of secondary and recrystallization of primary carbonates (calcite, butschliite, fairchildite, natrite, natrofairchildite, KCO_3, dolomite, magnesite) and formation of tertiary carbonates (kalicinite from K oxyhydroxides and KCO_3) Crystallization of secondary calcite due to the decomposition and carbonation of Ca oxalates Crystallization of secondary and recrystallization of primary chlorides (halite, sylvite) Probable formation of secondary Ca nitrates Formation of secondary amorphous (non-glass) material
500–700 °C	Combustion of residual char Crystallization of secondary silicates (quartz, cristobalite, kalsilite, leucite, plagioclases) Crystallization of secondary (lime, periclase, portlandite) and tertiary (portlandite from lime) oxyhydroxides Crystallization of secondary sulphates (anhydrite, arcanite) Crystallization of secondary phosphates (apatite and whitlockite) Crystallization of secondary carbonates (calcite, butschliite, fairchildite, KCO_3) and formation of tertiary carbonates (calcite from lime and portlandite and kalicinite from K oxyhydroxides and KCO_3) Crystallization of secondary chlorides (halite, sylvite) Formation of secondary amorphous (non-glass) material Initial formation of melt
700–900 °C	Combustion of residual char Crystallization of secondary silicates (quartz, cristobalite, tridymite, kalsilite, leucite, plagioclases) Crystallization of secondary (lime, periclase) and tertiary (portlandite from lime) oxyhydroxides Crystallization of secondary sulphates (anhydrite, arcanite) Crystallization of secondary phosphates (apatite and whitlockite) Crystallization of secondary carbonates (calcite, butschliite, fairchildite, KCO_3) and formation of tertiary carbonates (calcite from lime and portlandite and kalicinite from K oxyhydroxides and KCO_3) Crystallization of secondary chlorides (halite, sylvite) and their melting Formation of secondary amorphous (non-glass) material Formation of melt/glass
900–1100 °C	Crystallization of secondary silicates (quartz, cristobalite, tridymite, kalsilite, leucite, plagioclases) Crystallization of secondary (lime, periclase) and tertiary (portlandite from lime) oxyhydroxides Crystallization of secondary sulphates (anhydrite, arcanite) Crystallization of secondary phosphates (apatite) and transformation of whitlockite to apatite Crystallization of tertiary carbonates (calcite from lime and portlandite and kalicinite from K oxyhydroxides and KCO_3) and decomposition of secondary carbonates (calcite, butschliite, fairchildite, KCO_3) Melting of chlorides (halite, sylvite) Formation of secondary amorphous (non-glass) material Formation of melt/glass
1100–1300 °C	Crystallization of secondary silicates (quartz, cristobalite, tridymite, leucite), melting of feldspars and dissolution of kalsilite, lime and periclase in melt Crystallization of tertiary portlandite (from lime) Decomposition of secondary sulphates (anhydrite, arcanite) Crystallization of secondary apatite Crystallization of tertiary calcite from lime and portlandite Formation of secondary amorphous (non-glass) material Formation of melt/glass
1300–1500 °C	Crystallization of secondary silicates (quartz, cristobalite, tridymite) and dissolution of leucite, lime and apatite in melt Formation of secondary amorphous (non-glass) material Formation of melt/glass

and the approximate proportions of this material seem to be characteristic of BC, MM, PP > SS > CC > SG and, to a lesser extent, WS > RH (infused) based on the areas of amorphous halo and crystalline matter for the combustion products produced at these temperatures (Figs. 3–10). Hence, ashes with moderate to high contents of Ca, K, Si, Mg and P (Table 10) have a tendency for producing more glass. The microscopic investigations show that the first melt portions appear at ashes produced at 700 °C (CC, MM, SS, WS), 900 °C (BC, PP, SG) or 1300 °C (RH). Subsequently, the significant to intensive fusion of ashes proceeds at 900 °C (CC, MM, SG, WS) and 1100 °C (BC, PP, SS). Finally the complete ash melting was observed at 1100 °C (CC, SG) and 1300 °C (BC, MM, PP, SS, WS) excluding the RH sample. It should be stated that the melt formation in the combustion products can initiate at different temperature intervals depending on the phase composition of biomass and BA. For example, the fusion of: (1) K and Na nitrates and hydroxides (<500 °C); (2) some low-temperature K–Na silicate eutectics and Fe and Mn chlorides (500–700 °C); (3) K and Na chlorides and carbonates, as well as Na sulphate (700–900 °C); (4) K sulphate (900–1100 °C); (5) Mg sulphate, acid plagioclases, feldspars, illite and montmorillonite (1100–1300 °C); (6) Ca sulphate and basic plagioclases (1300–1500 °C); and (7) Ca and Mg silicates and oxides, kaolinite and silica minerals (>1500 °C); can be the major reasons for the initial liquid formation with increasing temperatures (Table 9).

DTA-TGA profiles of biomass and BA samples can specify some important temperatures related to melting of ashes. For example, it is well known that the complete fusion of biomass and coal ashes (hemispherical and mostly fluid ash-fusion temperatures) is detected as an endothermic reaction involving no

Table 15
Systematization of the leading physico-chemical processes during biomass combustion.

Process	Mineral, phase	Temperature (°C)
1. Oxidation and combustion of organic matter	Combustion of OM (cellulose, hemicellulose, lignin) and release of elements and compounds (Al, C, CH_4, C_2H_2, C_2H_6, CO, CO_2, Ca, Fe, H_2, H_2O, K, Mg, Mn, N_2, NO_X, Na, O_2, P, S, SO_X, Si, Ti, trace elements, others) associated with OM that: – escape the system as volatile components – react with each other – react with IM – form discrete inorganic phases (oxyhydroxides, carbonates, chlorides, sulphates, nitrates)	200–850
2. Transformation of minerals and inorganic phases		
2.1. Transformation in solid state		
2.1.1. Crystallization–recrystallization	Amorphous and cryptomere clay minerals	200–300
	Amorphous SiO_2	200–1100
	Opal, chalcedony	<300
2.1.2. Destruction of crystal lattice	Kaolinite	300–1100
	Zeolites	700–860
	Illite, muscovite	700–1100
	Montmorillonite, chlorite	800–1100
2.1.3. Polymorphic transformation	Marcasite → pyrite	100–400
	Aragonite → calcite	390–420
	α-quartz → β-quartz → tridymite → cristobalite	575–1500
	Orthoclase → sanidine	900–1000
2.2. Transformation with liberation of gas phases		
2.2.1. Decarbonation	Siderite	400–800
	Ankerite	500–800
	Calcite and dolomite	500–900
	Magnesite	560–650
	Ca–K carbonates	600–900
	K carbonate	830–1000
2.2.2. Dehydration	Kaolinite, illite, montmorillonite	50–200
	Ca oxalates, gypsum, hexahydrite, various hydrates	100–200
	Bassanite	200–400
2.2.3. Dehydroxylation	Jarosite	300–900
	Brucite	400–500
	Fe hydroxides	400–600
	Al hydroxides	450–580
	Portlandite	450–800
	Kaolinite, illite, muscovite, montmorillonite, chlorite	600–900
2.2.4. Desulphation	Fe sulphates	480–900
	Arcanite, thenardite	800–1100
	Anhydrite	800–1300
	Barite	900–1300
	Mg sulphates	1100–1200
2.2.5. Reduction	Hematite	900–1400
2.3. Transformation from solid to fluid state (melting) (see also Table 9)	K and Na hydroxides	318–406
	K and Na nitrates	330–370
	K silicates	600–980
	Mg and Ca chlorides	714–772
	K and Na chlorides	770–801
	K and Na carbonates	788–904
	K phosphates	800–1620
	Na silicates	874–1088
	Na sulphate	884
	Zeolites	896–1185
	Montmorillonite, illite, chlorite, muscovite, biotite, amphibole	1000–1300
	K sulphate	1067–1100
	Albite (acid plagioclase)	1118
	Feldspars (plagioclases and K feldspars)	1118–1553
	K feldspars (orthoclase, microcline, sanidine)	1170
	Apatite	1270–1660
	Ca–Mg silicates	1392–1554
	Ca sulphate	1450
	Nepheline	1526
	Ca silicates	1540–2130
	Anorthite (basic plagioclase)	1553
	Melilite	1554–1590
	Mg silicates	1557–1890
	Kaolinite, metakaolinite	1650–1810
	Kalsilite–kaliophilite	1684–1750
	Leucite	1686
	Quartz, cristobalite, tridymite, amorphous silica	1713
	Mullite, andalusite, sillimanite	1810
	Lime	2570–2597
	Periclase	2800

(*continued on next page*)

Table 15 (*continued*)

Process	Mineral, phase	Temperature (°C)
3. Reactions between minerals and phases		
3.1. Reactions between solid, liquid and gas phases		
3.1.1. Carbonation	Ca, K, Mg and Na oxyhydroxides and oxalates to:	
	– tertiary calcite, kalicinite	Ambient
	– secondary calcite, butschliite, fairchildite, natrite, natrofairchildite, dolomite	200–900
3.1.2. Chloridation	Na and K oxyhydroxides to halite and sylvite	500–700
3.1.3. Formation of inorganic amorphous (non-glass) material	Variable composition	Ambient-700
3.1.4. Hydration	Anhydrite and bassanite to tertiary gypsum	Ambient
	K–Mg sulphate to picromerite	Ambient
3.1.5. Hydroxylation	Lime, periclase and hematite to:	
	– tertiary portlandite, brucite, goethite	Ambient
	– secondary goethite	100–200
	– secondary brucite	300–400
	– secondary portlandite	300–600
3.1.6. Nitration	Ca oxyhydroxides to Ca nitrates	<500
3.1.7. Oxidation	– Fe sulphides	100–500
	– organically bound Ca, Mg, K, Na, Fe, Al to oxides	200–850
3.1.8. Phosphation	Ca oxyhydroxides to:	
	– whitlockite	500–900
	– apatite	500–1300
3.1.9. Silicate formation with liberation of gas phases	Reactions between:	
	– quartz and calcite to Ca silicates	400–800
	– quartz and anhydrite to Ca silicates	400–1300
	– calcite and wollastonite to larnite	500–900
3.1.10. Sulphation	Ca, K, Mg and Ba oxyhydroxides to:	
	– gypsum	Ambient
	– anhydrite	100–1100
	– barite	200–900
	– arcanite, Mg sulphate	200–1100
3.2. Solid-state reactions	Wollastonite	400–1300
	Kalsilite, feldspars (K feldspars, plagioclases)	500–1100
	Larnite	500–1200
	Leucite	500–1300
	Monticellite	600–1300
	Spinel	700–1200
	Melilite, rankinite	700–1300
	Anorthite	800–1100
	Mullite	800–1400
4. Processes in solutions and melts		
4.1. Crystallization of phases in melts	Kalsilite	1100
	Leucite, feldspars (K-feldspars, plagioclases), Ca and Ca–Mg silicates	1100–1300
	Hematite, magnetite	1100–1400
	Quartz, cristobalite, tridymite	1100–1500
	Mullite	1100–1600
4.2. Dissolution of minerals and solid phases in melts	Quartz, cristobalite, tridymite, Ca and Ca–Mg silicates, spinel, lime, periclase, hematite, magnetite, corundum, others	1100–1600
4.3. Glass formation	Glass	700–1600
4.4. Precipitation of inherited moisture	Halite, sylvite, arcanite, calcite, kalicinite, gypsum, magnesite, Ca oxalates, Ca nitrate hydrate, nitrocalcite, inorganic amorphous material	Ambient

change in mass or with limited mass loss [46,220,344,385]. Therefore, the temperatures related to the fluid state of the samples can be:

- 1193 °C for SG (Fig. 12a and b);
- 1230 °C for WS (Fig. 17a and b);
- 1233 °C for PP (1230–1235 °C in Fig. 14a and b);
- 1235 °C for CC (1230–1240 °C in Fig. 13a and b);
- 1236 °C for SS together with arcanite decomposition (Fig. 18a and b);
- 1240 °C for MM together with anhydrite decomposition (1230–1250 °C in Fig. 15a and b);
- 1300 °C for BC (Fig. 16b); and
- >1350 °C for RH (Fig. 11a and b).

It can be seen that these temperatures are in accordance with the fluid state observed visually in the crucibles after ash was produced at maximum temperatures in the electric oven (Table 10). The only exclusions are samples SG and CC which were transformed to liquid at $\leqslant$1100 °C (Table 10), which is significantly lower than determined by DTA, respectively 1193 °C and 1235 °C. The reason can be the prolonged time required for ash production in the electric oven (1 h at 1100 °C) in comparison with DTA-TGA analyses (10 °C min^{-1}) and the extensive dissolution of refractory minerals in the crucibles by the initial and active melts [3] of SG and CC ashes which have moderate silica contents (Table 10 and Fig. 1d). The ash fusion temperatures of various BAs have been reported recently [3], while the ash-melting behaviour of BAs and their types and sub-types will be characterised in Part II.

The reference investigations and present study reveal that glass is a characteristic phase in BAs (similar to coal ashes). This phase plays significant to major roles in all biomass combustion products (high, medium and low acid types and sub-types in Fig. 2) in comparison with other mineral classes during ash formation (see Part II).

3.4.9. Inorganic amorphous (non-glass) material

The inorganic amorphous (non-glass) material in BA has been described earlier [3]. Shortly, the reference investigations ([3] and references therein) show that this newly formed and mostly secondary product represents particles composed of non-fused phases and they were identified in BA produced from different biomass varieties. It is well known that phases such as clay, mica and silica minerals, zeolites and some hydroxides, sulphates and phosphates lose their crystallisation water at 300–1100 °C, resulting in structural collapse and consequent amorphization in this temperature range. For example, the presence of amorphous sulphate phases, poorly crystallised hydrohylapatite and non-crystalline needle-shaped silica grains or rounded to irregular shaped grains composed mostly of Si, K and Ca were observed in some BAs. Additionally, the formation of hydrated silicate phases and portlandite with amorphous, disordered or poorly crystallised structures during hydration of BA is also common ([3] and references therein).

The present study of eight biomass varieties and their HTAs confirmed some of the above observations. For example, the newly formed amorphous (non-glass) and poorly crystallised structures of inorganic matter in HTAs produced at 500 °C can be seen as maximums of amorphous halo in the range of 15–40° (2θ for CuKα radiation) on the base line of the XRD patterns (Figs. 3–6 and 10). This non-crystalline to semi-crystalline material seems to be characteristic of RH > SG ashes, to some extent CC > SS > MM > WS ashes, and occasionally other ashes (BC, PP) based on the areas of amorphous halo and crystalline matter for BAs generated at 500 °C. Ashes enriched in both Si and K and depleted in both Ca and Mg (Table 10) seem to have a stronger tendency for producing structurally disordered inorganic material at lower temperature intervals (500–700 °C) before the intensive fusion of BAs.

The reference investigations and present study reveal that inorganic amorphous (non-glass) material is typical of BAs (similar to coal ashes). This material plays a significant role in all biomass combustion products (high, medium and subordinately low acid types and sub-types in Fig. 2) in comparison with other mineral classes during ash formation (see Part II).

3.4.10. Other inorganic phases

The other inorganic phases identified in BA are listed in Table 7 and described earlier [3]. Shortly, the reference investigations ([3] and references therein) show that different metallic alloys and pure metals are typical minor and accessory phases in municipal solid waste ashes, other industrial ashes, and even some plants (Table 7). Hence, these metallic alloys and pure metals can occur as unchanged relics or impurities (additives or contaminants) in BA if they have relatively high decomposition and/or melting temperatures. For example, MPs of some elemental forms (Ag, Au, Cr, Cu, Fe, Mn, Ni, Pt, Si) are above 900 °C (Table 9). The presence of some unusual phases such as K–Mo selenide and margaritasite ($(Cs,K,H_3O)_2(UO_2)_2V_2O_8 \cdot (H_2O)$) in ashes produced from incomplete combustion of oil palm biomass waste (fibres from empty fruit bunches) and rice husks, respectively, has also been reported ([3] and references therein). Such accessory phases were not identified in the present study due to the low detection capability of XRD for minor and trace minerals, as well as using of natural biomass samples.

3.5. Systematization of physico-chemical transformations during biomass combustion

The reference and present data described above show that the physico-chemical transformations of OM and IM during biomass combustion are complex and include various interactions between solid, gas and liquid phases with original and newly formed genesis in such multicomponent system. A systematization of these transformations during combustion of eight biomass samples in the present study is given in Table 14. Additionally, the leading physico-chemical transformation processes during biomass combustion are summarized and systematized in Table 15 based on the combination of reference data (Tables 8 and 9) and present studies (Tables 11 and 14). It can be seen that the original OM and IM in biomass during combustion transform: (1) initially to devolatilization of OM and burning of combustible gases and char with formation of intermediate and less stable oxalates, nitrates, chlorides, hydroxides, carbonates, sulphates and inorganic amorphous (non-glass) material; (2) subsequently to more stable silicates, phosphates and oxides; (3) then to melting accompanied by dissolution of the refractory minerals; with increasing combustion temperatures in the system; and (4) followed by crystallisation of melt and formation of glass accompanied by some salt condensation and hydroxylation, hydration and carbonation of newly formed phases during cooling of BA. Finally, some post-combustion transformations of the newly formed minerals and phases to stable during weathering species among silicates, hydroxides, phosphates, sulphates, carbonates, chlorides and nitrates also occur due to their hydration, hydroxylation and carbonation by moisture and CO_2 in the air through storage of BA. Therefore, the detailed knowledge of OM and IM in biomass and its behaviour during combustion could predict and explain numerous technological and environmental problems resulting from the thermo-chemical conversion of biofuels (see Part II).

The present study also clearly shows that the ash formation mechanisms are strongly related to the presence, abundance, association and behaviour of the modes of element occurrence in biomass and BA. These chemical forms of combination of elements are represented by specific refractory (commonly silicates, oxyhydroxides and phosphates) or fluxing (normally chlorides, carbonates, sulphates and nitrates) mineral species, groups and classes or phases generated mainly as a result of chemical reactions in the BA system. Minerals are particularly illuminating in considering interpretations of ash formation mechanisms because their occurrence is a strong indicator of the processes during fuel combustion. It is well known that there are predictable end products of a definite set of physico-chemical conditions that provide an environment in which the minerals could be crystallised or in which they could form. Hence, such mineral crystallizations can be applied for reconstruction of the conditions and formation processes occurring during biomass combustion ([52,372,373,378,385,403] and references therein).

The detailed knowledge of the above issues can provide the most important information for the advanced and sustainable utilisation of biomass fuels and their thermo-chemical conversion products. Therefore, the specification of biomass varieties to proper organic and inorganic types and sub-types can play a leading role for prediction of their behaviour during biomass combustion and this topic will be evaluated in detail in Part II.

4. Conclusions

Some conclusions based on the present overview of the phase-mineral transformations of OM and IM during biomass combustion can be made:

(1) Biomass, similar to solid fossil fuels, is a complex heterogeneous mixture of OM (structural ingredients and organic minerals) and, to a lesser extent, IM (minerals, mineraloids and amorphous material), containing various intimately associated solid and fluid phases with different contents and natural (authigenic and detrital) or technogenic origin. The main structural organic components in biomass are cellulose, hemicellulose and lignin and these matrices contain

in addition various major, minor or accessory organic and inorganic phases.

(2) BA is the solid residue that results from the combustion of biomass and it is a complex inorganic–organic mixture with polycomponent, heterogeneous and variable composition, size and morphology, and contains: (1) mostly IM composed of non-crystalline (amorphous) and crystalline to semi-crystalline (mineral) constituents; (2) subordinately OM consisting of char and organic minerals; and (3) some fluid matter comprising moisture and gas and gas–liquid inclusions associated with both IM and OM.

(3) The physico-chemical transformations of OM and IM during biomass combustion include various interactions between solid, gas and liquid phases with original and newly formed genesis in such multicomponent system. General processes, namely: (1) combustion of OM (200–850 °C) (2) fragmentation (disintegration) of particles (500 °C); (3) initial (700–900 °C), significant (700–1100 °C) and extensive (700–1300 °C) agglomeration or occasionally swelling of particles; (4) initial (700 °C), extensive (900–1100 °C) and complete (1100–1500 °C) fusion of particles or minerals with different melting points; (5) various new phase crystallizations (500–1500 °C); and (6) melt/glass formation (700–1500 °C); were observed in BAs.

(4) OM of different biomass varieties tends to show similar combustion behaviour despite different phase and chemical composition, whereas IM of these biomass varieties has a tendency to reveal variable performance during combustion. The investigations also indicate that the thermal behaviour of IM and ash formation mechanisms of different BAs tend to be: (1) diverse between the inorganic "S", "C", "K" and "CK" types; and (2) similar within the inorganic types and sub-types.

(5) The proportions among cellulose, hemicellulose and lignin in biomass seem to have limited significance during combustion process and the two stage combustion behaviour of OM with increasing of temperature is basically related to: (1) devolatilization and burning of combustible volatile matter; and subsequently (2) char formation and combustion; simultaneously from the three structural components of the bulk OM with some temperature fluctuations depending on the content and distribution of structural components. The ill-defined structure, variable composition, different impurities and changeable properties of cellulose, hemicellulose and lignin in biomass varieties reflect directly on their variable and less predictable thermo-chemical conversion behaviour.

(6) Char particles encapsulated by newly formed chloride, carbonate, sulphate and silicate aggregates in the ashes obtained at 500–900 °C and even higher temperatures occur in BAs. The combustion of such residual char seems to follow closely the decomposition, recrystallization or melting of the above mineral layers or matrices containing this char.

(7) The minerals and phases found in BAs (291 identified) include more species and groups of species in comparison with coal ashes (188 found). The number of mineral species in BAs belongs to the mineral classes: silicates > oxides and hydroxides > sulphates > phosphates > carbonates > chlorides > nitrates > others. The common phases found in BAs comprise glass, char, silica minerals (quartz, cristobalite, tridymite), calcite, sylvite, leucite, plagioclases, amorphous (non-glass) material, arcanite, anhydrite, lime, periclase, hematite, portlandite, apatite, larnite, melilite, Ca phosphates, fairchildite, K carbonate, K feldspars, halite, K–Ca silicates, ankerite, clay minerals, siderite, Na silicate, merwinite, glaserite, gypsum, pyroxenes, olivines, others.

(8) BAs have highly variable chemical and phase-mineral composition and properties and these characteristics are more changeable and differ significantly in comparison with those of coal ashes. Most of the minerals and phases identified in coal ashes were also found in BAs. However, many mineral species among Ca–K–Mn silicates, Ca–Al–Mn oxides, K–Na–Ca chlorides and K–Ca–Mg–Na carbonates, sulphates and phosphates identified in BAs were normally not found in coal ashes. The reason for that could be the enrichment of elements such as Ca, Cl, K, Mg, Mn, Na and P in BAs compared to coal ashes. In contrast, typical Si-, Al-, Fe- and Ti-bearing minerals of coal ashes (quartz, clay and mica minerals, mullite, feldspars, Fe oxides and rutile), were not characteristic of many BAs probably due to limited contents of these elements in BAs.

(9) Phosphates, carbonates and chlorides (in contrast to coal ashes) plus glass and inorganic amorphous materials are characteristic of BAs because they play significant to major roles in almost all biomass combustion products in comparison with other mineral classes during ash formation. On the other hand, silicates, oxyhydroxides and sulphates are not typical of all BAs (in contrast to coal ashes) because they do not play such important roles in every biomass combustion product.

(10) The phases and minerals in BAs (similar to coal ashes) can be classified by origin as: (1) primary, namely pre-existing or original minerals and phases in biomass that have undergone no phase transformations during combustion (mostly refractory silicates, oxyhydroxides and phosphates); (2) secondary such as new phases formed during combustion process (species from all mineral classes plus glass and char); and (3) tertiary, namely new minerals or phases formed during transport and storage of BA (mainly carbonates and hydroxides).

(11) The systematization of physico-chemical transformations during biomass combustion show that the original OM and IM in biomass transform: (1) initially to devolatilization of OM and burning of combustible gases and char with formation of intermediate and less stable oxalates, nitrates, chlorides, hydroxides, carbonates, sulphates and inorganic amorphous (non-glass) material; (2) subsequently to more stable silicates, phosphates and oxides; (3) then to melting accompanied by dissolution of the refractory minerals; with increasing combustion temperatures in the system; and (4) followed by crystallisation of melt and formation of glass accompanied by some salt condensation and hydroxylation, hydration and carbonation of newly formed phases during cooling of BA. Finally, some post-combustion transformations of the newly formed minerals and phases to stable during weathering species among silicates, hydroxides, phosphates, sulphates, carbonates, chlorides and nitrates also occur due to their hydration, hydroxylation and carbonation by moisture and CO_2 in the air through storage of BA.

Finally, the present study shows that inorganic composition of biomass and BA is highly variable and the assignment of various biomass varieties to different inorganic types and sub-types could have primary importance when predicting the behaviour of a particular fuel during processing and potential applications of biomass conversion products. There is a big advantage when the biomass and BA classification systems are based on the identification and implementation of significant relationships between elemental concentrations, combined chemical and phase-mineral associations and especially on an application of genetic approaches for specification of the phases. In this case the reasons for different problems or benefits during biomass processing can be systematically identified and explained. Certain major associations related to the occurrence, content and origin of elements and phases were identified in the BA system and they include: (1) Si–Al–Fe–Na–Ti (mostly glass, silicates and oxyhydroxides); (2) Ca–Mg–Mn (commonly carbonates, oxyhydroxides, glass, silicates and some phosphates and sulphates); and (3) K–P–S–Cl (normally phosphates, sulphates, chlorides, glass and some silicates and carbonates). These associations were applied for classification of BAs to four types and six sub-types. Such systematic relationships have a key importance in both fundamental and applied aspects, namely their potential applications for classifications and indicator purposes connected with innovative and sustainable processing of biomass and BA.

The ash formation mechanisms and ash fusion behaviour, as well as some indications of potential technological problems and environmental risks during combustion of biomass types and sub-types and application of their BAs will be described in Part II of the present work.

Acknowledgements

The present work was carried out in part within the European Commission's research programme and in part within the research programme of the Bulgarian Academy of Sciences. Stanislav Vassilev would like to express his gratitude to the Joint Research Centre (European Commission) for the possibility to perform studies at the Institute for Energy and Transport (Petten, The Netherlands) as a Detached National Expert.

References

[1] Vassilev S, Baxter D, Andersen L, Vassileva C. An overview of the chemical composition of biomass. Fuel 2010;89:913–33.
[2] Vassilev S, Baxter D, Andersen L, Vassileva C, Morgan T. An overview of the organic and inorganic phase composition of biomass. Fuel 2012;94:1–33.
[3] Vassilev S, Baxter D, Andersen L, Vassileva C. An overview of the composition and application of biomass ash. Part 1. Phase-mineral and chemical composition and classification. Fuel 2013;105:40–76.
[4] Vassilev S, Baxter D, Andersen L, Vassileva C. An overview of the composition and application of biomass ash. Part 2. Potential utilization, technological and ecological advantages and challenges. Fuel 2013;105:19–39.
[5] Farrell AE, Gopal AR. Bioenergy research needs for heat, electricity, and liquid fuels. MRS Bullet 2008;33:373–80.
[6] Demirbas A. Biorefineries: current activities and future developments. Energ Convers Manage 2009;50:2782–801.
[7] Fouilland T, Grace JR, Ellis N. Recent advances in fluidized bed technology in biomass processes. Biofuels 2010;1(3):409–33.
[8] Zhang L, Xu C, Champagne P. Overview of recent advances in thermo-chemical conversion of biomass. Energ Convers Manage 2010;51:969–82.
[9] Izquierdo M, Querol X. Leaching behaviour of elements from coal combustion fly ash: an overview. Int J Coal Geol 2012;94:54–66.
[10] Ward SM, Braslaw J. Experimental weight loss kinetics of wood pyrolysis under vacuum. Combust Flame 1985;61:261–9.
[11] Kalkreuth W, Brouillard D, Roy C. Optical and chemical characterization of solid residues obtained from vacuum pyrolysis of wood (Aspen Poplar). Biomass 1986;10:27–45.
[12] Etiegni L, Campbell AG. Physical and chemical characteristics of wood ash. Bioresour Technol 1991;37:173–8.
[13] Baxter LL. Ash deposition during biomass and coal combustion: a mechanistic approach. Biomass Bioenerg 1993;4(2):85–102.
[14] Misra MK, Ragland KW, Baker AJ. Wood ash composition as a function of furnace temperature. Biomass Bioenerg 1993;4(2):103–16.
[15] Ulery AL, Graham RC, Amrhein C. Wood-ash composition and soil pH following intense burning. Soil Sci 1993;156(5):358–64.
[16] Williams PT, Besler S. The pyrolysis of rice husks in a thermogravimetric analyser and static batch reactor. Fuel 1993;72:151–9.
[17] Kanury AM. Combustion characteristics of biomass fuels. Combust Sci Technol 1994;97:469–91.
[18] Nordin A. Chemical elemental characteristics of biomass fuels. Biomass Bioenerg 1994;6(5):339–47.
[19] Miles TR, Miles JTR, Baxter LL, Bryers RW, Jenkins BM, Oden LL. Alkali deposits found in biomass power plants. A preliminary investigation of their extent and nature. Report of the National Renewable Energy Laboratory, (NREL/TZ-2-11226-1; TP-433-8142). Golden, CO., USA; 1995.
[20] Olanders B, Steenari B-M. Characterization of ashes from wood and straw. Biomass Bioenerg 1995;8(2):105–15.
[21] Raveendran K, Ganesh A, Khilar KC. Influence of mineral matter on biomass pyrolysis characteristics. Fuel 1995;74(12):1812–22.
[22] Bryers RW. Fireside slagging, fouling and high-temperature corrosion of heat transfer surface due to impurities in steam raising fuels. Prog Energ Combust 1996;22:29–120.
[23] Easterly JL, Burnham M. Overview of biomass and waste fuel resources for power production. Biomass Bioenerg 1996;10(2–3):79–92.
[24] Ghetti P, Ricca L, Angelini L. Thermal analysis of biomass and corresponding pyrolysis products. Fuel 1996;75:565–73.
[25] Jenkins BM, Bakker RR, Wei JB. On the properties of washed straw. Biomass Bioenerg 1996;10(4):177–200.
[26] Kristensen O. Combined heat and power production based on gasification of straw and woodchips. In: Chartier P, Ferrero GL, Henius UM, Hultberg S, Sachau J, Wiinblad M, editors. Proceedings of the 9th European bioenergy conference, vol. 1. Copenhagen, Denmark, Pergamon: Elsevier Science Ltd, Oxford UK, 24–27 June 1996. p. 272–7.
[27] Miles TR, Miles JTR, Baxter LL, Bryers RW, Jenkins BM, Oden LL. Boiler deposits from firing biomass fuels. Biomass Bioenerg 1996;10(2–3):125–38.
[28] Narodoslawsky M, Obernberger I. From waste to raw material - the route from biomass to wood ash for cadmium and other heavy metals. J Hazard Mater 1996;50:157–68.
[29] Pedersen LS, Nielsen HP, Kiil S, Hansen LA, Dam-Johansen K, Kildsig F, et al. Full-scale co-firing of straw and coal. Fuel 1996;75(13):1584–90.
[30] Raveendran K, Ganesh A, Khilar KC. Pyrolysis characteristics of biomass and biomass components. Fuel 1996;75(8):987–98.
[31] Someshwar AV. Wood and combination wood-fired boiler ash characterization. J Environ Qual 1996;25:962–72.
[32] Blander M, Pelton AD. The inorganic chemistry of the combustion of wheat straw. Biomass Bioenerg 1997;12(4):295–8.
[33] Faaij A, Van Doorn J, Curvers T, Waldheim L, Olsson E, Van Wijk A, et al. Characteristics and availability of biomass waste and residues in the Netherlands for gasification. Biomass Bioenerg 1997;12:225–40.
[34] Obernberger I, Biedermann F, Widmann W, Riedl R. Concentrations of inorganic elements in biomass fuels and recovery in the different ash fractions. Biomass Bioenerg 1997;12(3):211–24.
[35] Sander B. Properties of Danish biofuels and the requirements for power production. Biomass Bioenerg 1997;12(3):177–83.
[36] Steenari B-M, Lindqvist O. Stabilisation of biofuel ashes for recycling to forest soil. Biomass Bioenerg 1997;13:39–50.
[37] Turn SQ, Kinoshita CM, Ishimura DM. Removal of inorganic constituents of biomass feedstocks by mechanical dewatering and leaching. Biomass Bioenerg 1997;12(4):241–52.
[38] Baxter LL, Miles TR, Miles Jr TR, Jenkins BM, Milne T, Dayton D, et al. The behaviour of inorganic material in biomass-fired power boilers: field and laboratory experiences. Fuel Process Technol 1998;54(1–3):47–78.
[39] Jenkins BM, Baxter LL, Miles Jr TR, Miles TR. Combustion properties of biomass. Fuel Process Technol 1998;54(1–3):17–46.
[40] Kozinski JA, Saade R. Effect of biomass burning on the formation of soot particles and heavy hydrocarbons. An experimental study. Fuel 1998;77(4):225–37.
[41] Raveendran K, Ganesh A. Adsorption characteristics and pore-development of biomass-pyrolysis char. Fuel 1998;77(7):769–81.
[42] Steenari B-M, Lindqvist O. High-temperature reactions of straw ash and the anti-sintering additives kaolin and dolomite. Biomass Bioenerg 1998;14(1):67–76.
[43] Turn SQ, Kinoshita CM, Ishimura DM, Zhou J. The fate of inorganic constituents of biomass in fluidized bed gasification. Fuel 1998;77(3):135–46.
[44] Zevenhoven R, Hupa M. The reactivity of chars from coal, peat and wood towards NO, with and without CO. Fuel 1998;77(11):1169–76.
[45] Dayton DC, Jenkins BM, Turn SQ, Bakker RR, Williams RB, Belle-Oudry D, et al. Release of inorganic constituents from leached biomass during thermal conversion. Energ Fuel 1999;13:860–70.
[46] Hansen LA, Frandsen FJ, Dam-Johansen K, Sorensen HS, Skrifvars B-J. Characterization of ashes and deposits from high-temperature coal-straw co-firing. Energ Fuel 1999;13(4):803–16.
[47] Seggiani M. Empirical correlations of the ash fusion temperatures and temperature of critical viscosity for coal and biomass ashes. Fuel 1999;78:1121–5.
[48] Steenari B-M, Karlsson LG, Lindqvist O. Evaluation of the leaching characteristics of wood ash and the influence of ash agglomeration. Biomass Bioenerg 1999;16:119–36.
[49] Steenari B-M, Schelander S, Lindqvist O. Chemical and leaching characteristics of ash from combustion of coal, peat and wood in a 12 MW CFB – a comparative study. Fuel 1999;78:249–58.
[50] Thy P, Jenkins BM, Lesher CE. High-temperature melting behaviour of urban wood fuel ash. Energ Fuel 1999;13:839–50.
[51] Van der Drift A, Olsen A. Conversion of biomass, (private) prediction and solution methods for ash agglomeration and related problems. Project Report of ECN. Petten, The Netherlands; 1999. p. 89.
[52] Vassilev S, Braekman-Danheux C, Laurent P. Characterization of refuse-derived char from municipal solid waste. 1. Phase-mineral and chemical composition. Fuel Process Technol 1999;59:95–134.
[53] Vassilev S, Braekman-Danheux C. Characterization of refuse-derived char from municipal solid waste. 2. Occurrence, abundance and source of trace elements. Fuel Process Technol 1999;59:135–61.

[54] Vassilev S, Braekman-Danheux C, Laurent P, Thiemann T, Fontana A. Behaviour, capture and inertization of some trace elements during combustion of refuse-derived char from municipal solid waste. Fuel 1999;78:1131–45.

[55] Chirone R, Salatino P, Scala F. The relevance of attrition to the fate of ashes during fluidized-bed combustion of a biomass. Proc Combust Inst 2000;28:2279–86.

[56] Hansen LA, Nielsen HP, Frandsen FJ, Dam-Johansen K, Horlyck S, Karlsson A. Influence of deposit formation on corrosion at a straw-fired boiler. Fuel Process Technol 2000;64:189–209.

[57] Huggins FE, Shah N, Huffman GP, Robertson JD. XAFS spectroscopic characterization of elements in combustion ash and fine particulate matter. Fuel Process Technol 2000;65–66:203–18.

[58] Hus PJ, Tillman DA. Cofiring multiple opportunity fuels with coal at Bailly Generating Station. Biomass Bioenerg 2000;19:385–94.

[59] Jensen PA, Frandsen FJ, Dam-Johansen K, Sander B. Experimental investigation of the transformation and release to gas phase of potassium and chlorine during straw pyrolysis. Energ Fuel 2000;14:1280–5.

[60] Jones JM, Pourkashanian M, Williams A, Hainsworth D. A comprehensive biomass combustion model. Renew Energ 2000;19:229–34.

[61] Kalapathy U, Proctor A, Shultz J. Silica xerogels from rice hull ash: structure, density and mechanical strength as affected by gelation pH and silica concentration. J Chem Technol Biotechnol 2000;75:464–8.

[62] Kaufmann H, Nussbaumer T, Baxter L, Yang N. Deposit formation on a single cylinder during combustion of herbaceous biomass. Fuel 2000;79:141–51.

[63] Lind T, Valmari T, Kauppinen E, Nilsson K, Sfiris G, Maenhaut W. Ash formation mechanisms during combustion of wood in circulating fluidized beds. Proc Combust Inst 2000;28:2287–95.

[64] Nakbanpote W, Thiravetyan P, Kalambaheti C. Preconcentration of gold by rice husk ash. Miner Eng 2000;13(4):391–400.

[65] Nielsen HP, Frandsen FJ, Dam-Johansen K, Baxter LL. The implications of chlorine-associated corrosion on the operation of biomass-fired boilers. Prog Energ Combust 2000;26:283–98.

[66] Nielsen HP, Baxter LL, Sclippab G, Morey C, Frandsen FJ, Dam-Johansen K. Deposition of potassium salts on heat transfer surfaces in straw-fired boilers: a pilot-scale study. Fuel 2000;79:131–9.

[67] Schmieder H, Abeln J, Boukis N, Dinjus E, Kruse A, Kluth M, et al. Hydrothermal gasification of biomass and organic wastes. J Supercrit Fluids 2000;17:145–53.

[68] Thy P, Lesher CE, Jenkins BM. Experimental determination of high-temperature elemental losses from biomass slag. Fuel 2000;79:693–700.

[69] Tillman DA. Cofiring benefits for coal and biomass. Biomass Bioenerg 2000;19:363–4.

[70] Tillman DA. Biomass cofiring; the technology, the experience, the combustion consequences. Biomass Bioenerg 2000;19:365–84.

[71] Warnecke R. Gasification of biomass: comparison of fixed bed and fluidized bed gasifier. Biomass Bioenerg 2000;18:489–97.

[72] Werther J, Saenger M, Hartge E-U, Ogada T, Siagi Z. Combustion of agricultural residues. Prog Energ Combust 2000;26:1–27.

[73] Wieck-Hansen K, Overgaard P, Larsen OH. Cofiring coal and straw in a 150 MWe power boiler experiences. Biomass Bioenerg 2000;19:395–409.

[74] Zevenhoven-Onderwater M, Blomquist J-P, Skrifvars B-J, Backman R, Hupa M. The prediction of behaviour of ashes from five different solid fuels in fluidised bed combustion. Fuel 2000;79:1353–61.

[75] Zheng G, Kozinski JA. Thermal events occurring during the combustion of biomass residue. Fuel 2000;79:181–92.

[76] Allica JH, Mitre AJ, Bustamante JAG, Itoiz C, Blanco F, Alkorta I, et al. Straw quality for its combustion in a straw-fired power plant. Biomass Bioenerg 2001;21:249–58.

[77] Arvelakis S, Vourliotis P, Kakaras E, Koukios EG. Effect of leaching on the ash behavior of wheat straw and olive residue during fluidized bed combustion. Biomass Bioenerg 2001;20:459–70.

[78] Coll R, Salvado J, Farriol X, Montane D. Steam reforming model compounds of biomass gasification tars: conversion at different operating conditions and tendency towards coke formation. Fuel Process Technol 2001;74: 19–31.

[79] Dare P, Gifford J, Hooper RJ, Clemens AH, Damiano LF, Gong D, et al. Combustion performance of biomass residue and purpose grown species. Biomass Bioenerg 2001;21:277–87.

[80] Demeyer A, Voundi Nkana JC, Verloo MG. Characteristics of wood ash and influence on soil properties and nutrient uptake: an overview. Bioresource Technol 2001;77:287–95.

[81] Demirbas A. Biomass resource facilities and biomass conversion processing for fuels and chemicals. Energ Convers Manage 2001;42:1357–78.

[82] Folkedahl BC, Schmidt DD, Weber GF, Zygarlicke CJ. Barrier issues to the utilization of biomass. Semiannual Technical Progress Report of the Energy and Environmental Research Center: University of North Dakota, Grand Forks, ND, USA; 2001. p. 37.

[83] Gabra M, Nordin A, Ohman M, Kjellstrom B. Alkali retention/separation during bagasse gasification: a comparison between a fluidised bed and a cyclone gasifier. Biomass Bioenerg 2001;21:461–76.

[84] Hansen HK, Pedersen AJ, Ottosen LM, Villumsen A. Speciation and mobility of cadmium in straw and wood combustion fly ash. Chemosphere 2001;45:123–8.

[85] Henrich E, Dinjus E, Rumpel S, Stahl R. A two-stage pyrolysis/gasification process for herbaceous waste biomass from agriculture. In: Bridgwater AV, editor. Progress in thermochemical biomass conversion. Oxford: Blackwell Science Ltd.; 2001. p. 221–35. vol. 1.

[86] Jensen PA, Sander B, Dam-Johansen K. Pretreatment of straw for power production by pyrolysis and char wash. Biomass Bioenerg 2001;20:431–46.

[87] Jensen PA, Sander B, Dam-Johansen K. Removal of K and Cl by leaching of straw char. Biomass Bioenerg 2001;20:447–57.

[88] Kataki R, Konwer D. Fuelwood characteristics of some indigenous woody species of north-east India. Biomass Bioenerg 2001;20:17–23.

[89] Minkova V, Razvigorova M, Bjornbom E, Zanzi R, Budinova T, Petrov N. Effect of water vapour and biomass nature on the yield and quality of the pyrolysis products from biomass. Fuel Process Technol 2001;70:53–61.

[90] Paulrud S, Nilsson C. Briquetting and combustion of spring-harvested reed canary-grass: effect of fuel composition. Biomass Bioenerg 2001;20:25–35.

[91] Paulrud S, Nilsson C, Ohman M. Reed canary-grass ash composition and its melting behaviour during combustion. Fuel 2001;80:1391–8.

[92] Sami M, Annamalai K, Wooldridge M. Co-firing of coal and biomass fuel blends. Prog Energ Combust 2001;27:171–214.

[93] Savova D, Apak E, Ekinci E, Yardim F, Petrov N, Budinova T, et al. Biomass conversion to carbon adsorbents and gas. Biomass Bioenerg 2001;21:133–42.

[94] Soong Y, Schoffstall MR, Link TA. Triboelectrostatic beneficiation of fly ash. Fuel 2001;80:879–84.

[95] Van der Drift A, Van Doorn J, Vermeulen JW. Ten residual biomass fuels for circulating fluidized-bed gasification. Biomass Bioenerg 2001;20:45–56.

[96] Williams A, Pourkashanian M, Jones JM. Combustion of pulverised coal and biomass. Prog Energ Combust 2001;27:587–610.

[97] Zevenhoven-Onderwater M, Backman R, Skrifvars B-J, Hupa M. The ash chemistry in fluidised bed gasification of biomass fuels. Part I: predicting the chemistry of melting ashes and ash-bed material interaction. Fuel 2001;80:1489–502.

[98] Zevenhoven-Onderwater M, Backman R, Skrifvars B-J, Hupa M, Liliendahl T, Rosen C, et al. The ash chemistry in fluidised bed gasification of biomass fuels. Part II: ash behaviour prediction versus bench scale agglomeration tests. Fuel 2001;80:1503–12.

[99] Zhang F-S, Yamasaki S, Nanzyo M. Application of waste ashes to agricultural land – effect of incineration temperature on chemical characteristics. Sci Total Environ 2001;264:205–14.

[100] Zumerchik J, editor. Macmillan encyclopedia of energy. New York, USA: Macmillan Reference; 2001. p. 1284.

[101] Aho M, Skrifvars B-J, Yrjas P, Veijonen K, Taipale R, Lybeck E, et al. Benefits of biomass and coal co-combustion in fluidised bed boilers. In: Proceedings of the 12th European conference on biomass for energy, industry and climate protection. Amsterdam, The Netherlands, 17–21 June 2002. p. 456–60.

[102] Armesto L, Bahillo A, Veijonen K, Cabanillas A, Otero J. Combustion behaviour of rice husk in a bubbling fluidised bed. Biomass Bioenerg 2002;23:171–9.

[103] Arvelakis S, Koukios EG. Physicochemical upgrading of agroresidues as feedstocks for energy production via thermochemical conversion methods. Biomass Bioenerg 2002;22:331–48.

[104] Arvelakis S, Gehrmann H, Beckmann M, Koukios EG. Effect of leaching on the ash behavior of olive residue during fluidized bed gasification. Biomass Bioenerg 2002;22:55–69.

[105] Davidsson KO, Korsgren JG, Pettersson JBC, Jaglid U. The effects of fuel washing techniques on alkali release from biomass. Fuel 2002;81:137–42.

[106] Dogru M, Howarth CR, Akay G, Keskinler B, Malik AA. Gasification of hazelnut shells in a downdraft gasifier. Energy 2002;27:415–27.

[107] Kalapathy U, Proctor A, Shultz J. An improved method for production of silica from rice hull ash. Bioresource Technol 2002;85:285–9.

[108] McKendry P. Energy production from biomass (part 1): overview of biomass. Bioresource Technol 2002;83:37–46.

[109] McKendry P. Energy production from biomass (part 2): conversion technologies. Bioresource Technol 2002;83:47–54.

[110] McKendry P. Energy production from biomass (part 3): gasification technologies. Bioresource Technol 2002;83:55–63.

[111] Miller BB, Dugwell DR, Kandiyoti R. Partitioning of trace elements during the combustion of coal and biomass in a suspension-firing reactor. Fuel 2002;81:159–71.

[112] Oh GH, Park CR. Preparation and characteristics of rice-straw-based porous carbons with high adsorption capacity. Fuel 2002;81:327–36.

[113] Osan J, Alfoldy B, Torok S, Van Grieken R. Characterisation of wood combustion particles using electron probe microanalysis. Atmos Environ 2002;36:2207–14.

[114] Robinson AL, Junker H, Baxter LL. Pilot-scale investigation of the influence of coal-biomass cofiring on ash deposition. Energ Fuel 2002;16:343–55.

[115] Ross AB, Jones JM, Chaiklangmuang S, Pourkashanian M, Williams A, Kubica K, et al. Measurement and prediction of the emission of pollutants from the combustion of coal and biomass in a fixed bed furnace. Fuel 2002;81:571–82.

[116] Suarez-Garcia F, Martinez-Alonzo A, Llorente MF, Tascon JMD. Inorganic matter characterization in vegetable biomass feedstocks. Fuel 2002;81:1161–9.

[117] Van Loo S, Koppejan J. Handbook of biomass combustion and co-firing. Enschede, The Netherlands: Twente University Press; 2002. p. 348.

[118] Zhang F-S, Yamasaki S, Nanzyo M. Waste ashes for use in agricultural production: I. Liming effect, contents of plant nutrients and chemical characteristics of some metals. Sci Total Environ 2002;284:215–25.

[119] Zhang F-S, Yamasaki S, Nanzyo M. Waste ashes for use in agricultural production: II. Contents of minor and trace metals. Sci Total Environ 2002;286:111–8.

[120] Arvelakis S, Gehrmann H, Beckmann M, Koukios EG. Agglomeration problems during fluidized bed gasification of olive-oil residue: evaluation of fractionation and leaching as pre-treatments. Fuel 2003;82:1261–70.

[121] Attalla M, Chao C, Nelson PF. A review of tools for the modelling and prediction of trace element deportment in combustion processes. Research Report 36 of the Cooperative Research Centre for Coal in Sustainable Development, CSIRO Energy Technology, QCAT Technology Transfer Centre; 2003. p. 71.

[122] Bridgwater AV. Renewable fuels and chemicals by thermal processing of biomass. Chem Eng J 2003;91:87–102.

[123] Demirbas A. Sustainable cofiring of biomass with coal. Energ Convers Manage 2003;44:1465–79.

[124] Demirbas A. Trace metal concentrations in ashes from various types of biomass species. Energ Sources 2003;25:743–51.

[125] Gupta VK, Jain CK, Ali I, Sharma M, Saini VK. Removal of cadmium and nickel from wastewater using bagasse fly ash – a sugar industry waste. Water Res 2003;37:4038–44.

[126] Haykiri-Acma H. Combustion characteristics of different biomass materials. Energ Convers Manage 2003;44:155–62.

[127] Lin W, Dam-Johansen K, Frandsen F. Agglomeration in bio-fuel fired fluidized bed combustors. Chem Eng J 2003;96:171–85.

[128] Park B-D, Wi SG, Lee KH, Singh AP, Yoon T-H, Kim YS. Characterization of anatomical features and silica distribution in rice husk using microscopic and micro-analytical techniques. Biomass Bioenerg 2003;25:319–27.

[129] Risnes H, Fjellerup J, Henriksen U, Moilanen A, Norby P, Papadakis K, et al. Calcium addition in straw gasification. Fuel 2003;82:641–51.

[130] Sorum L, Frandsen FJ, Hustad JE. On the fate of heavy metals in municipal solid waste combustion. Part I. Devolatilisation of heavy metals on the grate. Fuel 2003;82:2273–83.

[131] Tsukada M, Yamada H, Kamiya H. Analysis of biomass combustion ash behavior at elevated temperatures. Adv Powder Technol 2003;14(6):707–17.

[132] Aho M, Silvennoinen J. Preventing chlorine deposition on heat transfer surfaces with aluminium-silicon rich biomass residue and additive. Fuel 2004;83:1299–305.

[133] Arvelakis S, Jensen PA, Dam-Johansen K. Simultaneous thermal analysis (STA) on ash from high-alkali biomass. Energ Fuel 2004;18:1066–76.

[134] Coda B, Cieplik MK, Jacobs JM, Kiel JHA. Impact of biomass co-firing on ash formation and ash behaviour in IGCC plants. Project Report of ECN, Petten, The Netherlands; 2004. p. 63.

[135] Cohen D, Dunn CE. Form and distribution of trace elements in biomass for power generation. Research Report 48 of the cooperative research centre for coal in sustainable development. University of New South Wales, QCAT Technology Transfer Centre: Technology Court Pullenvale, Australia; 2004. p. 66.

[136] Cordero T, Rodriguez-Mirasol J, Pastrana J, Rodriguez JJ. Improved solid fuels from co-pyrolysis of a high-sulphur content coal and different lignocellulosic wastes. Fuel 2004;83:1585–90.

[137] Cuiping L, Chuangzhi W, Yanyongjie, Haitao H. Chemical elemental characteristics of biomass fuels in China. Biomass Bioenerg 2004;27:119–30.

[138] Demirbas A. Combustion characteristics of different biomass fuels. Prog Energ Combust 2004;30:219–30.

[139] Eriksson G, Kjellstrom B, Lundqvist B, Paulrud S. Combustion of wood hydrolysis residue in a 150 kW power burner. Fuel 2004;83:1635–41.

[140] Feng Q, Lin Q, Gong F, Sugita S, Shoya M. Adsorption of lead and mercury by rice husk ash. J Colloid Interf Sci 2004;278:1–8.

[141] Feng W, Van der Kooi HJ, Arons JS. Biomass conversions in subcritical and supercritical water: driving force, phase equilibria, and thermodynamic analysis. Chem Eng Process 2004;43:1459–67.

[142] Knudsen JN, Jensen PA, Lin W, Frandsen FJ, Dam-Johansen K. Sulfur transformations during thermal conversion of herbaceous biomass. Energ Fuel 2004;18:810–9.

[143] Kwok QSM, Jones DEG, Nunez GF, Charland JP, Dionne S. Characterization of bio-fuel and bio-fuel ash. J Therm Anal Calorim 2004;78:173–84.

[144] Lapuerta M, Hernandez JJ, Rodriguez J. Kinetics of devolatilisation of forestry wastes from thermogravimetric analysis. Biomass Bioenerg 2004;27:385–91.

[145] Lavric ED, Konnov AA, De Ruyck J. Dioxin levels in wood combustion – a review. Biomass Bioenerg 2004;26:115–45.

[146] Meszaros E, Jakab E, Varhegyi G, Szepesvary P, Marosvolgyi B. Comparative study of the thermal behavior of wood and bark of young shoots obtained from an energy plantation. J Anal Appl Pyrol 2004;72:317–28.

[147] Obernberger I, Thek G. Physical characterisation and chemical composition of densified biomass fuels with regard to their combustion behaviour. Biomass Bioenerg 2004;27:653–69.

[148] Ohman M, Boman C, Hedman H, Nordin A, Bostrom D. Slagging tendencies of wood pellet ash during combustion in residential pellet burners. Biomass Bioenerg 2004;27:585–96.

[149] Ohman M, Nordin A, Hedman H, Jirjis R. Reasons for slagging during stemwood pellet combustion and some measures for prevention. Biomass Bioenerg 2004;27:597–605.

[150] Richaud R, Herod AA, Kandiyoti R. Comparison of trace element contents in low-temperature and high-temperature ash from coals and biomass. Fuel 2004;83:2001–12.

[151] Shim H-S, Hajaligol MR, Baliga VL. Oxidation behaviour of biomass chars: pectin and *Populus deltoides*. Fuel 2004;83:1495–503.

[152] Skrifvars B-J, Lauren T, Hupa M, Korbee R, Ljung P. Ash behaviour in a pulverized wood fired boiler – a case study. Fuel 2004;83:1371–9.

[153] Sorum L, Frandsen FJ, Hustad JE. On the fate of heavy metals in municipal solid waste combustion. Part II. From furnace to filter. Fuel 2004;83:1703–10.

[154] Srikanth S, Das SK, Ravikumar B, Rao DS, Nandakumar K, Vijayan P. Nature of fireside deposits in a bagasse and groundnut shell fired 20 MW thermal boiler. Biomass Bioenerg 2004;27:375–84.

[155] Tillman DA, Harding NS. Fuels of opportunity: characteristics and uses in combustion systems. Amsterdam, The Netherlands: Elsevier B.V.; 2004. p. 312.

[156] Vamvuka D, Zografos D. Predicting the behaviour of ash from agricultural wastes during combustion. Fuel 2004;83:2051–7.

[157] Yaman S. Pyrolysis of biomass to produce fuels and chemical feedstocks. Energ Convers Manage 2004;45:651–71.

[158] Yang YB, Sharifi VN, Swithenbank J. Effect of air flow rate and fuel moisture on the burning behaviours of biomass and simulated municipal solid wastes in packed beds. Fuel 2004;83:1553–62.

[159] Aho M, Ferrer E. Importance of coal ash composition in protecting the boiler against chlorine deposition during combustion of chlorine-rich biomass. Fuel 2005;84:201–12.

[160] Arvelakis S, Gehrmann H, Beckmann M, Koukios EG. Preliminary results on the ash behavior of peach stones during fluidized bed gasification: evaluation of fractionation and leaching as pre-treatments. Biomass Bioenerg 2005;28:331–8.

[161] Baxter L. Biomass-coal co-combustion: opportunity for affordable renewable energy. Fuel 2005;84:1295–302.

[162] Bergman PCA, Boersma AR, Zwart RWR, Kiel JHA. Torrefaction for biomass co-firing in existing coal-fired power stations. Project Report of ECN. Petten, The Netherlands; 2005. p. 72.

[163] Demirbas A. Potential applications of renewable energy sources, biomass combustion problems in boiler power systems and combustion related environmental issues. Prog Energ Combust 2005;31:171–92.

[164] Deydier E, Guilet R, Sarda S, Sharrock P. Physical and chemical characterisation of crude meat and bone meal combustion residue: "waste or raw material?". J Hazard Mater 2005;B121:141–8.

[165] Frandsen FJ. Utilizing biomass and waste for power production – a decade of contributing to the understanding, interpretation and analysis of deposits and corrosion products. Fuel 2005;84:1277–94.

[166] Hupa M. Interaction of fuels in co-firing in FBC. Fuel 2005;84:1312–9.

[167] Llorente MJF, Garcia JEC. Comparing methods for predicting the sintering of biomass ash in combustion. Fuel 2005;84:1893–900.

[168] Parikh J, Channiwala SA, Ghosal GK. A correlation for calculating HHV from proximate analysis of solid fuels. Fuel 2005;84:487–94.

[169] Park BB, Yanai RD, Sahm JM, Lee DK, Abrahamson LP. Wood ash effects on plant and soil in a willow bioenergy plantation. Biomass Bioenerg 2005;28:355–65.

[170] Pronobis M. Evaluation of the influence of biomass co-combustion on boiler furnace slagging by means of fusibility correlations. Biomass Bioenerg 2005;28:375–83.

[171] Skrifvars B-J, Yrjas P, Kinni J, Siefen P, Hupa M. The fouling behavior of rice husk ash in fluidized-bed combustion. 1. Fuel characteristics. Energ Fuel 2005;19:1503–11.

[172] Thy P, Grundvig S, Jenkins BM, Shiraki R, Lesher CE. Analytical controlled losses of potassium from straw ashes. Energ Fuel 2005;19:2571–5.

[173] Vasudevan P, Sharma S, Kumar A. Liquid fuel from biomass: an overview. J Sci Ind Res 2005;64:822–31.

[174] Wei X, Schnell U, Hein KRG. Behaviour of gaseous chlorine and alkali metals during biomass thermal utilisation. Fuel 2005;84:841–8.

[175] Yang YB, Ryu C, Khor A, Yates NE, Sharifi VN, Swithenbank J. Effect of fuel properties on biomass combustion. Part II. Modelling approach – identification of the controlling factors. Fuel 2005;84:2116–30.

[176] Amand L-E, Leckner B, Eskilsson D, Tullin C. Deposits on heat transfer tubes during co-combustion of biofuels and sewage sludge. Fuel 2006;85:1313–22.

[177] Elled A-L, Amand L-E, Leckner B, Andersson B-A. Influence of phosphorus on sulphur capture during co-firing of sewage sludge with wood or bark in a fluidised bed. Fuel 2006;85:1671–8.

[178] Feng J, Hong QY, Green AES. Analytical model of corn cob Pyroprobe-FTIR data. Biomass Bioenerg 2006;30:486–92.

[179] Fryda L, Panopoulos K, Vourliotis P, Pavlidou E, Kakaras E. Experimental investigation of fluidised bed co-combustion of meat and bone meal with coals and olive bagasse. Fuel 2006;85:1685–99.

[180] Grammelis P, Skodras G, Kakaras E. Effects of biomass co-firing with coal on ash properties. Part I: characterisation and PSD. Fuel 2006;85:2310–5.

[181] Grammelis P, Skodras G, Kakaras E, Karangelos DJ, Petropoulos NP, Anagnostakis MJ, et al. Effects of biomass co-firing with coal on ash properties. Part II: leaching, toxicity and radiological behaviour. Fuel 2006;85:2316–22.

[182] Huber GW, Iborra S, Corma A. Synthesis of transportation fuels from biomass: chemistry, catalysts, and engineering. Chem Rev 2006;106:4044–98.

[183] Kaer SK, Rosendahl LA, Baxter LL. Towards a CFD-based mechanistic deposit formation model for straw-fired boilers. Fuel 2006;85:833–48.

[184] Kastanaki E, Vamvuka D. A comparative reactivity and kinetic study on the combustion of coal-biomass char blends. Fuel 2006;85:1186–93.

[185] Llorente MJF, Garcia JEC. Concentration of elements in woody and herbaceous biomass as a function of the dry ashing temperature. Fuel 2006;85:1273–9.

[186] Llorente MJF, Laplaza JMM, Cuadrado RE, Garcia JEC. Ash behaviour of lignocellulosic biomass in bubbling fluidised bed combustion. Fuel 2006;85:1157–65.

[187] Lokare SS, Dunaway JD, Moulton D, Rogers D, Tree DR, Baxter LL. Investigation of ash deposition rates for a suite of biomass fuels and fuel blends. Energ Fuel 2006;20(3):1008–14.

[188] Martirena F, Middendorf B, Day RL, Gehrke M, Roque P, Martinez L, et al. Rudimentary, low tech incinerators as a means to produce reactive pozzolan out of sugar cane straw. Cement Concrete Res 2006;36:1056–61.

[189] Mohan D, Pittman JCU, Steele PH. Pyrolysis of wood/biomass for bio-oil: a critical review. Energ Fuel 2006;20(3):848–89.

[190] Nair DG, Jagadish KS, Fraaij A. Reactive pozzolanas from rice husk ash: an alternative to cement for rural housing. Cement Concrete Res 2006;36:1062–71.

[191] Obernberger I, Brunner T, Barnthaler G. Chemical properties of solid biofuels – significance and impact. Biomass Bioenerg 2006;30:973–82.

[192] Pronobis M. The influence of biomass co-combustion on boiler fouling and efficiency. Fuel 2006;85:474–80.

[193] Ryu C, Yang YB, Khor A, Yates NE, Sharifi VN, Swithenbank J. Effect of fuel properties on biomass combustion: part I. Experiments – fuel type, equivalence ratio and particle size. Fuel 2006;85:1039–46.

[194] Shuangning X, Zhihe L, Baoming L, Weiming Y, Xueyuan B. Devolatilization characteristics of biomass at flash heating rate. Fuel 2006;85:664–70.

[195] Srivastava VC, Mall ID, Mishra IM. Equilibrium modelling of single and binary adsorption of cadmium and nickel onto bagasse fly ash. Chem Eng J 2006;117:79–91.

[196] Srivastava VC, Mall ID, Mishra IM. Characterization of mesoporous rice husk ash (RHA) and adsorption kinetics of metal ions from aqueous solution onto RHA. J Hazard Mater 2006;B134:257–67.

[197] Theis M, Mueller C, Skrifvars B-J, Hupa M, Tran H. Deposition behaviour of model biofuel ash in mixtures with quartz sand. Part 1: experimental data. Fuel 2006;85:1970–8.

[198] Theis M, Skrifvars B-J, Hupa M, Tran H. Fouling tendency of ash resulting from burning mixtures of biofuels. Part 1: deposition rates. Fuel 2006;85:1125–30.

[199] Theis M, Skrifvars B-J, Zevenhoven M, Hupa M, Tran H. Fouling tendency of ash resulting from burning mixtures of biofuels. Part 2: deposit chemistry. Fuel 2006;85:1992–2001.

[200] Theis M, Skrifvars B-J, Zevenhoven M, Hupa M, Tran H. Fouling tendency of ash resulting from burning mixtures of biofuels. Part 3: influence of probe surface temperature. Fuel 2006;85:2002–11.

[201] Thy P, Jenkins BM, Grundvig S, Shiraki R, Lesher CE. High temperature elemental losses and mineralogical changes in common biomass ashes. Fuel 2006;85:783–95.

[202] Thy P, Jenkins BM, Lesher CE, Grundvig S. Compositional constrains on slag formation and potassium volatilization from rice straw blended wood fuel. Fuel Process Technol 2006;87:383–408.

[203] Tite MS, Shortland A, Maniatis Y, Kavoussanaki D, Harris SA. The composition of the soda-rich and mixed alkali plant ashes used in the production of glass. J Archaeol Sci 2006;33:1284–92.

[204] Vamvuka D, Troulinos S, Kastanaki E. The effect of mineral matter on the physical and chemical activation of low rank coal and biomass materials. Fuel 2006;85(12–13):1763–71.

[205] Wzorek Z, Jodko M, Gorazda K, Rzepecki T. Extraction of phosphorus compounds from ashes from thermal processing of sewage sludge. J Loss Prevent Proc 2006;19:39–50.

[206] Arvelakis S, Frandsen FJ. Melting behavior of ashes from the co-combustion of coal and straw. Energ Fuel 2007;21(5):3004–9.

[207] Bridgeman TG, Darvell LI, Jones JM, Williams PT, Fahmi R, Bridgwater AV, et al. Influence of particle size on the analytical and chemical properties of two energy crops. Fuel 2007;86:60–72.

[208] Davidsson KO, Amand L-E, Leckner B, Kovacevik B, Svane M, Hagstrom M, et al. Potassium, chlorine, and sulphur in ash, particles, deposits, and corrosion during wood combustion in a circulating fluidized-bed boiler. Energ Fuel 2007;21:71–81.

[209] Fahmi R, Bridgwater AV, Darvell LI, Jones JM, Yates N, Thain S, et al. The effect of alkali metals on combustion and pyrolysis of *Lolium* and *Festuca* grasses, switchgrass and willow. Fuel 2007;86:1560–9.

[210] Frandsen FJ, van Lith SC, Korbee R, Yrjas P, Backman R, Obernberger I, et al. Quantification of the release of inorganic elements from biofuels. Fuel Process Technol 2007;88:1118–28.

[211] Gulyurtlu I, Crujeira AT, Abelha P, Cabrita I. Measurements of dioxin emissions during co-firing in a fluidised bed. Fuel 2007;86:2090–100.

[212] Ioannidou O, Zabaniotou A. Agricultural residues as precursors for activated carbon production – a review. Renew Sust Energ Rev 2007;11:1966–2005.

[213] Jimenez S, Ballester J. Formation of alkali sulphate aerosols in biomass combustion. Fuel 2007;86:486–93.

[214] Joller M, Brunner T, Obernberger I. Modeling of aerosol formation during biomass combustion for various furnace and boiler types. Fuel Process Technol 2007;88:1136–47.

[215] Koukouzas N, Hamalainen J, Papanikolaou D, Tourunen A, Jantti T. Mineralogical and elemental composition of fly ash from pilot scale fluidized bed combustion of lignite, bituminous coal, wood chips and their blends. Fuel 2007;86(14):2186–93.

[216] Koyuncu T, Pinar Y. The emissions from a space-heating biomass stove. Biomass Bioenerg 2007;31:73–9.

[217] Liao C, Wu C, Yan Y. The characteristics of inorganic elements in ashes from a 1 MW CFB biomass gasification power generation plant. Fuel Process Technol 2007;88:149–56.

[218] Llorente MJF, Cuadrado RE. Influence of the amount of bed material on the distribution of biomass inorganic elements in a bubbling fluidized bed combustion pilot plant. Fuel 2007;86:867–76.

[219] Martins FM, Martins JM, Ferracin LC, da Cunha CJ. Mineral phases of green liquor dregs, slaker grits, lime mud and wood ash of a Kraft pulp and paper mill. J Hazard Mater 2007;147:610–7.

[220] Masia AAT, Buhre BJP, Gupta RP, Wall TF. Characterising ash of biomass and waste. Fuel Process Technol 2007;88:1071–81.

[221] Masia AAT, Buhre BJP, Gupta RP, Wall TF. Use of TMA to predict deposition behaviour of biomass fuels. Fuel 2007;86(15):2446–56.

[222] McIlveen-Wright DR, Huang Y, Rezvani S, Wang Y. A technical and environmental analysis of co-combustion of coal and bimass in fluidized bed technologies. Fuel 2007;86(14):2032–42.

[223] Miller SF, Miller BG. The occurrence of inorganic elements in various biofuels and its effect on ash chemistry and behavior and use in combustion products. Fuel Process Technol 2007;88:1155–64.

[224] Nevalainen H, Jegoroff M, Saastamoinen J, Tourunen A, Jantti T, Kettunen A, et al. Firing of coal and biomass and their mixtures in 50 kW and 12 MW circulating fluidized beds – phenomenon study and comparison of scales. Fuel 2007;86(14):2043–51.

[225] Nutalapati D, Gupta R, Moghtaderi B, Wall TF. Assessing slagging and fouling during biomass combustion: a thermodynamic approach allowing for alkali/ash reactions. Fuel Process Technol 2007;88:1044–52.

[226] Prasad S, Singh A, Joshi HC. Ethanol as an alternative fuel from agricultural, industrial and urban residues. Resour Conserv Recy 2007;50:1–39.

[227] Schroder E, Thomauske K, Weber C, Hornung A, Tumiatti V. Experiments on the generation of activated carbon from biomass. J Anal Appl Pyrol 2007;79:106–11.

[228] Senneca O. Kinetics of pyrolysis, combustion and gasification of three biomass fuels. Fuel Process Technol 2007;88:87–97.

[229] Tobiasen L, Skytte R, Pedersen LS, Pedersen ST, Lindberg MA. Deposit characteristic after injection of additives to a Danish straw-fired suspension boiler. Fuel Process Technol 2007;88:1108–17.

[230] Tranvik AC, Ohman M, Sanati M. Bed material deposition in cyclones of wood fuel fired circulating fluidized beds (CFBs). Energ Fuel 2007;21:104–9.

[231] Wigley F, Williamson J, Malmgren A, Riley G. Ash deposition at higher levels of coal replacement by biomass. Fuel Process Technol 2007;88:1148–54.

[232] Wiinika H, Gebart R, Boman C, Bostrom D, Ohman M. Inflence of fuel ash composition on high temperature aerosol formation in fixed bed combustion of woody biomass pellets. Fuel 2007;86:181–93.

[233] Yang H, Yan R, Chen H, Lee DH, Zheng C. Characteristics of hemicellulose, cellulose and lignin pyrolysis. Fuel 2007;86:1781–8.

[234] Yanik J, Ebale S, Kruse A, Saglam M, Yuksel M. Biomass gasification in supercritical water: part 1. Effect of the nature of biomass. Fuel 2007;86(15):2410–5.

[235] Zheng Y, Jensen PA, Jensen AD, Sander B, Junker H. Ash transformation during co-firing coal and straw. Fuel 2007;86(7–8):1008–20.

[236] Zhou H, Jensen PA, Frandsen FJ. Dynamic mechanistic model of superheater deposit growth and shedding in a biomass fired grate boiler. Fuel 2007;86:1519–33.

[237] Aho M, Gil A, Taipale R, Vainikka P, Vesala H. A pilot-scale fireside deposit study of co-firing Cynara with two coals in a fluidised bed. Fuel 2008;87:58–69.

[238] Bridgeman TG, Jones JM, Shield I, Williams PT. Torrefaction of reed canary grass, wheat straw and willow to enhance solid fuel qualities and combustion properties. Fuel 2008;87:844–56.

[239] Demirbas A. Biofuels sources, biofuel policy, biofuel economy and global biofuel projections. Energ Convers Manage 2008;49:2106–16.

[240] Di Blasi C. Modelling chemical and physical processes of wood and biomass pyrolysis. Prog Energ Combust 2008;34:47–90.

[241] Fahmi R, Bridgwater AV, Donnison I, Yates N, Jones JM. The effect of lignin and inorganic species in biomass on pyrolysis oil yields, quality and stability. Fuel 2008;87:1230–40.

[242] Goyal HB, Seal D, Saxena RC. Bio-fuels from thermochemical conversion of renewable resources: a review. Renew Sust Energ Rev 2008;12:504–17.

[243] Izquierdo M, Moreno N, Font O, Querol X, Alvarez E, Antenucci D, et al. Influence of the co-firing on the leaching of trace pollutants from coal fly ash. Fuel 2008;87:1958–66.

[244] Jimenez S, Perez M, Ballester J. Vaporization of trace elements and their emission with submicrometer aerosols in biomass combustion. Energ Fuel 2008;22:2270–7.

[245] Lapuerta M, Hernandez JJ, Pazo A, Lopez J. Gasification and co-gasification of biomass wastes: effect of the biomass origin and the gasifier operating conditions. Fuel Process Technol 2008;89:828–37.

[246] Lima AT, Ottosen LM, Pedersen AJ, Ribeiro AB. Characterization of fly ash from bio and municipal waste. Biomass Bioenerg 2008;32(3):277–82.

[247] Llorente MJF, Garcia JEC. Suitability of thermo-chemical corrections for determining gross calorific value in biomass. Thermochim Acta 2008;468:101–7.

[248] Lu G, Yan Y, Cornwell S, Whitehouse M, Riley G. Impact of co-firing coal and biomass on flame characteristics and stability. Fuel 2008; 87:1133–40.

[249] Miccio F, Kalisz S, Baxter D, Svoboda K. Combustion of liquid bio-fuels in an internal circulating fluidized bed. Chem Eng J 2008;143:172–9.

[250] Monti A, Virgilio ND, Venturi G. Mineral composition and ash content of six major energy crops. Biomass Bioenerg 2008;32(3):216–23.

[251] Pettersson A, Amand L-E, Steenari B-M. Leaching of ashes from co-combustion of sewage sludge and wood – part I: recovery of phosphorus. Biomass Bioenerg 2008;32(3):224–35.

[252] Pettersson A, Amand L-E, Steenari B-M. Leaching of ashes from co-combustion of sewage sludge and wood – part II: the mobility of metals during phosphorus extraction. Biomass Bioenerg 2008;32(3):236–44.

[253] Pettersson A, Zevenhoven M, Steenari B-M, Amand L-E. Application of chemical fractionation methods for characterisation of biofuels, waste derived fuels and CFB co-combustion fly ashes. Fuel 2008;87:3183–93.

[254] Ross AB, Jones JM, Kubacki ML, Bridgeman T. Classification of macroalgae as fuel and its thermochemical behaviour. Bioresour Technol 2008;99:6494–504.

[255] Rulkens W. Sewage sludge as a biomass resource for the production of energy: overview and assessment of the various options. Energ Fuel 2008;22:9–15.

[256] Scala F, Chirone R. An SEM/EDX study of bed agglomerates formed during fluidized bed combustion of three biomass fuels. Biomass Bioenerg 2008;32(3):252–66.

[257] Schmidl C, Marr IL, Caseiro A, Kotianova P, Berner A, Bauer H, et al. Chemical characterisation of fine particle emissions from wood stove combustion of common woods growing in mid-European Alpine regions. Atmos Environ 2008;42:126–41.

[258] Umamaheswaran K, Batra VS. Physico-chemical characterisation of Indian biomass ashes. Fuel 2008;87(6):628–38.

[259] Vamvuka D, Zografos D, Alevizos G. Control methods for mitigating biomass ash-related problems in fluidized beds. Bioresour Technol 2008;99:3534–44.

[260] Van Loo S, Koppejan J. The handbook of biomass combustion and co-firing. London - Sterling (VA): Earthscan; 2008. p. 442.

[261] Wang S, Jiang XM, Han XX, Wang H. Fusion characteristic study on seaweed biomass ash. Energ Fuel 2008;22(4):2229–35.

[262] Yin CY, Kadir SASA, Lim YP, Syed-Ariffin SN, Zamzuri Z. An investigation into physicochemical characteristics of ash produced from combustion of oil palm biomass waste in a boiler. Fuel Process Technol 2008;89:693–6.

[263] Zhang J. Hydrogen production by biomass gasification in supercritical water. Energeia 2008;19(6):1–3.

[264] Bakisgan C, Dumanli AG, Yurum Y. Trace elements in Turkish biomass fuels: ashes of wheat straw, olive bagasse and hazelnut shell. Fuel 2009;88:1842–51.

[265] Bhattacharya P, Steele PH, Barbary E, Hassan M, Mitchell B, Ingram L, et al. Wood/plastic copyrolysis in an auger reactor: chemical and physical analysis of the products. Fuel 2009;88:1251–60.

[266] Dahl O, Nurmesniemi H, Poykio R, Watkins G. Comparison of the characteristics of bottom ash and fly ash from a medium-size (32 MW) municipal district heating plant incinerating forest residues and peat in a fluidized-bed boiler. Fuel Process Technol 2009;90:871–8.

[267] Demirbas A. Progress and recent trends in biodiesel fuels. Energy Convers Manage 2009;50:14–34.

[268] Demirbas MF. Biorefineries for biofuel upgrading: a critical review. Appl Energ 2009;86:S151–61.

[269] Demirbas MF, Balat M, Balat H. Potential contribution of biomass to the sustainable energy development. Energ Convers Manage 2009;50:1746–60.

[270] Di Blasi C. Combustion and gasification rates of lignocellulosic chars. Prog Energ Combust 2009;35:121–40.

[271] Doshi V, Vuthaluru HB, Korbee R, Kiel JHA. Development of a modelling approach to predict ash formation during co-firing of coal and biomass. Fuel Process Technol 2009;90:1148–56.

[272] Duong DNB, Tillman DA. Chlorine issues with biomass cofiring in pulverized coal boilers: sources, reactions, and consequences – a literature review. Foster Wheeler Technical Papers: Clinton, NJ, USA; 2009. p. 1–13.

[273] Fermoso J, Arias B, Plaza MG, Pevida C, Rubiera F, Pis JJ, et al. High-pressure co-gasification of coal with biomass and petroleum coke. Fuel Process Technol 2009;90:926–32.

[274] Khan AA, de Jong W, Jansens PJ, Spliethoff H. Biomass combustion in fluidized bed boilers: Potential problems and remedies. Fuel Process Technol 2009;90:21–50.

[275] Kiel JHA, Ciepilk MK, Pels JR, van de Kamp WL, Saraber A, van Eijk RL. Biomass co-firing in high percentages – Dutch R&D consortium pushing the limits. In: Proceedings of the 4th international conference on clean coal technologies in conjunction with the 3rd international Freiberg conference in IGCC & XtL Technol. Dresden, Germany, 18–21 May 2009. p. 13.

[276] Kiel JHA, Verhoeff F, Gerhauser H, van Daalen W, Meuleman B. BO2-technology for biomass upgrading into solid fuel – an enabling technology for IGCC and gasification-based BtL. In: Proceedings of the 4th international conference on clean coal technologies in conjunction with the 3rd international freiberg conference in IGCC & XtL Technol. Dresden, Germany, 18–21 May 2009. p. 10.

[277] Kirubakaran V, Sivaramakrishnan V, Nalini R, Sekar T, Premalatha M, Subramanian P. A review on gasification of biomass. Renew Sust Energ Rev 2009;13(1):179–86.

[278] Koukouzas N, Ward CR, Papanikolaou D, Li Z, Ketikidis C. Quantitative evaluation of minerals in fly ashes of biomass, coal and biomass-coal mixture derived from circulating fluidised bed combustion technology. J Hazard Mater 2009;169:100–7.

[279] Madhiyanon T, Sathitruangsak P, Soponronnarit S. Co-combustion of rice husk with coal in a cyclonic fluidized-bed combustor (Ψ-FBC). Fuel 2009;88:132–8.

[280] Pallares J, Gil A, Cortes C, Herce C. Numerical study of co-firing coal and *Cynara cardunculus* in a 350 MWe utility boiler. Fuel Process Technol 2009;90:1207–13.

[281] Pettersson A, Amand L-E, Steenari B-M. Chemical fractionation for the characterization of fly ashes from co-combustion of biofuels using different methods for alkali reduction. Fuel 2009;88:1758–72.

[282] Poykio R, Ronkkomaki H, Nurmesniemi H, Peramaki P, Popov K, Valimaki I, et al. Chemical and physical properties of cyclone fly ash from the grate-fired boiler incinerating forest residues at a small municipal district heating plant (6 MW). J Hazard Mater 2009;162:1059–64.

[283] Rajamma R, Ball RJ, Tarelho LAC, Allen GC. Characterisation and use of biomass fly ash in cement-based materials. J Hazard Mater 2009;172:1049–60.

[284] Sarenbo S. Wood ash dilemma-reduced quality due to poor combustion performance. Biomass Bioenerg 2009;33:1212–20.

[285] Shen DK, Gu S, Luo KH, Bridgwater AV, Fang MX. Kinetic study on thermal decomposition of woods in oxidative environment. Fuel 2009;88:1024–30.

[286] Szemmelveisz K, Szucs I, Palotas AB, Winkler L, Eddings EG. Examination of the combustion conditions of herbaceous biomass. Fuel Process Technol 2009;90:839–47.

[287] Thy P, Esbensen KH, Jenkins BM. On representative sampling and reliable chemical characterization in thermal biomass conversion studies. Biomass Bioenerg 2009;33:1513–9.

[288] Vamvuka D. Comparative fixed/fluidized bed experiments for the thermal behaviour and environmental impact of olive kernel ash. Renew Energ 2009;34:158–64.

[289] Vamvuka D, Pitharoulis M, Alevizos G, Repouskou E, Pentari D. Ash effects during combustion of lignite/biomass blends in fluidized bed. Renew Energ 2009;34:2662–71.

[290] Wang C, Wang F, Yang Q, Liang R. Thermogravimetric studies of the bahavior of wheat straw with added coal during combustion. Biomass Bioenerg 2009;33(1):50–6.

[291] Zbogar A, Frandsen F, Jensen PA, Glarborg P. Shedding of ash deposits. Prog Energ Combust 2009;35:31–56.

[292] Abbasi T, Abbasi SA. Biomass energy and the environmental impacts associated with its production and utilization. Renew Sust Energ Rev 2010;14:919–37.

[293] Abreu P, Casaca C, Costa M. Ash deposition during the co-firing of bituminous coal with pine sawdust and olive stones in a laboratory furnace. Fuel 2010;89:4040–8.

[294] Ahmaruzzaman M. A review on the utilization of fly ash. Prog Energ Combust 2010;36:327–63.

[295] Arvelakis S, Frandsen FJ. Rheology of fly ashes from coal and biomass co-combustion. Fuel 2010;89:3132–40.

[296] Bajus M. Pyrolysis of woody material. Petrol Coal 2010;52(3):207–14.

[297] Brebu M, Ucar S, Vasile C, Yanik J. Co-pyrolysis of pine cone with synthetic polymers. Fuel 2010;89:1911–8.

[298] Brennan L, Owende P. Biofuels from microalgae – a review of technologies for production, processing, and extractions of biofuels and co-products. Renew Sust Energ Rev 2010;14:557–77.

[299] Darvell LI, Jones JM, Gudka B, Baxter XC, Saddawi A, Williams A, et al. Combustion properties of some power station biomass fuels. Fuel 2010;89:2881–90.

[300] Demirbas A. Use of algae as biofuel sources. Energ Convers Manage 2010;51:2738–49.

[301] Fryda L, Sobrino C, Cieplik M, Van de Kamp WL. Study on ash deposition under oxyfuel combustion of coal/biomass blends. Fuel 2010;89:1889–902.

[302] Gao C, Vejahati F, Katalambula H, Gupta R. Co-gasification of biomass with coal and oil sand coke in a drop tube furnace. Energ Fuel 2010;24:232–40.

[303] Kajitani S, Zhang Y, Umemoto S, Ashizawa M, Hara S. Co-gasification reactivity of coal and woody biomass in high-temperature gasification. Energ Fuel 2010;24:145–51.

[304] Kumar M, Patel SK, Mishra S. Studies on characteristics of some shrubaceous non-woody biomass species and their electricity generation potentials. Energ Source, Part A 2010;32:786–95.

[305] Kwapinski W, Byrne CMP, Kryachko E, Wolfram P, Adley C, Leahy JJ, et al. Biochar from biomass and waste. Waste Biomass Valoriz 2010;1:177–89.

[306] Li W, Li W, Liu H. The resource utilization of algae – preparing coal slurry with algae. Fuel 2010;89:965–70.

[307] Mulligan CJ, Strezov L, Strezov V. Thermal decomposition of wheat straw and mallee residue under pyrolysis conditions. Energ Fuel 2010;24:46–52.

[308] Naik S, Goud VV, Rout PK, Jacobson K, Dalai AK. Characterization of Canadian biomass for alternative renewable biofuel. Renew Energ 2010;35:1624–31.

[309] Naik SN, Goud VV, Rout PK, Dalai AK. Production of first and second generation biofuels: a comprehensive review. Renew Sust Energ Rev 2010;14:578–97.

[310] Niu Y, Tan H, Wang X, Liu Z, Liu H, Liu Y, et al. Study on fusion characteristics of biomass ash. Bioresour Technol 2010;101:9373–81.

[311] Piotrowska P, Zevenhoven M, Davidsson K, Hupa M, Amand L-E, Barisic V, et al. Fate of alkali metals and phosphorus of rapeseed cake in Circulating Fluidized Bed Boiler. Part 1. Combustion with wood. Energ Fuel 2010;24:333–45.

[312] Ross AB, Biller P, Kubacki ML, Lea-Langton A, Jones JM. Hydrothermal processing of microalgae using alkali and organic acids. Fuel 2010;89:2234–43.

[313] Sims REH, Mabee W, Saddler JN, Taylor M. An overview of second generation biofuel technologies. Bioresour Technol 2010;101:1570–80.
[314] Stam AF, Livingston WR, Cremers MFG, Brem G. Review of models and tools for slagging and fouling prediction for biomass co-combustion. Review article for IEA. Task 2010;32:1–18.
[315] Steenari B-M, Fedje KK. Addition of kaolin as potassium sorbent in the combustion of wood fuel – effects on fly ash properties. Fuel 2010;89:2026–32.
[316] Weller N, Zeng T, Lenz V. Combustion behavior of straw pellets and its potential optimisation by fuel improvement. Report 18th European biomass conference and exhibition. Lyon, France, 03–07 May 2010. p. 5.
[317] Xu XG, Li S-Q, Li G-D, Yao Q. Effect of co-firing straw with two coals on the ash deposition behaviour in a down-fired pulverized coal combustor. Energ Fuel 2010;24:241–9.
[318] Yip K, Tian F, Hayashi J-I, Wu H. Effect of alkali and alkaline earth metallic species on biochar reactivity and syngas compositions during steam gasification. Energ Fuel 2010;24:173–81.
[319] Zhang M, Qi W, Liu R, Su R, Wu S, He Z. Fractionating lignocellulose by formic acid: characterization of major components. Biomass Bioenerg 2010;34:525–32.
[320] Abdullah H, Wu H. Direct utilisation of biomass for bioenergy generation: key technical challenges and pre-treatment technologies. Proceedings of the UMTAS 2011 empowering science, technology and innovation towards a better tomorrow 2011;EO2:1–17.
[321] Ban CC, Ramli M. The implementation of wood waste ash as a partial cement replacement material in the production of structural grade concrete and mortar: an overview. Resour Conserv Recy 2011;55:669–85.
[322] Demirbas A. Competitive liquid biofuels from biomass. Appl Energ 2011;88:17–28.
[323] Font O, Cordoba P, Querol X, Coca P, Garcia-Pena F. Co-gasification of biomass: effect on the fate of trace elements. In: 2011 World of coal ash conference (WOCA). Denver, CO., USA, 9–12 May 2011. p. 10.
[324] Giuntoli J, Gout J, Verkooijen AHM, De Jong W. Characterization of fast pyrolysis of dry distiller's grains (DDGS) and palm kernel cake using a heated foil reactor: nitrogen chemistry and basic reactor modelling. Ind Eng Chem Res 2011;50(8):4286–300.
[325] Gubba SR, Ma L, Pourkashanian M, Williams A. Influence of particle shape and internal thermal gradients of biomass particles on pulverised coal/biomass co-fired flames. Fuel Process Technol 2011;92(11):2185–95.
[326] Kumar M, Patel SK, Hamid PF. Characteristics of some forestry non-woody biomass species and estimation of their power generation potentials. Energ Sources, Part A 2011;33:1616–24.
[327] Mansha M, Javed SH, Kazmi M, Feroze N. Study of rice husk ash as potential source of acid resistance calcium silicate. Adv Chem Eng Sci 2011;1:147–53.
[328] Nigam PS, Singh A. Production of liquid biofuels from renewable resources. Prog Energ Combust 2011;37:52–68.
[329] Quaranta N, Unsen M, Lopez H, Giansiracusa C, Roether JA, Boccaccini AR. Ash from sunflower husk as raw material for ceramic products. Ceram Int 2011;37:377–85.
[330] Saidur R, Abdelaziz EA, Demirbas A, Hossain MS, Mekhilef S. A review on biomass as a fuel for boilers. Renew Sustain Energ Rev 2011;15(5):2262–89.
[331] Singh S, Ram LC, Masto RE, Verma SK. A comparative evaluation of minerals and trace elements in the ashes from lignite, coal refuse, and biomass fired power plants. Int J Coal Geol 2011;87:112–20.
[332] Skreiberg A, Skreiberg O, Sandquist J, Sorum L. TGA and macro-TGA characterisation of biomass fuels and fuel mixtures. Fuel 2011;90:2182–97.
[333] Tan Z, Lagerkvist A. Phosphorus recovery from the biomass ash: a review. Renew Sust Energ Rev 2011;15:3588–602.
[334] Tateda M, Okura M, Kim Y, Athapattu BCL. Production of safe charcoal from waste construction wood treated with citric acid. J Environ Protect 2011;2:1134–42.
[335] Tumuluru JS, Sokhansanj S, Wright CT, Boardman RD, Yancey NA. A review on biomass classification and composition, co-firing issues and pretreatment methods. In: Proceedings of the 2011 ASABE annual international meeting. Louisville, Kentucky, USA, 7–10 August 2011. p. 31.
[336] Vamvuka D, Kakaras E. Ash properties and environmental impact of various biomass and coal fuels and their blends. Fuel Process Technol 2011;92:570–81.
[337] Van der Stelt MJC, Gerhauser H, Kiel JHA, Ptasinski KJ. Biomass upgrading by torrefaction for the production of biofuels: a review. Biomass Bioenerg 2011;35:3748–62.
[338] Wang C, Wu Y, Liu Q, Yang H. Study of the characteristics of the ashing process of straw/coal combustion. Fuel 2011;90(9):2939–44.
[339] Wang L, Shahbazi A, Hanna MA. Characterization of corn stover, distiller grains and cattle manure for thermochemical conversion. Biomass Bioenerg 2011;35:171–8.
[340] Wang X, Si J, Tan H, Zhao Q, Xu T. Kinetics investigation on the reduction of NO using straw char based on physicochemical characterization. Bioresour Technol 2011;102(16):7401–6.
[341] Werkelin J, Lindberg D, Bostrom D, Skrifvars B-J, Hupa M. Ash-forming elements in four Scandinavian wood species. Part. 3. Combustion of five spruce samples. Biomass Bioenerg 2011;35:725–33.
[342] Wilson L, Yang W, Blasiak W, John GR, Mhilu CF. Thermal characterization of tropical biomass feedstocks. Energ Convers Manage 2011;52:191–8.
[343] Xiao R, Chen X, Wang F, Yu G. The physicochemical properties of different biomass ashes at different ashing temperature. Renew Energ 2011;36:244–9.
[344] Baxter XC, Darvell LI, Jones JM, Barraclough T, Yates NE, Shield I. Study of *Miscanthus* × *giganteus* ash composition – variation with agronomy and assessment method. Fuel 2012;95:50–62.
[345] Boonjob W, Zevenhoven M, Ek P, Hupa M, Ivaska A, Miro M. Automatic dynamic chemical fractionation method with detection by plasma spectrometry for advanced characterization of solid biofuels. J Anal Atom Spectrom 2012;27(5):841–9.
[346] Bostrom D, Skoglund N, Grimm A, Boman C, Ohman M, Brostrom M, et al. Ash transformation chemistry during combustion of biomass. Energ Fuel 2012;26:85–93.
[347] Chandrasekaran SR, Hopke PK. Kinetics of switch grass pellet thermal decomposition under inert and oxidizing atmospheres. Bioresour Technol 2012;125:52–8.
[348] Diaz-Ramirez M, Boman C, Sebastian F, Royo J, Xiong S, Bostrom D. Ash characterization and transformation behavior of the fixed-bed combustion of novel crops: poplar, brassica, and cassava fuels. Energ Fuel 2012;26(6):3218–29.
[349] Eberhardt TL, Pan H. Elemental analyses of chars isolated from a biomass gasifier fly ash. Fuel 2012;96:600–3.
[350] Fernandez RG, Garcia CP, Lavin AG, Bueno de las Heras JL. Study of main combustion characteristics for biomass fuels used in boilers. Fuel Process Technol 2012;103:16–26.
[351] Fournel S, Godbout S, Heitz M, Brassard P, Palacios J. Gaseous emissions from agricultural biomass combustion: influence of biomass characteristics. In: Proceedings of the NABEC-CSBE/SCGAB 2012 (Paper # NABEC/CSBE 12–070), joint meeting and technical conference northeast agricultural & biological engineering conference. Canadian Society for Bioengineering, Lakehead University, Orillia, Ontario, 15–18 July 2012. p. 7.
[352] Fournel S, Godbout S, Heitz M. Gaseous emissions from agricultural biomass combustion: a modelling approach. In: Proceedings of the NABEC-CSBE/SCGAB 2012 (Paper # NABEC/CSBE 12–071), joint meeting and technical conference northeast agricultural & biological engineering conference. Canadian Society for Bioengineering, Lakehead University, Orillia, Ontario, 15–18 July 2012. p. 10.
[353] Garcia R, Pizarro C, Lavin AG, Bueno JL. Characterization of Spanish biomass wastes for energy use. Bioresour Technol 2012;103:249–58.
[354] Gudka B, Darvell LI, Jones JM, Williams A, Kilgallon PJ, Simms NJ, et al. Fuel characteristics of wheat-based dried distillers grains and solubles (DDGS) for thermal conversion in power plants. Fuel Process Technol 2012;94(1):123–30.
[355] Hupa M. Ash-related issues in fluidized-bed combustion of biomasses: recent research highlights. Energ Fuel 2012;26:4–14.
[356] Jordan CA, Akay G. Speciation and distribution of alkali, alkali earth metals and major ash forming elements during gasification of fuel cane bagasse. Fuel 2012;91:253–63.
[357] Lassesson H, Steenari B-M. Possibilities of ash speciation with synchrotron based X-ray absorption spectroscopy (XAS). In: Proceedings of the 21st international conference on fluidized bed combustion. Naples, Italy, June 3–6, 2012. p. 195–202.
[358] Medic D, Darr M, Shah A, Potter B, Zimmerman J. Effects of torrefaction process parameters on biomass feedstock upgrading. Fuel 2012;91:147–54.
[359] Mehmood S, Reddy BV, Rosen MA. Energy analysis of a biomass co-firing based pulverized coal power generation system. Sustainability 2012;4:462–90.
[360] Miccio F, Ruoppolo G, Kalisz S, Andersen L, Morgan TJ, Baxter D. Combined gasification of coal and biomass in internal circulating fluidized bed. Fuel Process Technol 2012;95:45–54.
[361] Rocca S, Van Zomeren A, Costa G, Dijkstra JJ, Comans RNJ. Characterisation of major component leaching and buffering capacity of RDF incineration and gasification bottom ash in relation to reuse or disposal scenarios. Waste Manage 2012;32:759–68.
[362] Sethupathy SB, Natarajan E. Hydrodynamic study on gasification of biomass in a fluidized bed gasifier. Int J Eng Sci Technol 2012;4(1):316–23.
[363] Sommersacher P, Brunner T, Obernberger I. Fuel indexes: a novel method for the evaluation of relevant combustion properties of new biomass fuels. Energ Fuel 2012;26:380–90.
[364] Viana H, Vega-Nieva DJ, Torres LO, Lousada J, Aranha J. Fuel characterization and biomass combustion properties of selected native woody shrub species from central Portugal and NW Spain. Fuel 2012;102:737–45.
[365] Wang G, Shen L, Sheng C. Characterization of biomass ashes from power plants firing agricultural residues. Energ Fuel 2012;26(1):102–11.
[366] Williams A, Jones JM, Ma L, Pourkashanian M. Pollutants from the combustion of solid biomass fuels. Prog Energ Combust 2012;38(2):113–37.
[367] Xu M, Sheng C. Influences of the heat-treatment temperature and inorganic matter on combustion characteristics of cornstalk biochars. Energ Fuel 2012;26:209–18.
[368] Lindberg D, Backman R, Chartrand P, Hupa M. Towards a comprehensive thermodynamic database for ash-forming elements in biomass and waste combustion – current situation and future developments. Fuel Process Technol 2013;105:129–41.
[369] Nordgren D, Hedman H, Padban N, Bostrom D, Ohman M. Ash transformations in pulverised fuel co-combustion of straw and woody biomass. Fuel Process Technol 2013;105:52–8.
[370] Piotrowska P, Zevenhoven M, Hupa M, Giuntoli J, de Jong W. Residues from the production of biofuels for transportation: characterization and ash sintering tendency. Fuel Process Technol 2013;105:37–45.

[371] Weber R, Mancini M, Schaffel-Mancini N, Kupka T. On predicting the ash behaviour using computational fluid dynamics. Fuel Process Technol 2013;105:113–28.

[372] Vassilev S, Vassileva C. Occurrence, abundance and origin of minerals in coals and coal ashes. Fuel Process Technol 1996;48:85–106.

[373] Vassilev S, Vassileva C. Mineralogy of combustion wastes from coal-fired power stations. Fuel Process Technol 1996;47:261–80.

[374] Vassilev S, Vassileva C. Geochemistry of coals, coal ashes and combustion wastes from coal-fired power stations. Fuel Process Technol 1997; 51:19–45.

[375] Vassilev S, Menendez R, Alvarez D, Diaz-Somoano M, Martinez-Tarazona MR. Phase-mineral and chemical composition of coal fly ashes as a basis for their multicomponent utilization. 1. Characterization of feed coals and fly ashes. Fuel 2003;82(14):1793–811.

[376] Vassileva C, Vassilev S. Behaviour of inorganic matter during heating of Bulgarian coals. 1. Lignites. Fuel Process Technol 2005;86(12–13):1297–333.

[377] Vassileva C, Vassilev S. Behaviour of inorganic matter during heating of Bulgarian coals. 2. Subbituminous and bituminous coals. Fuel Process Technol 2006;87:1095–116.

[378] Vassilev S, Vassileva C. A new approach for the classification of coal fly ashes based on their origin, composition, properties, and behaviour. Fuel 2007;86:1490–512.

[379] Vassileva C, Vassilev S, Daher D. Preliminary results on chemical and phase-mineral composition of Syrian petroleum coke and ash. Compt rend Acad Bulg Sci 2010;63(1):129–36.

[380] Stach E, Mackowsky M, Teichmuller M, Taylor G, Chandra D, Teichmuller R. Stach's textbook of coal petrology. Berlin: Gebruder Borntraeger; 1982. p. 535.

[381] Taylor GH, Teichmuller M, Davis A, Diessel CFK, Littke R, Robert P. Organic petrology. Berlin-Stuttgart: Gebruder Borntraeger; 1998. p. 704.

[382] Vassilev S, Tascon J. Methods for characterization of inorganic and mineral matter in coal: a critical overview. Energ Fuel 2003;17:271–81.

[383] Vassilev S, Vassileva C. Methods for characterization of composition of fly ashes from coal-fired power stations: a critical overview. Energ Fuel 2005;19(3):1084–98.

[384] Vassilev S, Vassileva C, Baxter D, Andersen L. A new approach for the combined chemical and mineral classification of the inorganic matter in coal. 2. Potential applications of the classification systems. Fuel 2009;88:246–54.

[385] Vassilev S, Kitano K, Takeda S, Tsurue T. Influence of mineral and chemical composition of coal ashes on their fusibility. Fuel Process Technol 1995;45:27–51.

[386] Franzle S, Markert B. The biological system of the elements (BSE). Part II: a theoretical model for establishing the essentiality of chemical elements. The application of stoichiometric network analysis to the biological system of the elements. The Sci Total Environ 2000;249:223–41.

[387] Vassilev S, Eskenazy G, Vassileva C. Contents, modes of occurrence and behaviour of chlorine and bromine in combustion wastes from coal-fired power stations. Fuel 2000;79:923–37.

[388] Cenni R, Janisch B, Spliethoff H, Hein KRG. Legislative and environmental issues on the use of ash from coal and municipal sewage sludge co-firing as construction material. Waste Manage 2001;21:17–31.

[389] Vassileva C, Vassilev S. Some environmental aspects related to sulphur emissions during combustion of Bulgarian coals. Compt rend Acad Bulg Sci 2004;57(9):29–32.

[390] Lin S, Wang Y, Suzuki Y. High-temperature CaO hydration/$Ca(OH)_2$ decomposition over a multitude of cycles. Energ Fuel 2009;23:2855–61.

[391] Saidur R, Boroumandjazi G, Mekhilef S, Mohammed HA. A review on exergy analysis of biomass based fuels. Renew Sust Energ Rev 2012;16(2):1217–22.

[392] Kubaschewski O, Alcock CB. Metallurgical thermochemistry. Oxford: Pergamon Press; 1983. p. 449.

[393] Voitkevich GV, Kokin AV, Miroshnikov AE, Prohorov VG. Geochemical handbook. Nedra, Moscow; 1990. p. 480 (in Russian).

[394] Skrifvars B-J, Hupa M, Backman R, Hiltunen M. Sintering mechanisms of FBC ashes. Fuel 1994;73:171–6.

[395] Railsback LB. Some fundamentals of mineralogy and Geochemistry. Department of Geology, University of Georgia, Athens, Georgia, USA; 2012. A web-based document <www.gly.uga.edu/railsback/FundamentalsIndex.html>.

[396] Mitchell RS, Gluskoter HJ. Mineralogy of ash of some American coals: variations with temperature and source. Fuel 1976;55(4):90–6.

[397] Nankervis J, Furlong R. Phase changes in mineral matter of North Dakota lignites caused by heating to 1200 °C. Fuel 1980;59(6):425–30.

[398] Vassilev S, Eskenazy G, Vassileva C. Contents, modes of occurrence and origin of chlorine and bromine in coal. Fuel 2000;79:903–21.

[399] Vassilev S, Vassileva C, Karayigit A, Bulut Y, Alastuey A, Querol X. Phase-mineral and chemical composition of composite samples from feed coals, bottom ashes and fly ashes at the Soma power station, Turkey. Int J Coal Geol 2005;61(1–2):35–63.

[400] Vassilev S, Vassileva C. A new approach for the combined chemical and mineral classification of the inorganic matter in coal. 1. Chemical and mineral classification systems. Fuel 2009;88:235–45.

[401] Ververis C, Georghiou K, Danielidis D, Hatzinikolaou DG, Santas P, Santas R, et al. Cellulose, hemicelluloses, lignin and ash content of some organic materials and their suitability for use as paper pulp supplements. Bioresource Technol 2007;98:296–301.

[402] Kostov I. Mineralogy. Technika, Sofia; 1993. p 734 (in Bulgarian).

[403] Vassilev S, Vassileva C, Baxter D, Andersen L. Relationships between chemical and mineral composition of coal and their potential applications as genetic indicators. Part 2. Mineral classes, groups and species. Geologica Balcanica 2010;39(3):43–67.